THE UNIVERSITY of ADELAIDE

Enhancing Green Hydrogen Production during One and Two Stage Catalytic Pyrolysis of Biomass with Mechano-chemically Prepared Char Supported Iron Catalyst

by

Richard Thomson

Submitted in fulfilment of the requirements for the degree of Doctor of Philosophy

School of Chemical Engineering and Advanced Materials
The University of Adelaide

August 2022

DECLARATION

I certify that this work contains no material which has been accepted for the award of any other degree or diploma in my name, in any university or other tertiary institution and, to the best of my knowledge and belief, contains no material previously published or written by another person, except where due reference has been made in the text. In addition, I certify that no part of this work will, in the future, be used in a submission in my name, for any other degree or diploma in any university or other tertiary institution without the prior approval of The University of Adelaide and where applicable, any partner institution responsible for the joint award of this degree. I give permission for the digital version of my thesis to be made available on the web, via the University's digital research repository, the Library Search and also through web search engines, unless permission has been granted by the University to restrict access for a period of time. I acknowledge the support I have received for my research through the provision of an Australian Government Research Training Program Scholarship.

Richard Thomson

20th August 2022

ABSTRACT

Thermo-chemical conversion of biomass is one route to create a pathway to renewably sourced energy, including hydrogen; and precursor products for the manufacture of transport fuels and chemicals. While this prospect is tantalising, the three realities of economics, complexities of processing, and securing feedstock supplies currently hinder the transition.

The aims of this work were to hasten the use of biomass conversion by improving its economics. Two key considerations were the catalyst system and the type of thermochemical process, pyrolysis or gasification, as both have the potential to not only influence reaction rates and yields, but also both capital and operating costs.

Pyrolysis was selected as the process. A new catalyst system was devised based on a mechano-chemical preparation method, suitable for direct addition of the catalyst to the biomass. The catalyst components were iron, being plentiful, low cost and an established catalyst in biomass processing; and char, generated internally during pyrolysis. Almond residues were the primary biomass used.

Using thermogravimetric analysis the impact of this catalyst on reaction kinetics was assessed over a range of pyrolysis temperatures (450 – 750°C) with catalyst iron loading of 2%, 4% and 6%(wt./wt. biomass). Char yields were reduced, the major ligno-cellulose components had lower onset and peak decomposition temperatures, increased total mass loss and reduced apparent activation energies. The extent of each of these changes reflected catalyst loadings (Chapter 2).

A one-stage laboratory fixed bed reactor was used to conduct a series of catalytic pyrolysis trials over a similar range of temperature and catalyst loadings, using almond residue and pine chips as biomass. Overall product gas volumes and hydrogen production were higher with increasing pyrolysis temperature and catalyst loadings. Notably, char yields reduced as hydrogen production increased. The impact of the catalyst on different biomass was essentially the same.

Commercial iron ore (CIO) and waste iron ore tailings (IOT) were selected as alternatives to replace iron oxide prepared from AR grade ferric nitrate (LFN). The mechano-chemical preparation method was progressively simplified for each of CIO and IOT. At the lower catalyst loadings and pyrolysis temperatures each catalyst type produced similar yields. Above 650°C yields from CIO and IOT types were lower by around 15% with a 30% divergence evident at peak temperature and catalyst loading.

Nevertheless, at these conditions, hydrogen production by all catalyst types was over 175% of that from baseline pyrolysis at 600°C.

A two-stage catalytic pyrolysis process was developed, with both stages operating at the same temperature. Product from the first stage passed to the second, where char residue, containing the catalyst, supported reforming reactions. Total gas and hydrogen production, was essentially double that achieved in equivalent one-stage processing. Increases (up to 60%) in syngas production were also assisted by higher CO production at higher pyrolysis temperatures, bringing improved H_2/CO ratios. IOT proved equally as effective as LFN in these experiments. This further enhances the development of this process for producing green hydrogen through recycling of waste ore.

ACKNOWLEDGEMENTS

I would first and foremost wish to thank my primary supervisor Dr. Philip Kwong for his encouragement, guidance, patience, and support throughout my studies. His knowledge has proved invaluable to my development as a researcher and making the adjustment from industry back to academia. His feedback and incisive comments often resulted in developing new insights to the project, from which I have no doubt this thesis has benefitted.

Sincere thanks must go Dr. Tony Hall for his outstanding analytical chemistry abilities that have provided me with much valuable data for this work, and whose work ethic just goes ‘above and beyond’. Another extremely important supporter and friend has been ECMS technician Jason Peak, providing continuous support, ensuring I had a high quality, operational experimental rig; and also taking time out occasionally to discuss a common interest, sailing.

There are countless other colleagues at the University and friends in the wider community that have helped in numerous ways, and I thank them for their companionship and support on this journey.

To my family; first, my wife and soul-mate, Pamela, who advised sagely, showed much forbearance, and provided all the support and encouragement that one could hope for to allow me to indulge in these four years of research; words will never adequately express my thanks. Secondly, to my children, Andrew and Sophie, who both showed much love, support and encouragement for “the old man” to do his thing.

TABLE OF CONTENTS

LIST OF TABLES

LIST OF FIGURES

.

LIST OF ABBREVIATIONS

The following list displays the abbreviations used throughout this thesis.

AAE	Apparent Activation Energy
AAME	Alkali and Alkaline Earth Metallic species
AR	Almond residue
BECCS	Bioenergy with Carbon Capture and Storage
C	Carbon
CH_4	Methane
CIO	Commercial iron ore
CO	Carbon monoxide
CO_2	Carbon dioxide
dia	Diameter
DSC	Differential scanning calorimetry
DTG	Differential thermogravimetry
Fe	Iron
g	Gram
GC	Gas chromatograph
GC-MS	Gas chromatograph – mass spectrometer
GHG	Greenhouse gas
He	Helium
H	Hydrogen
IOT	Iron ore tailings
kJ	kilo-joules
LFN	Laboratory ferric nitrate
mg	milligram
µm	micrometre
mm	millimetres
mL	millilitres
mol	moles
MW	molecular weight
N	Nitrogen

Nm^3	Cubic metres at STP
O	Oxygen
PC	Pine chips
PM	Particulate matter
PAH	Polycyclic aromatic hydrocarbon
S/B	Steam to biomass ratio (wt/wt)
T_f	Final temperature
TGA	Thermogravimetric analysis
T_o	Onset temperature
tpa	tonnes per annum
T_{pn}	Peak temperature at Stage n
VM	Volatile matter
WtE	Waste-to-energy
WtH	Waste-to-hydrogen
wt.	Weight

LIST OF RESEARCH OUTPUT

Journal Article

R. Thomson, P. Kwong, E. Ahmad and K. D. P. Nigam Clean syngas from small commercial biomass gasifiers; a review of gasifier development, recent advances and performance evaluation. *International Journal of Hydrogen Energy*, 2020, Vol. 45 Issue 41 Pages 21087-21111

DOI: 10.1016/j.ijhydene.2020.05.160

Elsevier Reference Series

R. Thomson, P. Kwong, Production and Applications of Synthesis Gas. In: *Reference Module in Chemistry Molecular Sciences and Chemical Engineering,* Elsevier 2020

DOI https://doi.org/10.1016/B978-0-12-409547-2.14429-4

https://www.sciencedirect.com/science/article/pii/B9780124095472144294

Conference Poster

R. Thomson, P. Kwong, Enhanced hydrogen production using ball-milled, char supported iron catalyst during pyrolysis of biomass. N**ature Conference:** *Waste Management and Valorisation for a Sustainable Future* October 26 – 28, 2021 | LG Science Park, Seoul, Korea

Chapter 1: Introduction

1.1 The role of biomass as a renewable energy source

The replacement of fossil fuels is seen as a critical step in meeting the challenge of greenhouse gas effect as well as tackling the problem of depleting fossil fuels (Johnsson, Kjärstad & Rootzén 2018). Biomass, organic material derived from plants, contains the energy in the chemical bonds created as plants convert sunlight into plant material through photosynthesis. Consequently, biomass is a renewable resource and is one of the alternatives capable of replicating the role of fossil fuels, whereby its energy can be converted into electricity and heat, as well as transportation fuels and chemical precursors as a replacement for petrochemicals. It therefore represents a very versatile renewable energy source. In fact, biomass has always been a significant energy source for humanity and is currently assessed to provide approximately 10–14% of the world's energy supply (World Energy Resources | 2016 ; World Energy Resources Waste to Energy | 2016).

One of the primary concerns in the use of biomass for production of hydrogen, or syngas and its downstream products, is the risk of unsustainable, over-exploitation of natural resources. Biomass production inevitably requires access to land, and this raises the inescapable competition between food and industrial use. Therefore, the availability of biomass for industrial purposes has to be assessed in this light, with one estimate being that up to 1bn tonnes can be made available, 50% from agricultural residue and waste and 50% from purpose grown energy crops (OECD Meeting Policy Challenges for a Sustainable Bioeconomy 2018). In the context of competing demands, an important consideration is the development of processes directed at improving the efficiency of conversion of biomass.

However, utilisation of biomass has significant potential to deliver socio-economic benefits too. People can be engaged at each stage within the industry. This, together with developing higher efficiencies within the industry, will raise living standards and broaden the demographics of those that can be engaged usefully in income generating employment (World Energy Resources | 2016).

Several technologies have now been developed for the conversion of biomass into fuels and chemicals, out of which gasification remains a promising technology to produce syngas, useful for power generation and to produce liquid transportation fuel

(Ahmad et al. 2016; Sansaniwal, Rosen & Tyagi 2017). Moreover, biomass pyrolysis and gasification is reported as a potential process to produce hydrogen (Pandey, Prajapati & Sheth 2019).The contribution of biomass to the overall energy system has opportunities for reducing oil dependency through the production of hydrogen and other biofuels for land transportation and aviation and maritime transportation. Electricity generation is critically important as the increasing use of renewable energy sources create grid intermittency problems, and the products of biomass conversion can be used as a grid stabiliser with the added benefit of ready storage of raw material versus the more expensive option of product storage.

1.2 Biomass – a potential source of hydrogen, and hydrogen enriched syngas

While the scientific community has long recognised the need to de-carbonise the world's energy sources, the realisation has finally resonated with governments that action must now be taken (UN Climate Change Conference UK 2021 2021). This has led to a renewed focus on hydrogen as one of the preferred energy sources to replace fossil fuels used for transport and to become both an energy carrier and a fuel. Currently production of hydrogen is around 70 million tpa of which approximately 96% is sourced from fossil fuels (Kaur R. 2019).

The challenge now is to not only replace that production with hydrogen from renewable sources but to increase renewably sourced hydrogen, and hydrogen enriched syngas production very significantly to meet the other demands created through the wider de-carbonisation thrust. At present the sources of renewable hydrogen are limited to biomass processes and water splitting processes both of which have production costs substantially higher than those of fossil fuels. Major research efforts have now been supported by governments to more swiftly tackle the technical issues associated with developing scale production of renewably sourced hydrogen at acceptable costs (IEA 2019). Costs for solar PV and wind generation continue to decline and this may assist in developing a low-cost supply option for hydrogen, based around electrolysers at preferred production locations. Similarly an important development associated with biomass processing has been to focus on the utilisation of wastes as feedstock as this addresses two problems concurrently. Firstly, it reduces the waste disposal burden; and secondly, reduces the input costs for the biomass conversion process (Lui et al. 2020). Biomass also offers the prospect of carbon

negative emissions when combined with carbon capture and storage (BECCS) (Kemper 2015).

It is probable that with the huge potential market developing for hydrogen, and hydrogen enriched syngas that all current, and yet to-be-developed means, of renewable hydrogen and syngas production will find opportunities to participate.

1.3 Production of hydrogen, and hydrogen enriched syngas, using thermochemical conversion of biomass

Biomass can be converted to useful products using the process options of bio-chemical or thermochemical routes with the latter considered the more advanced in respect of hydrogen production. Within the thermochemical conversion options both pyrolysis and gasification are considered to be the best potential process routes for large scale hydrogen production.

1.3.1 Hydrogen production using gasification

Biomass gasification technology involves higher temperatures (generally in the range 900-1200°C), partial oxidation of biomass in the presence of a gasifying agent (either air, oxygen, steam, carbon dioxide, or mixtures of these components), then gas purification, and conditioning to produce syngas and/or hydrogen (Figure 1.1). Prior to conditioning the gas product is of a low-to-medium heating value producer gas, that contains carbon monoxide, hydrogen, carbon dioxide, methane, and nitrogen, the proportions being determined by the specific oxidiser (Richardson, Drobek, et al. 2015).

Primarily three processes have been studied in regard to hydrogen production by gasification, each specific to the oxidant, air, oxygen or steam. The key differences reported were the average hydrogen content of the produced gas, being 15%, 40% and 40% respectively, and H_2/CO ratios of 0.75, 1.0 and 1.6 respectively (Basu 2010; Parthasarathy & Narayanan 2014; Yang, H & Chen 2015). These typical outcomes have supported a move to steam gasification, which also offers the opportunity to utilise biomass with higher moisture contents (up to 35%) (de Lasa et al. 2011). While the gasification step produces a typical gas product dominated by carbon monoxide and carbon dioxide, and char and tars, it is the steam reforming process that is critical. In this stage the structure of the tars is altered, producing significant quantities of

hydrogen. This is generally followed by the water-gas-shift (WGS) reaction which converts carbon monoxide in the presence of steam to additional hydrogen. At this stage the gas is primarily hydrogen and carbon dioxide and a carbon capture system known as Sorption-Enhanced Hydrogen Production (SEHP) (Harrison 2008) combined with Pressure Swing Adsorption (PSA) delivers a very high purity hydrogen product (Yao, J et al. 2017).

Additional developments in gasification, aimed primarily at reducing tar production and the formation of high temperature agglomerations, has been the development of two stage processes. This foreshadowed successful process design developments. Each included some form of staging of the pyrolysis and gasification steps, in either separate reactors or separate zones in the same reactor. In the case of gasification, the Dual Fluidised Bed (DFB) has been recognised as an important development in the pursuit of enhancing hydrogen production from gasification.

1.3.2 Limitations on hydrogen production from gasification

Despite the claim that biomass gasification for hydrogen production is a mature technology pathway (Hydrogen Production: Biomass Gasification) the fact is that many gasification units have been built but the vast majority are small scale (IEA Bioenergy The past, present and future of gasification 2020) and while successful, are not suitable for large scale hydrogen production. Researchers have recognised how capital and operating costs reflect the process complexity, and the way in which this reduced the competitiveness of the biomass gasification processes used to produce syngas and hydrogen. Much focus has been placed on improving reactor design to improve the potential by reducing the complexity of current large-scale gasification units. DFB reactor designs have been proposed and while a demonstration plant has operated successfully, all commercial plants have been closed. The MILENA technology, a broadly similar process, had been suggested as an alternative but there is no evidence of commercial application. Other concerns include the high temperatures required for the second stage (>1000°C), the poor H_2/CO ratio that requires additional processing for both downstream syngas applications or hydrogen production. This requires water-gas-shift (WGS) catalysed fixed bed reactors downstream of the gasification, often post a catalytic hot gas cleaning unit to remove tars (Binder et al. 2018).

1.3.3 Hydrogen production using pyrolysis

Of the thermochemical processes available, pyrolysis is one of the simplest. Conventional pyrolysis leads to the conversion of biomass to liquid, solid and gaseous fractions by heating the biomass in the absence of air to temperatures between 400-900°C. With the focus on hydrogen and hydrogen enriched sngas, the target has been to increase the gaseous yield at the expense of the liquid yield, thereby increasing hydrogen production. Initially, one-stage catalytic pyrolysis was almost universally adopted as the best means of achieving this outcome (Bru et al. 2007; Khelfa et al. 2009; Pütün 2010). However through the development of a conceptual picture of the pyrolysis process (Figure 1.2), it was recognised that there were two stages to the process (Neves, D. et al. 2011) which became the basis for the development of two-stage catalytic pyrolysis-reforming process. This development took two paths, one where the bio-oil was treated in a second stage to produce hydrogen, and another where in-line catalytic steam reforming was combined with pyrolysis to more directly produce hydrogen. The latter has gained greater appeal given the capability of optimising each of the pyrolysis and reforming stages, and the avoidance of impurities in the reforming stage.

Several advantages accrue in this process scheme, firstly, the ease of scaling up to a continuous feed design, secondly, the components of bio-oil are dealt with prior to condensation and therefore avoids the secondary volatilisation step and, thirdly, the gas product is completely free of tars, a significant advantage over gasification. Various reactor designs have developed for the pyrolysis step but notably, almost invariably, the in-line reforming stage is a fixed catalyst bed (Arregi, Aitor et al. 2018). Consequently, another critical aspect is the selection of catalyst for the reforming stage.

1.3.4 Limitations on hydrogen production from pyrolysis

It is apparent that single stage pyrolysis will always suffer from relatively low yields of hydrogen, and that the product streams still carry significant contaminants. Yield is of fundamental importance given the low hydrogen content of biomass (from 5% to 7.5% depending on the biomass source) (Yang, H & Chen 2015) as it impacts on the quantity of material that requires to be processed to meet specific production requirements. Two stage in-line processing provides significantly better yields but the optimisation of catalyst systems is necessary, particularly addressing the de-activation

and regeneration of the second stage fixed bed catalysts. In the case of pyrolysis nearly all the research has been at laboratory scale (Arregi, Aitor et al. 2018) and there is an urgent need to move to larger scale, continuous operation testing to prove up some of the concepts developed, particularly two-stage pyrolysis, and other options for process improvement.

1.3.5 A comparison between pyrolysis and gasification

A detailed study (Arregi, Aitor et al. 2018) of the alternatives of gasification or pyrolysis was undertaken which concluded that hydrogen production using steam gasification could produce 4g$_{H2}$/100g biomass without catalysis and 7g$_{H2}$/100g biomass with catalysts. The primary issues remaining to be addressed were assessed as reduction of tar content, optimising the catalyst, and reducing the energy requirements and material costs. This was compared to two step pyrolysis-reforming process considered to be capable of producing 5g$_{H2}$/100g biomass operating batch-wise, and twice that amount in continuous operation although there was no actual data to support this assertion. The remaining challenges in this case were scale up of the process, and optimising the catalyst.

Nevertheless, because of the greater promise of the pyrolysis route it has been selected as the thermochemical conversion process for this project.

1.4 Catalyst selection

1.4.1 The wide range of roles for iron as a catalyst

In recent times the drive for lower cost environmentally benign catalysts has seen a growing interest in the use of non-noble metal catalysts, and, in particular, iron based catalysts. Well recognised uses of iron catalyst have been in the Haber-Bosch process for ammonia synthesis, and the Fischer-Tropsch process for conversion of syngas into liquid hydrocarbons (Du et al. 2020). And while the latter process has traditionally used fossil fuel feedstocks it may be equally applied to biomass processing. Likewise long-established iron based coal liquefaction catalysts, limonite and hematite iron ore, have also been adopted for the catalytic reforming and cracking conversions of biomass feedstocks. More recent applications have included the use of iron or its compounds in biomass pretreatment, pyrolysis and gasification processing, and biomass liquefaction. Other uses for iron based catalysts are found in specific biomass processes directed towards transport fuels and chemical feedstocks.

The attractiveness of iron-based catalysts is driven by a number of special characteristics that set it apart, especially in commercial applications. Firstly, iron is the second most abundant element in the Earth's crust leading to a wide range of iron compounds being readily available and plentiful; secondly, iron's catalytic impacts are well understood, with many compounds easily prepared and some being usable directly; thirdly, the metal and many of its compounds are seen as being nontoxic from a human perspective as well as having very low environmental impacts; and, the magnetic properties provide one of the means of achieving efficient catalyst recycling. A number of researchers have investigated the use of iron based catalysts to develop gas yield increases and tar reduction strategies in biomass thermochemical processing. A study was conducted to examine the influence of iron granules on tar reduction during biomass gasification ((Nordgreen et al. 2012). That study reported tar reductions of over 50% and noted improved performance when the catalyst was in metallic state rather than the oxide. Another study investigated the use of both Ni and Fe catalysts, and were one of the early research groups to explore impregnation of the catalysts prior to pyrolysis or gasification (Bru et al. 2007)). Their results showed significant increases in gas yield with very large increases in hydrogen content. They noted the superior performance of Ni over Fe, but importantly, also recognised more toxic products were produced by the former. Haematite has been reported as being a versatile catalyst for steam gasification and pyrolysis increasing gas yields and reducing the tar levels substantially (Khelfa et al. 2009).

More broadly iron based catalysts find a role in both low temperature and high temperature Fischer-Tropsch processing, sometimes with alkalis added as promoters. In Japan there is now a national program focussed on developing iron based catalysts to replace catalysts using noble metals or other scarce materials (Kamitani 2021). Further afield, a recent article places strong emphasis on the role of iron catalysis in organic synthesis (Guethmundsson & Backvall 2020). The article notes the traditional role of noble transition metals like palladium, platinum and ruthenium as catalysts but toxicity and scarcity has focussed attention on developing more benign base metals in this role. Iron is seen as particularly good, not only because it is plentiful but also its other features: a wide redox potential range, and tuneable properties due to multiple oxidation states. They conclude with the observation that iron is used as a cornerstone in the chemistry of living processes.

1.4.2 Metallic catalyst choice for enhanced hydrogen production

Because there are a number of roles for catalysis in gasification the identification of the best combination of catalysts is not simple. Many alternative catalysts have been researched for the gasification role including Ni-based catalysts, alkaline metal oxides and aluminium and alumino-silicates. For the gasification process itself, olivine has been favoured but also dolomite, and nickel-based compounds have been used. A survey of catalysts used in steam gasification for hydrogen production (Arregi, Aitor et al. 2018) (mostly from bench scale tests) identified that olivine in the first stage with a nickel based secondary catalyst produced 14.5% H_2 (wt % biomass), and another using dolomite in conjunction a nickel based catalyst yielded 11.0% H_2 (wt % biomass) while replacing the secondary catalyst with a Ni-La-Fe catalyst provided 12.1% H_2 (wt % biomass). Given the elemental hydrogen content of the biomass (~5.5% wt% biomass) it may be deduced that between 50% and 70% of the hydrogen must have been sourced from the injected steam. These results were more than 20% higher than alternative tests reported, although both catalyst loadings and biomass sources varied. For the downstream reforming in WGS reactors Fe-Cr based catalysts are used. Some are better suited to improving gas composition whereas others are more effective in reducing impurities in the gas (Balat, M. 2008).

Results for pyrolysis combined with in-line reforming reported from the same survey indicated that almost universally some form of nickel-based catalyst was used for the reforming step, occasionally integrated with iron. The best result was a yield of 11.0% H_2 (wt % biomass) using a commercial nickel catalyst on an aluminium oxide support. Notably this is of the same order of that achieved by steam gasification. There have also been catalysts used in the primary pyrolysis reaction such as the impregnation of biomass with nickel salts prior to pyrolysis and subsequent gasification (Richardson et al. 2010). This was reported to have enhanced the hydrogen production and also reduced the tar production.

It has been amply demonstrated that the catalysis of biomass conversion reactions can be improved by using char as a carrier for metal catalysts (Guo, FQ et al. 2018; Kastner, Mani & Juneja 2015; Shen, YF, Chen, et al. 2015; Wang, Y et al. 2013). The choice of metal is largely driven by the proportionate improvement in performance against the cost and complexity of producing the catalyst. More recently, this choice has chiefly been nickel or iron (Li, H et al. 2017; Shen, YF, Zhao, et al. 2015), with a preference for iron due to its cost efficiency and its benign environmental character despite nickel providing higher hydrogen yields.

1.4.3 Bio-char as a catalyst for enhanced hydrogen production

It has been well recognised that char is an excellent catalyst (Abu El-Rub, Bramer & Brem 2004; Abu El-Rub, Bramer & Brem 2008; Guan et al. 2016; Qian et al. 2015; Xiong et al. 2017). Initially interest in bio-char as a catalyst was focused around its potential role in tar reduction during gasification (Abu El-Rub, Bramer & Brem 2004). However recognising that tar cracking was an important pathway to improved hydrogen yields interest in the role of bio-char grew substantially. Significant research was undertaken into various aspects of bio char including investigations to unravel the mechanism of catalytic cracking using model tars (Zhang, YL et al. 2014); the preparation of bio char as an adsorbent (Shen, Y 2015) ; and the preparation of bio char-supported catalysts (Shen, YF et al. 2014; Wang, Y et al. 2013; Yao, D et al. 2016; Zhang, S et al. 2015). This high level of interest in the potential roles of char in catalysis demonstrated that char had been recognised as a key element in catalytic systems for biomass pyrolysis and gasification. It has been established that both the process in which the char is formed and the original biomass influence its catalytic properties (Yao, D et al. 2016). While using char alone has been demonstrated to be an effective catalyst, particularly if AAEMs are present in the char, its use as a carrier for reactive metal catalysts has been shown to be superior (Yao, D et al. 2016).

Char-supported catalysts are attractive as char is a natural product of pyrolysis and gasification and meets several of the classic qualities of good catalyst support such as large surface area, desirable pore size, low cost and low environmental impact. One of the challenges is to better understand the potential for improving the specific properties of char and the development of new char metal catalyst matrices that further enhance catalytic performance (Li, Y et al. 2020). Another of the challenges is to find an improved method of impregnating the metal catalyst into the char. Methods of producing char-supported metal catalysts have been relatively complex. For char supported catalysts used in pyrolysis and gasification two general methods are used to attach the active catalyst to the support, precipitation and impregnation. Other methods have been developed (Cheng & Li 2018; Mohan, B., Park, J. C. & Park, K. H. 2016; Ralphs, Hardacre & James 2013; Xu et al. 2015) that offer promise of a simpler preparation for these catalysts. In particular, mechano-chemical synthesis has the potential to provide simpler techniques, with high reproducibility, with little or no added solvents. These catalysts generally have lower environmental impact yet provide similar or improved performance to other preparation methods. Mechano-chemical

catalyst preparation can be a simple two-step process in which the metal salt is dry mixed with the char support followed by calcination in an inert atmosphere (Figure 1.3).

As mechano-chemical preparation methods offer such advantages it has been selected as the preferred method of catalyst preparation for this project.

1.5 Significance of this Thesis

Hydrogen has long been recognised as a preferred energy source/carrier. More recently its relevance has increased as the move to decarbonise the world's energy sources gathers pace. Thermochemical biomass conversion processes, pyrolysis and gasification, offer potential routes for producing hydrogen, and hydrogen enriched syngas from renewable sources. Yet there remain numerous obstacles to be overcome before becoming commercially viable. These include the dispersed nature of the feedstock, relatively high capital cost of combustion and gasification equipment for large scale operations. Also, of concern are the high operating temperatures leading to thermal inefficiencies, and the use of relatively exotic catalyst systems to increase hydrogen recovery, many of which carry with them environmental concerns if widely adopted. While multi-stage gasification has done much to reduce costs and produce an acceptable fuel gas, much less has been achieved in respect of improving hydrogen yields (Thomson et al. 2020).

The efficient conversion of waste biomass to syngas and hydrogen using catalytic pyrolysis offers an advantageous approach for both sustainable waste management and the production of a critical clean energy source. If an effective catalyst can be developed that is simple to produce, low cost and recyclable then a form of the lower temperature pyrolysis process could challenge gasification processes as a preferred pathway for the primary gas products, syngas and hydrogen.

Enhancing the production of green hydrogen from biomass offers an exciting strategy for increasing the value of this renewable feedstock; more so, if it can be achieved through simple pyrolysis rather than gasification. Importantly, another product of the process, syngas, has established an essential renewables role not only as a chemical building block, and a source of liquid fuels but critically in the production of hydrogen itself. This may, in fact, become its dominant role if the world transforms to a hydrogen economy.

This thesis has therefore focused on developing catalyst systems (low temperature, environmentally benign, recyclable) and design (reactor layout, catalyst

flow) and operating principles (pyrolysis temperature) that improve the performance of low temperature pyrolysis processes to deliver lower capital and operating costs, improved hydrogen and syngas yield, and a sustainable catalyst system. This quest seeks to establish a basis for waste valorisation for a wide range of biomass that is currently not utilised, or simply combusted, through a process that seeks to be economical for both small- and large-scale operations. Waste valorisation is one of the key planks in improving the environment and increasing the level of sustainability in resource consumption, while hydrogen is seen as a key to resolving many of the energy issues associated with climate change. This work is a crucial step in realising these outcomes.

Solely using pyrolysis in either one- or two-stage processes reduces both capital and operating costs, ameliorating the importance of scale of operations as well as complex operating controls, and thereby encouraging the process to be adopted more widely. This outcome supports the application of the process in lesser developed economies and provides community benefits of a local circular economy that is directly supplying a usable energy source while reducing GHG emissions.

Therefore, the overall goal of this project is to increase hydrogen and syngas production from one- and two-stage pyrolysis, using a newly developed char-supported catalyst system that can be mixed with biomass feed and recovered and recycled at the completion of the process, or alternatively offering a char product suitable as a coke or coal substitute for the iron and steel industry.

1.6 Aims of this thesis

To realise the goals outlined for this research project the following aims were set:

1. Using TGA, and kinetic analysis, investigate the potential of a mechano-chemically prepared catalyst, compare it to a traditionally prepared catalyst, in a biomass pyrolysis process, over a range of pyrolysis temperatures.
2. Using a laboratory fixed bed single-stage reactor understand the changes in production of char, liquids and product gas, and the component composition of product gas, particularly hydrogen; and tars, for arrange of catalyst loadings and pyrolysis temperatures during biomass pyrolysis using a mechano-chemically prepared catalyst.
3. Investigate and compare the above outcomes for at least two biomass sources.

4. Investigate and compare the above outcomes using alternative, lower cost resources and reduced processing in the production of the catalyst system.
5. Investigate and compare the above outcomes when operating a two-stage fixed bed pyrolysis system.

1.7 Outline of thesis

This thesis is prepared in a “thesis by publication” format. It comprises of 6 chapters. Chapters 2-5 are papers prepared for submission to journals pending the outcome of an assessment of patent application in respect of potentially novel developments arising from this work.

Chapter 1 provides some background to the opportunity for biomass to have a significant role in the future production of hydrogen. It briefly examines the two key thermochemical processes of gasification and pyrolysis, outlining for these processes the current preferred methods for producing hydrogen, as well as their limitations. There is a broad review of catalysts used to enhance hydrogen production and the role of bio-char as a catalyst and as catalyst support in these processes. The relevance and aims of the thesis are also outlined.

In Chapter 2, the preparation of a char supported iron catalyst, prepared by a mechano-chemical method is described and its use in the catalytic pyrolysis of almond residues (AR) investigated using a thermo-gravimetric analyser. The catalytic impact on char yields, the temperatures of the onset of mass loss, peak rates of mass loss, overall mass loss as well as reaction kinetics are presented for a range of pyrolysis temperatures (450 – 750°C) and catalyst loadings (1.6%Fe – 5.0%Fe). The aim of this chapter is to demonstrate that the newly developed catalyst is effective in positively influencing the outcomes of catalytic pyrolysis in terms of reaction kinetics and the products of pyrolysis; and further that it has additional benefits of simpler preparation and reduced resource use compared with traditionally prepared catalysts.

Chapter 3 investigates the catalytic performance of the mechano-chemically prepared catalyst in greater detail using a laboratory single-stage packed bed pyrolysis unit. Both catalysed almond residue (AR) and pine chips (PC) are pyrolysed at a range of peak temperatures (600°C - 750°C) at three different catalyst loadings (1.6%Fe, 2.9%Fe and 5.0%Fe). The produced gas has the pyrolysis liquids removed, then a slip stream is removed for component analysis in a microGC, with the produced gas volume being measured and recorded. Residual char is recovered, and the tars recovered from the produced liquids for quantitative assessment and analysis with GC-

MS. The aim of this chapter is to better understand how the production of char, liquids and product gas change, and the component composition of gases, particularly hydrogen; and tars, change with catalyst loading and pyrolysis temperature.

In Chapter 4 alternative sources of iron for incorporation in the mechano-chemically prepared catalyst are investigated to determine whether commercially available iron ore (CIO) or waste iron ore tailings (IOT) could effectively replace laboratory prepared ferric nitrate (LFN) as sources of iron. This is an important step in establishing a catalyst system that incorporates the valorisation of a waste product without reducing its effectiveness. Each iron source requires individual preparation techniques to prepare it for ball milling with the char carrier. A suite of experiments similar to those described in Chapter 3 is conducted with each of the catalysts. The performance of each of the catalysts is compared, with particular emphasis on the quantity of hydrogen produced in gas product stream, the overall product composition and changes in tar production and composition.

Chapter 5 introduces the concept of two-stage pyrolysis as a means for further enhancing hydrogen production from biomass. While this process concept is not novel of itself the way this experimental work is conducted offers a different approach to the traditional post pyrolysis reforming process. In addition to the fixed bed catalytic pyrolysis sample, described in Chapter 3, a bed of recovered catalytic pyrolysis char was placed downstream to provide second stage treatment of the primary pyrolysis products. The whole process is conducted at the same peak temperature mirroring a constant temperature moving bed pyrolyser. The same sampling and analysis procedures are conducted as described in Chapter 3. Experiments using both the laboratory-based catalyst system (LFN) and the catalyst system using a waste product (IOT) are carried out. The outcomes of the two-stage pyrolysis are compared with single stage pyrolysis and the implications of this development discussed.

Chapter 6 presents a summary of the key findings of this thesis and outlines the potential for pyrolysis only processes to provide an effective, efficient production method for green hydrogen and contribute towards the global challenges of delivering waste valorisation and energy decarbonisation. Recommendations for future work are also discussed.

Chapter 2: Catalytic pyrolysis of almond residues with mechano-chemically prepared char supported iron catalyst: A kinetic study

Richard Thomson[a], Philip Kwong[b,*]

School of Chemical Engineering and Advanced Materials,

Postal Address. The University of Adelaide South Australia 5005 AUSTRALIA

[a] richard.thomson@adelaide.edu.au; ORCID: 0000-0003-2304-8261

[b],* Author for correspondence

P: +618 8313 0724 E:philip.kwong@adelaide.edu.au

Statement of Authorship

Title of Paper	Mechano-chemically prepared char supported iron catalyst for catalytic pyrolysis of almond residues – a kinetic study
Publication Status	☐ Published ☐ Accepted for Publication ☐ Submitted for Publication ☑ Unpublished and Unsubmitted w ork w ritten in manuscript style
Publication Details	

Principal Author

Name of Principal Author (Candidate)	Richard Thomson		
Contribution to the Paper	Design of experimental work and methodology; performance of experiments and interpretation of results. Responsible for drafting the paper and revision in preparation for publication		
Overall percentage (%)	70%		
Certification:	This paper reports on original research I conducted during the period of my Higher Degree by Research candidature and is not subject to any obligations or contractual agreements with a third party that would constrain its inclusion in this thesis. I am the primary author of this paper.		
Signature		Date	20 Apr 2022

Co-Author Contributions

By signing the Statement of Authorship, each author certifies that:

i. the candidate's stated contribution to the publication is accurate (as detailed above);

ii. permission is granted for the candidate in include the publication in the thesis; and

iii. the sum of all co-author contributions is equal to 100% less the candidate's stated contribution.

Name of Co-Author	Philip Kwong		
Contribution to the Paper	Corresponding author. Provided original idea of the study. Reviewed experimental design and methodology. Major contributor to the critical analysis of results and to writing and revision of the paper.		
Signature		Date	20/4/2022

Name of Co-Author			
Contribution to the Paper			
Signature		Date	

Please cut and paste additional co-author panels here as required.

ABSTRACT

A new type of char supported iron catalyst, prepared by a mechano-chemical method, for the catalytic pyrolysis of almond residues was investigated. The catalytic performance and reaction kinetics were evaluated using thermo-gravimetric analyser over a range of pyrolysis temperatures (450 – 750°C). Pyrolysis at 750°C gave char yields of baseline biomass of 32.7%, whereas in chars containing supported iron catalyst, normalised char yields were reduced to 29.3%, 26.7% and 25.5% with catalyst iron loading of 2%, 4% and 6%, respectively. Deconvolution of DTG data showed the major ligno-cellulose components responded to the char supported iron catalyst, lowering the onset decomposition temperature, reducing the temperature at which peak rates were achieved while developing up to 40% higher decomposition rates. Total mass loss for hemi-cellulose and cellulose increased by 20% and for lignin by over 100%. Kinetic analysis also revealed that for almond residue pyrolysed with char supported catalyst at 6% iron loading, the required apparent activation energy reduced from 103 to 82 kJ/mol, 40 to 30kJ/mol and from 10 to 8 kJ/mol during the decomposition of hemicellulose, cellulose and lignin, respectively. The mechano-chemically prepared catalyst was demonstrated to create lower apparent activation energies in more highly catalysed settings and offers simpler preparation with minimum resource requirements compared to the catalyst prepared by incipient wetness impregnation method.

Key words: thermogravimetry, biomass, catalysis, pyrolysis, kinetics, iron

DECLARATIONS

Funding: The authors did not receive support from any organisation for the submitted work.

Conflicts of interest: The authors have no conflicts of interest to declare that are relevant to the content of this article.

Availability of data: If requested additional data associated with this research project can be accessed by contacting the authors.

Code availability: Not applicable

2.1 Introduction

The use of catalysts in biomass gasification has been investigated over many years and a very large volume of work has developed around different approaches to thermal and catalytic cracking systems to promote tar destruction (Anis & Zainal 2011). The aim of the catalysts is largely directed at reducing tars in the product gas as this can have a major influence on the downstream processing requirements and the complexity of gas clean-up (Anis & Zainal 2011; Woolcock & Brown 2013). A wide range of catalysts including dolomites, transition metals, alkali metals and noble metals have been investigated for tar removal. Transition metal catalysts have shown relatively good performance in tar reduction. Often such catalyst systems are complex, and the catalysts are expensive. Other approaches have focused on tar minimisation in the gasifier by manipulation of the various parameters. None of these approaches has been universally successful and a continuing area of investigation is the use of catalysts, in particular, to modify the products of the process; with a focus on tar reduction and elimination, in both the pyrolysis and gasification stage (Al-Rahbi, Onwudili & Williams 2016; Park, HJ et al. 2010; Park, J, Lee & Ryu 2016; Qian & Kumar 2017). Generally, the effectiveness of catalysts has been variable, their preparation complex, their supports expensive, and regeneration difficult or uneconomical.

For some time researchers have sought an alternative and developed catalysts based on biomass char and also char as a support for metallic catalysts (Cao, Sun & Sun 2017; Klinghoffer, Castaldi & Nzihou 2012; Shen, Y 2015). Despite the variability in the properties of char due to the biomass source and process conditions, the attractiveness of its availability, and its role as a reactant in gasification has led to it being a preferred catalyst support. Char has been recognised as having catalytic properties (Abu El-Rub, Bramer & Brem 2008; Xiong et al. 2017), but performance can be further improved using char as a carrier for metal catalysts (Guo, FQ et al. 2018; Kastner, Mani & Juneja 2015; Shen, YF, Chen, et al. 2015; Wang, Y et al. 2013). The choice of metal is largely driven by the proportionate improvement in performance against the cost and complexity of producing the catalyst. More recently, this choice has narrowed to

nickel or iron (Shen, YF, Zhao, et al. 2015), with iron being preferred on a cost basis and because of its benign environmental character.

Two general methods have been used to attach the active catalyst to the support, precipitation (for loadings >20%) and impregnation for lower loadings (Shen, YF, Zhao, et al. 2015; Wang, Y et al. 2013). The precipitation method uses two steps to interact the precipitate and the support. Impregnation is a three-step process, steeping the catalyst support in the solution, removing excess solution by drying the support and then calcination or reduction to activate the catalyst. Methods of producing bio-char or char-supported metal catalysts have been relatively complex with pre-treatment of the bio-char by boiling with a mineral acid, followed water washes, and then drying.

Over the last decade there has been the emergence of many mechano-chemical catalyst preparation methods which have been discussed in detail (Ralphs, Hardacre & James 2013). These methods, it is argued, provide potentially more sustainable routes for catalyst preparation, particularly avoiding the use of solvents. Within the general description of mechano-chemical catalyst preparation there are numerous different methodologies. A comprehensive summary has been published of the various methods of synthesising nanomaterials for catalytic application and the mechanisms involved utilising a dry milling method for creating char supported iron catalysts (Xu et al. 2015).

Mechano-chemical catalyst preparation can be a simple two-step process with the metal salt being dry mixed with the char support followed by calcination in an inert atmosphere. So, the recent increased focus on mechano-chemical methods reflects the same objectives as are being sought in this project, and supports its selection delivering simple preparation, relatively low cost, scalable and reproducible catalyst outcomes, with low environmental impact.

The study of catalytic pyrolysis has been limited but several researchers have investigated the use of metal catalysts during pyrolysis. The use of a nickel salt introduced with the biomass at the pyrolysis stage as been explored, achieving high conversion of aromatic hydrocarbon molecules and limited tar production during pyrolysis (Richardson et al. 2013). Using a char supported iron catalyst it was found that a char supported catalyst with 20% Fe loading, produced by incipient wetness impregnation method, could reduce producer gas

tar content to below 100mg/Nm^3 (Malek, Asadullah & Sauki 2015) . Both nickel and iron, and combinations, have been investigated (Shen, YF, Zhao, et al. 2015), who reported both the tar yield and CO_2 concentration were improved because the metal oxides, through in-situ thermal reduction, were transformed to metallic states.

The objective of this paper is to examine the effect of mechano-chemically prepared catalysts on the pyrolysis of samples of almond residue, at peak pyrolysis temperatures (PPT) ranging from 450°C to 750°C, using a thermogravimetric analyser. The work investigates the reaction kinetics, char yield and the decomposition of biomass components; assesses the impact of iron catalyst loading, and compares the relative performance of alternate catalyst preparation methods. The impact of catalysis on gas composition was not possible as no equipment was available to allow contemporaneous gas analysis.

2.2 Experimental

2.2.1 Materials

2.2.1.1 Biomass

Almond residue was sourced from a local almond processing mill (Laragon Pty Ltd, Renmark, South Australia). Biomass was prepared by drying at 105°C for 6 hours, grinding in a DeLonghi DEDICA coffee grinder, and sieving material to <500µm for experimentation. The prepared material was allowed to re-absorb moisture from the atmosphere prior to pyrolysis.

2.2.1.2 Catalyst support

Prepared biomass was pyrolysed to produce char as the support for the catalyst. Weighed quantities of biomass were pyrolysed in a ceramic boat, located in a horizontal tubular furnace (60mm diameter and 650mm long) for 30 minutes at peak pyrolysis temperatures (PPT) of 450°C, 550°C, 650°C and 750°C, using a heating rate of approximately 50°C per minute, in a nitrogen atmosphere. The samples were cooled to ambient temperature and the yield of char recorded. The chars were then ground to <200µm prior to loading with catalyst.

2.2.2 Catalyst preparation

Two methods of catalyst preparation were used so that the relative effectiveness of mechano-chemically prepared catalyst could be compared to the incipient wetness impregnation method. Iron nitrate was selected as an appropriate salt from which to produce both catalysts as it dissociates fully to ferric oxide (Fe_2O_3) at temperatures below 250°C (Melnikov et al. 2013). All char supported catalyst was prepared at 11.6% Fe (wt./wt.) basis and different ratios of the char supported catalyst used to make biomass/catalyst mixtures with different catalyst loadings.

2.2.2.1 Mechano-chemically prepared catalyst

The general procedure for preparing the catalyst was to mix equal weights of $Fe(NO_3)_3.9H_2O$ (Chem-Supply (Australia), AR grade: 98.0% minimum assay) solution and char (produced at one of the selected PPTs). This mixture was then heat treated at 350°C for 2 hours in nitrogen atmosphere to thermally decompose iron nitrate to ferric oxide (Fe_2O_3). The calcined product was then milled in a ball mill (Fritsch *Pulverisette 7* planetary mill) using 50g of 3mm zirconia balls with 6g catalyst, at 700 rpm for 120 minutes. This was repeated for chars produced at each of the selected PPTs to produce the range of char supported catalyst samples to be used to mix with biomass for subsequent pyrolysis.

2.2.2.2 Incipient Wetness Impregnation prepared catalyst

The general procedure was to prepare a 0.84mol/L solution using the same $Fe(NO_3)_3.9H_2O$ as used for mechano-chemical catalyst preparation. The mass of water required to saturate 1g char was determined, and the equivalent volume of solution and water was added to char (produced at one of the selected PPT) to produce mixtures having a Fe loading of 11.6% (wt./wt.). The mixtures were calcined in a nitrogen atmosphere for 2 hours at 350°C and homogenised in a ball mill (Fritsch *Pulverisette 23* vibrating mill) for 10 minutes at 25cps, using a single 1mm zirconia ball with 6g catalyst.

A selection of the catalyst samples was analysed for particle size distribution (Malvern Mastersizer 2000 particle size analyser). In each case 0.5g of char supported catalyst was placed in 20ml water and agitated for 2 hours prior to adding to the circulating water in the analyser. Sufficient of the sample was added

to meet the obscuration range for the analysis. Calcined samples of the prepared catalysts, in powder form, were placed directly on sample plates for XRD (Rigaku Miniflex 600), scanning from 3-80°, at 10°/min. The resultant scans confirmed the catalyst was in the form of ferric oxide (Fe_2O_3).

2.2.3 Thermogravimetric analysis (TGA)

An experimental matrix was developed to examine, during pyrolysis, the effect of PPTs (450, 550, 650 and 750°C), the effect of catalyst loading, using 3 levels of loading on biomass, and the effect of catalyst preparation, using 2 methods of catalyst preparation.

Biomass was prepared as described in Section 2.2.1.1. Samples for TGA were prepared by adding one of three aliquots of catalyst to 0.5g of biomass, and mixing, by agitating in a ball mill (Fritsch *Pulverisette 23)* for 10 minutes at 25cps, using a single 1mm ball. “Baseline” samples consisted solely of biomass, and “Char” samples consisted of biomass with only char support added. The nomenclature for samples is shown in Table: 2.1 including that for a series of samples prepared for each of the PPTs using the incipient wetness impregnation method. In each case the char carrier was manufactured at the same PPT for which it was to be used in subsequent catalytic biomass pyrolysis.

Additionally almond residue samples were prepared for pyrolysis with char carrier only, at 10% and 50wt% without catalyst. These were used to identify whether there was any significant catalytic impact of the char alone.

Thermal analysis was undertaken using a Mettler Toledo TGA/DSC2. Each sample was heated from room temperature at 15°C/minute, using nitrogen as carrier gas (50mL/min), to 105°C, then held for 10 minutes, after which heating continued to the PPT of either 450°C, 550°C, 650°C or 750°C which was maintained for 30 minutes. The carrier gas was then switched to oxygen to oxidise the sample over a period of 30 minutes.

The reported Normalised char yields have been calculated on the basis that both the char carrier and char produced during pyrolysis can participate in the pyrolysis reactions.

2.2.4 Kinetic modelling of the catalytic pyrolysis process

For this work a classical non-isothermal model was used to analyse the data to determine apparent activation energies, E_A (kJ/mol), and the pre-exponential coefficient A (min^{-1}) for both the catalysed and the baseline pyrolysis samples.

Using the equations below together with TGA data, the reaction rate constants can be determined:

$$\frac{dX(t)}{dt} = k \quad (1)$$

With the pyrolysis conversion being expressed as

$$X = (\mathrm{m} - m_f)/(m_0 - m_f) \quad (2)$$

Where m_0 is the initial weight of dry biomass, m is the weight at time t (excluding char support and catalyst), and m_f is the weight at end of pyrolysis (excluding char support and catalyst).

This approach is based upon a first order rate equation being appropriate for the pyrolysis processes being represented as outlined in Equation (3), and is suitable where a single heating rate has been used. Nevertheless, it is recognised that many factors can influence the estimates including sample heterogeneity and heat and mass transfer limitations within these heterogeneous reactions (Babu 2008).

$$Biomass \rightarrow Volatiles + Char \quad (3)$$

Under this approach the Arrhenius equation is used to determine the rate of reaction in a similar manner to others (Fiori et al. 2012; Mallick et al. 2018) and described by:

$$dx/dt = A \times \exp(-\frac{E}{RT})(1 - x) \quad (4)$$

where A (min^{-1}) is the pre-exponential constant, E ($kJmol^{-1}$) is the activation energy, T (°K) is the reaction temperature, R ($kJ.mol^{-1}.K^{-1}$)is the universal gas constant and x is the fractional conversion.

2.3 Results and Discussion

2.3.1 Characterisation of biomass, catalysts, and char

2.3.1.1 Biomass

The characteristics of the almond residue feedstock are shown in Table 2.2. The high volatile content of the proximate analysis indicates that significant gaseous production may be expected on pyrolysis and gasification. There will be a reduced char yield consistent with the low fixed carbon and ash contents. The proximate analysis is typical of those reported for almond shells whereas almond husks show higher ash (6%) and consequently lower fixed carbon.

The ligno-cellulosic component composition of almond residue has been estimated from the deconvoluted DTG graphical analysis for the baseline biomass pyrolysed at each of the PPT. The compositional analysis is broadly consistent with that found by other researchers (Li, X et al. 2018) who reported 28.8%, 38.5% and 29.5% for hemi-cellulose, cellulose, and lignin fractions respectively.

2.3.1.2 Chars and char support

Initially a char yield (Char yield; catalyst mass constant) was calculated by reducing the mass of residue by the mass of char supported catalyst added to the biomass as if neither the char carrier nor the iron catalyst participated in the pyrolysis process. The reported Normalised Char Yield is based on recognising that the char carrier had been produced from virgin biomass, and not exposed to a catalytic environment. Thus, it could participate in the catalytic pyrolysis in the same manner as char being formed from the degradation of the biomass. In the normalised char yield calculation both the char formed from the biomass and the char carrier were assumed to have participated equally in catalytic degradation reactions that led to the lower residues than that of baseline pyrolysis samples (Table: 2.3).

The iron oxide catalyst mass used to calculate the char component of the residue was the same at the beginning and end when samples were weighed, having returned to its original state post pyrolysis, even if there was catalyst reduction during the pyrolysis process.

The char yields of baseline samples reduced as the PPT increased trending to a minimum char yield at 750°C, and catalysed char yields further decreased, largely proportionate to catalyst loadings. Normalised char yield reductions for the highest catalyst loadings were 32%, 17%, 9% and 15% for 750, 650, 550 and 450 samples, respectively. The elemental analysis (Table: 2.4) shows that chars produced above 550°C have higher carbon contents and this is consistent with reported results (Klinghoffer, Castaldi & Nzihou 2012), who also observed such chars exhibit more porous structures, providing much greater surface areas for the encapsulation of catalytic species.

2.3.1.3 Catalyst

The particle size distributions of catalyst produced with and without ball milling are shown in Figure: 2.1, (each being the average of 3 measurements). The average volume based mean particle sizes were 1.50μm and 27.22μm respectively, and the specific area estimation was 5.2m^2/g and 0.40m^2/g, respectively. The ball milling had reduced the mean particle size by a factor of approximately 18, but more importantly, increased the specific surface area (calculated using the material density and Sauter diameter) available by a factor of approximately 13. This difference in available surface is one of the keys to the relatively higher catalytic impacts observed during pyrolysis.

2.3.2 Mass loss of almond residue, with and without catalyst

Figure 2.2 a) indicated that the mass loss patterns of all three of the baseline biomass samples (750-B, 750-010 and 750-050) were very similar and confirmed that the impact of char carrier alone was minimal. While the mass loss patterns of the three catalysed samples- 750-2, 750-4, 750-6 were of similar form, the mass loss was greater as the catalyst loading increased. The difference in mass loss is evident early in Stage 1, at around 200°C indicating that the catalyst is influencing the reaction from the very early stages of decomposition. The measured mass loss increases significantly above approximately 670°C (illustrated by 750-6 non-normalised) and this is attributed to decomposition of Fe_2O_3 to metallic iron together with surface reactions between the char and released oxygen (Zieliński et al. 2010).

2.3.3 Effect of catalyst on the decomposition of biomass components

DTG analysis in Figure 2.2 b) shows the stages of the rate of mass loss during the decomposition of the biomass components. Six distinct decomposition stages were identified during the pyrolysis for catalysed samples at PPTs greater than 650°C, while only five stages were identified for baseline samples and catalysed samples with PPTs below 600°C.

Stage 1 and 2 are attributed to largely hemi-cellulose degradation with some contribution from cellulose. Stage 3 is considered to be predominantly cellulose degradation while Stage 4 and 5 are attributed largely to decomposition of lignin (Pecha et al. 2019) (Figure 2.3 a)). Stage 6 commences when the temperature of catalysed samples approached 680°C, and was marked by further significant mass loss and an intense endothermic stage followed by exothermic activity. This event was not observed in the baseline sample, and is attributed in part to the reduction of the iron oxide to metallic iron (Pineau, Kanari & Gaballah 2006) (Figure 2.2 b)).

In Stage 1 (125-230°C) the maximum decomposition rate was 0.079 mg/sec.g for sample 750-6 (6% Fe loading) which was 10% higher than the baseline sample (0.072 mg/sec.g). The maximum decomposition rate for the intermediate catalysed samples increased with increasing iron loading. For Stage 2 (230-280°C) maximum decomposition rates were 0.074, 0.085 and 0.100 mg/sec.g for the catalysed samples 750-2, 750-4, 750-6 respectively being 10%, 27% and 49% higher than the baseline sample.

Stage 3 (280-340°C) showed a different response with the catalysed samples and baseline sample having essentially the same maximum decomposition rate of 0.110 mg/sec.g. which was the highest rate recorded of all stages. It is this stage during which the major component undergoing decomposition is considered to be cellulose (Yang, HP et al. 2007).

Stage 4 (340-550°C) is a period of lignin decomposition (Yang, HP et al. 2007) , and again reflected the effect of catalyst with maximum decomposition rates of 0.023, 0.026 and 0.030 mg/sec.g for the catalysed samples 750-2, 750-4, 750-6 respectively being 5%, 18% and 36% higher than the baseline sample. Stage 5 (550-735°C) is similarly a period of lignin decomposition but with the

lowest peak rates of 0.007, 0.008, and 0.011 mg/sec.g for the catalysed samples 750-2, 750-4, 750-6 respectively being 75%, 100% and 175% higher than the baseline sample.

Stage 6 is not observed in baseline samples, but the catalysed samples had maximum decomposition rates of 0.012, 0.043 and 0.066 mg/sec.g, reflecting catalyst loading.

Table: 2.5 records the onset, final temperatures, and peak temperature in each reaction stage. Extrapolated onset temperature (T_o) has been defined as the point of intersection of the starting-mass baseline and the tangent to the TGA curve at the point of maximum gradient; and the final temperature (T_f) has been defined as the temperature at which 98% of the total mass loss has occurred. Stage temperatures (T_{pn}) have been defined as those temperatures at which the decomposition rate on the DTG curves reaches a local maximum. It was found that the baseline sample has the highest onset temperature (T_o) and the lowest final temperature (T_f) whereas the reverse is observed for the sample with the highest catalyst loading where the onset temperature has reduced by 10°C and the final temperature increased by almost 50°C. This represents a significant change and together with the data in (Figure 2.2 b), it is evident that the catalyst is effective in promoting an earlier commencement of the reaction as well as extending the reaction and is consistent with the extended lignin reaction and reduced char yields observed. The trend of the peak stage temperatures (T_{p1}-T_{p6}) mirrors that of the onset temperatures, with occurrence of peaks being at lower temperatures as the catalyst loading increases.

In Stage 1 these reductions were minor only being around 3°C but become more significant in Stage 2 when the reduction was greater than 10°C in peak temperature. A similar reduction is noted in Stage 3 even though the effect of the catalyst on maximum degradation rates in this stage were negligible. In Stages 4 and 5, it has been noted that the catalyst had major impacts on the maximum degradation rates, and the reductions in peak temperatures reinforce the degree to which the catalyst is influencing the process. It should be noted that Stage 6 represents the dissociation of the catalyst.

2.3.4 Decomposition of the components: hemicellulose, cellulose and lignin

The degradation process has also been examined using deconvoluted curve analysis of the DTG data as depicted in Figure 2.3 a), with each of the stages identified in Figure 2.2b) now being seen to correspond with specific decomposition zones (Figure 2.3 a). Stage 1 almost solely encompasses the first stage decomposition of hemicellulose, with some overlap of initial portion of the second stage hemicellulose decomposition which predominantly occurs in Stage 2. This is accompanied by the commencement of the cellulose decomposition which starts around 230°C (almost at the beginning of stage 2) and continues through its peak decomposition rate almost to completion in Stage 3. These are the zones reflecting periods of dehydration, and fragmentation and secondary reactions over the temperature zone from 200°C to 400°C.

Like hemi-cellulose lignin has been interpreted as a two-stage decomposition commencing from as low as 150°C and certainly from 200°C (Yang, HP et al. 2007). Stage 4 includes the last of the cellulose reaction, but is dominated by lignin decomposition. The peak degradation is observed at around 400-420°C with this stage extending to 550°C. The next stage extends to the end of the pyrolysis process at 750°C and is almost exclusively the second stage of lignin decomposition producing a peak decomposition rate at approximately 630°C. These observations are consistent with studies carried out on single components of biomass, with lignin decomposition being demonstrated to occur over a wide temperature range including at the lower temperatures when the cellulosic components are decomposing (Kok & Ozgur 2017; Stefanidis et al. 2014). The second stage reaction of lignin is likely to be associated largely with the char formation reactions.

Figure: 2.3 b) allows a more detailed examination of the differences created by catalysis in the component decomposition. In the first of the hemi-cellulose decomposition reactions the relative mass decomposed by the catalytic reaction (area contained by the curve) is 20% greater, the peak rate of degradation is 7% greater and occurs at both a lower temperature and earlier. In the Stage 2, the continuation of hemicellulose decomposition, the impact of the catalyst increases

with the relative mass decomposed by the catalytic reaction being 23% greater, the peak rate of degradation 42% greater and occurs 10°C lower and 35s earlier.

In Stage 3, where a significant proportion of the cellulose was decomposed, the maximum degradation rates recorded in the DTG raw data for this stage were the same for catalysed and baseline samples, suggesting that the catalyst had little effect on cellulose. However, the deconvoluted data supports the proposition that the catalyst impacts on each component as the relative mass of cellulose decomposed by the catalytic reaction was 23% greater, the peak rate of degradation being 42% greater and the peak occurring 10°C lower, and earlier, than the baseline sample.

Stage 4 represents largely the remaining degradation of the first lignin stage and the small residual cellulose decomposition. The relative mass of lignin decomposed in the catalysed sample was 14% greater than the baseline sample, and the peak rate of decomposition 31% higher, but the peaks occurred at essentially the same temperature.

Stage 5 represents the second stage of lignin decomposition, and the impact of catalyst is quite pronounced with the relative mass decomposed being 260% greater and the peak rate of decomposition 130% greater than that of the baseline sample.

2.3.5 The influence of catalysts on reaction kinetics

Figure: 2.4 shows the first order reactions identified during the pyrolysis of almond residues. Four major reaction zones, closely aligned with the temperature ranges of the first four stages of decomposition identified in the analysis of the DTG data were identified from the kinetic analysis. These reactions are first order, with high linear correlation coefficients. The effects of peak pyrolysis temperatures, catalyst loading, and catalyst preparation methods can be examined using this kinetic data.

2.3.6 The effect of catalyst loading on apparent activation energy (AAE)

Figure: 2.5 shows that for Reaction 1 (130°C to 205°C) the apparent activation energy (AAE) for baseline samples was approximately 105 kJ/mol.

Samples catalysed with 6%Fe show a reduction in AAE, being 83 kJ/mol for 450 PPT, 76 kJ/mol at 550 PPT and 73 kJ/mol at 650°C PPT, representing reductions of 21%, 28% and 29% respectively. At 750 PPT the AAE was 82 kJ/mol giving a reduction in AAE of only 22% and not mirroring the previous pattern of reduction. Nevertheless, these significant reductions confirm the iron catalyst is influencing the decomposition of hemi-cellulose from the outset of the pyrolysis process.

In Reaction 2 (215°C-270°C), which represent further hemi-cellulose and minor cellulose decomposition, the baseline samples had an AAE of approximately 28 kJ/mol and the catalyst had little positive effect on the AAE. The 6%Fe loaded samples recorded 31, 28, 27, and 33 kJ/mol at each of the PPT from 450-750°C respectively.

Reaction 3 (270°C -335°C) where cellulose decomposition dominates, the baseline sample had AAEs of approximately 40 kJ/mol and reflected a similar pattern to Reaction 1, with 6%Fe loaded samples having AAEs of 32, 33, and 30 kJ/mol, or a 20% reduction at each of the PPT from 450-650°C respectively, while at 750 PPT the AAE was 26 kJ/mol giving a 35% reduction.

Reaction 4 (345°C - 485°C),where decomposition is predominantly lignin, had uncatalyzed samples with AAEs of approximately 10 kJ/mol. The samples loaded with 6%Fe had AAEs of 9, 5, and 8 kJ/mol for 550, 650 and 750°C samples respectively representing reductions in AAEs of 10%, 50% and 20% while at 450 PPT the AAE was 12 kJ/mol, 20% higher than the baseline samples.

AAEs for samples with intermediate catalyst loadings of 2%Fe and 4%Fe, for all PPT, lay between that of the baseline sample and the sample with 6%Fe loading, and were consistent with the catalyst loading.

2.3.7 The effect of char support production temperature on AAE

It is apparent from Figure:2.5 that there is a relatively consistent pattern within the individual reaction results whereby for catalysed samples the greatest improvement in AAE is not achieved at the highest PPT (750°C) but rather at 650°C. Further, there is a trend suggesting the next best performance may be at PPT 550°C with PPTs of 450°C and 750°C providing the lowest level of improvement. This is considered to be an artefact of the catalyst support, and the temperature at which it has been produced and the different physical

characteristics that are developed. This is consistent with the results reported that the maximum surface area developed by chars is frequently in the pyrolysis temperature range of 600-700°C (Chatterjee et al. 2020).

2.3.8 The effect of preparation method

Figure: 2.5 also provides the AAEs for samples with catalyst loadings of 6% Fe prepared by the conventional incipient wetness impregnation method (450-6-IWI to 750-6-IWI). Reaction 1 shows the AAEs of this catalyst were consistently higher than that of the mechano-chemically prepared catalyst by between 5-10%. In Reaction 2, where catalytic influence appears low as observed in Section 2.3.4, the samples prepared by either method generally reflect similar AAEs. This is also the situation in Reaction 3 where the only substantive difference is observed with the samples with the highest PPT (reduced by 21%). In Reaction 4 the mechano-chemically prepared catalyst reduced AAEs by 8%, 26%, 12% and 11% as PPTs increased. This difference in performance of the catalysts is attributed to the smaller particle size of the ball milled catalyst providing a larger surface area for the catalytic activity to occur but the effect was masked when catalyst effectiveness was generally weak.

The activation energies determined in this work are within the range reported by others for baseline reactions. A comprehensive review of activation energy assessments for various nutshells using a range of models has been presented (White, Catallo & Legendre 2011). For almond residue it was reported that for single step first order reactions values of 42, 93 and 100 kJ/mol, and significantly higher values of 120-250 kJ/mol using alternative models. Other researchers reported values of 80-95 kJ/mol for hazelnut shells, depending on the model (Kok & Ozgur 2017); while interestingly, using a first order model, values of 38 kJ/mol (210-330°C) and 14 kJ/mol (330-530°C) were determined for non-catalysed palm oil decanter cake pyrolysis (Dewayanto, Isha & Nordin 2014); values that closely approximate those of Reaction 2 (215°C-270°C) and Reaction 4 (345°C - 485°C) in this work (Figure: 2.5). Impregnating catalysts into biomass prior to pyrolysis has been investigated, (Bru et al. 2007) with increasing gas yields at the cost of liquid yield being reported, as well as both H_2 and CO_2 production being increased. In a similar study (Collard et al. 2012), found that iron catalysed both dehydration and decarboxylation reactions that encouraged char

production and supressed depolymerisation of cellulose. These observation are consistent with AAEs determined in the various reaction zones, with depolymerisation of hemi-cellulose and cellulose occurring in the temperature range of Reaction 2 (little catalytic influence) while dehydration reactions are occurring in the temperature ranges of Reactions 1 and 3. It was also reported that iron favoured rearrangement of the aromatic rings in lignin, which would be expected to occur in Reaction 4 (reduced AAEs) and contributed to a reduction of aromatics in the tar.

2.4 Conclusions

This study has demonstrated the successful application of a char supported iron (2%-6% Fe) catalyst, prepared by a mechano-chemical method. Catalytic pyrolysis of almond residue has produced reductions in normalised char yields, from 37.6% (baseline) to 31.9% (6%Fe) at 450°C and from 32.7% (baseline) to 25.5% (6%Fe) at 750°C. Overall the responses to the catalyst were proportional to the catalyst loading.

Catalytic activity is observed from the onset of pyrolysis with five distinct decomposition stages identified. In all except Stage 3 (280-340°C), catalysed samples had higher rates of decomposition, by 15% to over 100% as iron loading in the catalyst increased.

The progress of ligno-cellulose component decomposition was revealed using deconvolution of DTG data. Catalysed samples (6% Fe) had mass losses greater than baseline samples by 20% and 23% for the two hemicellulose stages, 23% for the cellulose stage and 14% and 260% for each of the lignin stages.

This analysis was supported by kinetic analysis which identified first order reactions showing samples with 6% Fe loading reducing AAEs from approximately 105 to 80kJ/mol during the first stage of hemi-cellulose degradation, from 40 to 30 kJ/mol during the cellulose decomposition and from 10 to 8kJ/mol during the first stage of lignin degradation.

Of the two methods of catalyst preparation the results from mechano-chemically prepared catalysts were generally superior to that of the incipient impregnation wetness method.

Overall, this work demonstrates that a mechano-chemically prepared char supported catalyst provides a simpler, more environmentally benign method of catalyst preparation and is effective in promoting decomposition processes when used in biomass pyrolysis. Potentially it could enhance the value of waste biomass by improving the products of pyrolysis while utilising considerably reduced resources.

Chapter 3: Enhancing hydrogen yield during catalytic pyrolysis of almond residues and pine chips, using mechano-chemically prepared char supported iron catalyst

Richard Thomson[a], Philip Kwong[b,*]

School of Chemical Engineering and Advanced Materials,
Postal Address. The University of Adelaide South Australia 5005 AUSTRALIA
[a] richard.thomson@adelaide.edu.au
[b],* Author for correspondence
P: +618 8313 0724 E:philip.kwong@adelaide.edu.au

Statement of Authorship

Title of Paper	Enhancing hydrogen yield during catalytic pyrolysis of almond residues and pine chips, using mechano-chemically prepared char supported iron catalyst
Publication Status	☐ Published ☐ Accepted for Publication ☐ Submitted for Publication ☑ Unpublished and Unsubmitted work written in manuscript style
Publication Details	

Principal Author

Name of Principal Author (Candidate)	Richard Thomson
Contribution to the Paper	Developed the concept of the study and the experimental design. Design, construction and development of experimental apparatus. Performance of the experiments and interpretation of results. Responsible for the drafting and revision of the paper.
Overall percentage (%)	75%
Certification:	This paper reports on original research I conducted during the period of my Higher Degree by Research candidature and is not subject to any obligations or contractual agreements with a third party that would constrain its inclusion in this thesis. I am the primary author of this paper.
Signature	Date: 20 Apr 2022

Co-Author Contributions

By signing the Statement of Authorship, each author certifies that:

i. the candidate's stated contribution to the publication is accurate (as detailed above);

ii. permission is granted for the candidate to include the publication in the thesis; and

iii. the sum of all co-author contributions is equal to 100% less the candidate's stated contribution.

Name of Co-Author	Philip Kwong
Contribution to the Paper	Corresponding author. Assisted in development of the concept of the study and the experimental design. Major contributor to critical analysis of experimental results. Significant contribution to the revision of the paper.
Signature	Date: 22/4/2022

Name of Co-Author	
Contribution to the Paper	
Signature	Date:

Please cut and paste additional co-author panels here as required.

DECLARATIONS

Funding: The authors did not receive support from any organization for the submitted work.

Conflicts of interest: The authors have no conflicts of interest to declare that are relevant to the content of this article.

Availability of data: If requested additional data associated with this research project can be accessed by contacting the authors.

Code availability: Not applicable

ABSTRACT

With the increased emphasis for green hydrogen production a mechano-chemically prepared, char supported catalyst was developed for use in single stage pyrolysis of almond residues and pine chips. Using peak pyrolysis temperatures from 600°C to 750°C and catalyst loadings of 0%, 1.6%Fe, 2.9%Fe and 5.0%Fe the influence of the catalyst on the conversion, yields and composition of the pyrolysis products was studied with particular focus on hydrogen production.

The catalyst enhanced the hydrogen production, increasing from 6.4 g/kg (600°C, baseline) and 8.4 g/kg (750°C, baseline) to 9.2g/kg (600°C 5.0%Fe) and 13.0 g/kg (750°C, 5.0%Fe), the latter representing over 20% recovery of hydrogen contained in biomass. The influence of the catalyst was different between the two biomass, with the increase in hydrogen yield being significantly higher for pine chips, as was CO production. Char yields reduced as hydrogen production increased, with product gas volumes being 20% higher at 5.0%Fe catalyst loading. The recovered char contained all the initial iron catalyst.

The higher yield of hydrogen demonstrated with this single stage pyrolysis is a key step in developing a lower cost strategy for green hydrogen production. Pyrolysis offers a simpler process conducted at lower temperatures compared to gasification, and the valorising of waste biomass makes this an exciting prospect for producing H_2 from renewable raw materials and wastes.

Key words: hydrogen, catalytic pyrolysis, biomass, waste valorisation

3.1 Introduction

Hydrogen has long been recognised as a preferred energy source/carrier but of recent times its relevance has changed as the move to decarbonise the world's energy sources gathers pace. Critically the costs of producing hydrogen and its utilisation in existing infrastructure have been substantial hurdles in encouraging commercial developments, and remain so, to a significant extent (Fernyhough, J. 2021).

The sources of hydrogen are diverse; hydrogen can be produced through reforming and combustion processes as well as pyrolysis using fossil fuels; and when using renewable sources, biomass can deliver hydrogen through biological and thermal processes and renewable electricity can produce hydrogen through electrolysis. Steam reforming and partial oxidation of fossil fuels remain the dominant source of hydrogen today but there is a strongly developing thrust to accelerate the emerging renewable hydrogen production technologies (Kalamaras & Efstathiou 2013).

Biomass offers one of the potential renewable sources of hydrogen and while developing biomass as a source of bio-oil and char has been an attractive target for researchers for many years, more recently the focus has changed to hydrogen and synthesis gas, primarily through thermochemical conversions or biochemical routes. The primary thermochemical processes are pyrolysis and gasification and two of the more common approaches to produce hydrogen from biomass are reforming the bio-oil produced during pyrolysis and steam gasification (Arregi, Aitor et al. 2018).

Pyrolysis processes are generally classified into slow or conventional pyrolysis, fast pyrolysis, and flash pyrolysis. The products of the pyrolysis process are primarily determined from the constituents of the biomass, the heating rate, maximum pyrolysis temperature and residence time. Clearly the ligno-cellulosic composition of the biomass is critical with each component pyrolysing at different rates and through different routes. This has made it difficult to develop a model to predict yield and composition of final products (Uddin, Daud & Abbas 2013).

In the context of hydrogen production, with biomass often only containing 5%-8% hydrogen, and even with high recoveries, much material must be processed to produce significant amounts of hydrogen; and so, the remainder of

the biomass products also must be used efficiently and economically. This has led to an examination of the influence of pyrolysis process variables to identify factors that would deliver a hydrogen product more economically and efficiently (Uddin, Daud & Abbas 2013). The conclusions were that hydrogen production was favoured by higher moisture content (but that reduced process efficiencies), reduced particle size, higher heating rates, higher pyrolysis temperatures, and the use of catalysts, with the latter potentially having the greatest impact. Because of the multiple variables involved in the pyrolysis process a significant amount of research has been undertaken to identify the preferred conditions for hydrogen production.(Basu 2010; Bridgwater 2012; Demirbas 2004; Demirbaş 2002; Derimbas 2001)

Of the various thermochemical processes that offer a pathway to hydrogen from biomass, pyrolysis has been increasingly seen to be a preferred route. Compared with gasification, the primary benefits are that pyrolysis allows a separation of any downstream reforming processes, and thereby individual control of process variables at each stage; and importantly the process occurs at lower temperatures. The simplest of the processes is a single step process using biomass impregnated with metal salts providing an in-situ catalytic process. Other processes become of increasing complexity, including fast pyrolysis and reforming, catalytic conversion of bio-oil and integrated pyrolysis and gasification. Catalytic processes can also benefit from the separation where the pyrolysis step may produce conditions that poison the reforming catalyst. Consequently, a number of researchers have used two stage fixed bed reactors, pyrolysing the biomass in the first stage and catalytically reforming the gaseous stream as the second stage.(Kaur R. 2019)

Catalytic pyrolysis is used to improve the yield of H_2 from biomass, and to achieve this at lower temperatures, and with reduced char and tar yields. Nickel based catalysts have been widely used, various zeolite catalysts and the use of oxide catalysts also researched.(Saxena et al. 2008) A detailed review of experimental work involving catalytic pyrolysis using transition metals, metal oxides and zeolites has also been reported (Kabakcı & Hacıbektaşoğlu 2017).

More recently the focus has moved to using char supported catalysts with catalytic pyrolysis performed both in-situ (where catalyst and biomass are mixed

together) and ex-situ (where the catalyst is above the biomass bed in the product stream). The latter provides benefits with separate temperature zones making the system more flexible. For char supported catalysts it is generally accepted that Ni metal catalysts provide the greatest benefit, but Fe catalysts may be preferred due to being readily available, low cost and environmentally benign and this has led to a consideration of iron based catalysts (Hongbo et al. 2020; Xia et al. 2019) and char as a catalyst support (Kastner, Mani & Juneja 2015).

This study is designed to further investigate the use of char supported iron catalysts used in-situ during single stage pyrolysis, building on previous work, using thermogravimetric analysis to study the impact of a ball-milled char supported iron catalyst on the pyrolysis of almond residues (AR) as biomass. That study found that samples treated with a char supported iron catalyst exhibit significant reductions in residual char compared with non-catalysed biomass, possibly leading to increased non-condensable gas yields and reduced tar yields.

This work uses a laboratory scale packed bed to investigate the effects of ball-milled char supported iron catalysts during biomass pyrolysis. The use of this catalyst reflects the ready availability of both components; char from the reaction, and iron which may be sourced directly as iron oxides, providing a simple, low cost, environmentally benign, catalyst system. Key areas of interest are the influence of the catalyst on hydrogen production, quantity and composition of tars, and residual char.

3.2 Experimental

3.2.1 Experimental setup

A laboratory scale packed bed sample container (38.1mm dia, 225mm long) was mounted inside a reactor chamber (44.5mm dia, 800mm long) which was encased by a series of separately controllable electrical heating elements (each 300mm long) formed the basis of the experimental vertical furnace. When assembled the base of the sample container was located 185mm from the entry of the furnace, so that the centre of the sample container was approximately at the mid-point of the first element. Thermocouples were located at 170mm, 250mm (inside the sample container) and 790mm at the reactor outlet.

The sample container was packed with biomass or biomass/catalyst mixture (approximately 40g) and heated to one of four pyrolysis peak temperatures (PPT). Thermocouples at the entry to the packed bed, within the packed bed and at the produced gas outlet provided a record of the temperatures during the reaction. The product gas passed through an exit line and via a cylindrical heater and particle filter then entered the gas scrubbing train. This gas scrubbing train was set up in accordance with the CEN Technical Specification (van de Kamp W. 2006) to collect condensable vapours and tars. Non-condensable gases passed through a fine filter before being sampled for GC analysis and metered to determine production volumes. A small nitrogen purge (0.1 litres/min) passed through the thermocouple inlet while a larger nitrogen sweeping flow (2 litres/min) entered at the base of the reactor to carry the produced gas out of the reactor and through the process train (Figure 3.1). After cooling the residual mass was recovered from the packed bed.

3.2.2 Materials

3.2.2.1 Biomass

Biomass feedstocks were waste products; almond residues (AR) were sourced from a local almond processing mill (Laragon Pty Ltd, Renmark, South Australia) while pine chips (PC) were obtained from a local timber mill (Plantation Treated Timber Pty Ltd, Kalangadoo, South Australia).

Biomass was prepared by drying at 105°C for 6 hours, grinding in a DeLonghi DEDICA coffee grinder, and sieving to provide material of <500µm for experimentation. The prepared material was allowed to re-absorb moisture from the atmosphere prior to pyrolysis.

3.2.2.2 Catalyst support

Prepared biomass was pyrolysed to produce char as the support for the catalyst. Weighed quantities of biomass were pyrolysed in the packed bed reactor using a heating rate of approximately 15°C per minute, in a N_2 atmosphere to peak temperatures of 600°C, 650°C, 700°C and 750°C which were maintained for 30 minutes. The samples were cooled to ambient temperature and the yield of char recorded. The char was ground in a pestle and mortar prior to use as catalyst support.

3.2.2.3 Mechano-chemically prepared catalyst

Iron nitrate was selected as an appropriate salt from which to produce the catalyst as its solution is readily absorbed by char, and when dried, the catalyst mixture can be calcined at temperatures below 250°C during which the nitrate fully dissociates to Fe_2O_3 (Melnikov et al. 2013; Vander Wall 1962). The general procedure for preparing the catalyst was to make up a primary solution of 80g $Fe(NO_3)_3.9H_2O$ (Chem-Supply (Australia), AR grade: 98.0% minimum assay) in 200ml distilled water, and 2 additional solutions by diluting with distilled water, the primary solution 1:1, and another 1:3. Each of these solutions were then added to chars (produced at one of the selected PPTs) at the rate of 5ml per 1g char. Each mixture was heated to 250°C for 2 hours in air to thermally decompose the iron nitrate to Fe_2O_3. The decomposition was confirmed by measuring the weight loss (Melnikov et al. 2013; Vander Wall 1962). The calcined product was then milled in duplicate 6g batches in a Fritsch *Pulverisette 7* planetary mill at 700 rpm for 120 minutes using 70g of 3mm zirconia balls in a 45 ml zirconia grinding bowl. This produced, for each of the selected peak pyrolysis temperatures (PPT), a range of char supported catalyst samples with either 6.30%, 11.55% or 19.82% Fe (wt./wt.). When mixed (1:3) with biomass for subsequent pyrolysis the iron loading within the biomass/catalyst mixture was 1.6%Fe, 2.9%Fe or 5.0%Fe.

The catalysts were characterised by the particle size analysis. A selection of the catalyst samples was analysed for particle size distribution using a Malvern Mastersizer 2000 particle size analyser. In each case 0.5g of char supported catalyst was placed in 20ml water and agitated for 2 hours prior to adding to the circulating water in the analyser. Sufficient of the sample was added to meet the obscuration range for the analysis.

3.2.3 Experimental Procedure

An experimental matrix was developed to examine the products of pyrolysis of biomass, at four PPTs (600, 650, 700 and 750°C), and using four levels of catalyst loading (Baseline, 1.6%Fe, 2.9%Fe, and 5.0%Fe). Base line non-catalysed samples were conducted in triplicate and several catalysed samples were conducted in duplicate to confirm consistency of results.

Biomass was prepared as described in Section 2.2.1. Catalysed samples were prepared by adding 10g catalyst to 30g of biomass so that each catalysed sample had approximately the same catalyst support char loading, and Fe loading of either 1.6%, 2.9% or 5.0%. The biomass/catalyst samples were mixed in a DeLonghi DEDICA coffee grinder for 45 seconds. Previous work with AR demonstrated that during pyrolysis the catalytic impact of the char support alone was minimal. The biomass mixture was loaded into a weighed sample carrier and inserted into the vertical furnace. The nitrogen purge and sweeping flows were used to purge the sample chamber for 15 minutes. The heating rate was set at 50°C/min up to the relevant PPT and then maintained at this temperature for 30 minutes. At the product outlet from the reactor a pre-weighed particle filter was installed within a cylindrical heater which operated at 250°C. This led the pyrolysis product to a gas scrubbing assembly. The non-condensable gases leaving the scrubbing train passed through a coalescing filter and then to a flow recorder.

3.2.4 Sampling and analysis

3.2.4.1 Gas analysis

Samples for GC analysis were delivered by a bypass line prior to the flow measurement. A three column Agilent 470 microGC was used but only columns one and two were used. Column one, MS5 mol sieve, measures major gases such as He, H_2, O_2, N_2, CH_4, and CO, and column two, PoraPLOT U (PPU), measures CO_2, C_2H_4, C_2H_6, and C_2H_2.

The data acquisition system provided recorded data from the thermocouples and the product gas flow after tar extraction, with the GC providing a sequential analysis of the gas composition. A series of trials were undertaken to establish a relationship between reactor temperature, sweeping gas flow and time difference between acquired data and microGC sampling to time align all data for processing.

3.2.4.2 Tar analysis

At the completion of the experiment the sample container and particle filter assembly were cooled in a nitrogen atmosphere and then re-weighed to determine residual mass and particle content of the product gas, respectively. Ultimate analysis of the residual mass was carried out using a CHNS elemental

determinator (PerkinElmer , 2400 Series II CHNS/O). The ultimate analysis for C, H, N, S, and O was carried out following ASTM D5373. The O content was determined by difference. The isopropanol and bio-oil mixture in the gas bubbler train was collected, mixed, weighed and sub-sampled for roto vacuum distillation to recover the tars. The tars were analysed using GC-MS. PAH analysis of the tar samples was carried out by extracting 1 mL of representative tar in 1 mL of dichloromethane and 1µl of 2mg/ml Semi-volatile Internal Standard Mix of deuterated PAHs (Supelco 4-8902) was added prior to analysis.

Analysis was conducted on an Agilent 5977B GCMS system by direct injection of 1µl of extract. Separation was conducted using a 30m, 0.25mm ID DB-5MS capillary column with helium carrier gas at a constant flow rate of 1ml/min over the temperature program from 50^{o}C, held for 1 min. ramped to 300^{o}C at 8^{o}C/min and held for 7 mins. Compounds were detected using SIM/scan mode with selected ion groups of ion mass/charge ratio being Group 1; 128, 136, Group 2; 152, 154, 166 178,188, Group 3; 202, 228, 240, Group 4; 252, 264, 276 & 278 monitored and a full scan range of ion mass/charge ratio from 45 to 400. Quantification of the EPA16 target PAHs was conducted against a calibration curve generated by injecting known quantities of PAH Mix (Sigma-Aldrich CRM47543) diluted in dichloromethane using the SIM grouping ions.

3.2.5 Mass balance

The normalised char was calculated on the basis that char formed from biomass degradation and char present as catalyst carrier were equally likely to participate in reactions involving chars, as the char carrier was originally produced in a non-catalytic environment.

As the mass of total liquids was the least reliable direct measurement it was determined by difference from the mass of all other reactants and products. The mass balance was calculated from the following:

$$M_{bt} - C_{fe} - C_{ch} - M_p - (V_{gT} \times F_i \times \rho_i) - M_{bc} = M_{liq}$$

Where: M_{bt} is the total mass of biomass mix loaded

C_{fe} is the mass of iron oxide included , if any

C_{ch} is the mass of char carrier included , if any

M_p is the mass of particulates collected on the gas filter

V_{gT} is the temperature corrected volume of gas

F_i is the fraction of the gas volume attributable to component *i*

ρ_i is the density of component *i*

M_{bc} is the mass of residual char attributable to the biomass, and

M_{liq} is the mass of liquids and tar

The total mass of liquids was subsequently divided into liquids other than tar (essentially bio-oil and water) and gravimetrically determined tars.

3.3 Results and Discussion

3.3.1 Characterisation of biomass and catalyst

3.3.1.1 Biomass

The characteristics of the almond residue feedstock are shown in Table 3.1. The high volatile content of the proximate analysis indicates that significant gaseous production may be expected on pyrolysis and gasification and that there will be a reduced char yield consistent with the low fixed carbon and ash contents. The proximate analysis is typical of those reported for almond shells whereas almond husks show higher ash (6%) and consequently lower fixed carbon. The characteristics of the pine chip feedstock are also shown in Table 3.1 and are in reasonable agreement with other results for pine.(Phyllis2 2020)

3.3.1.2 Catalyst

The catalyst was prepared mechano-chemically by ball milling the char supported ferric oxide to produce a powder with particle size characteristics typically of a mean size of 3 μm, 10% less than 1 μm and 10% larger than 7 μm.

3.3.2 Impact of catalyst at different pyrolysis temperatures on product distribution

Figure 3.2 shows the distribution of the primary products of gas, liquids, tars, char and particulates over a range of PPTs and catalyst loadings.

3.3.2.1 Normalised char yields

Char yields reported have been normalised as described in Section 2.2.5. The char yields of non-catalysed samples reduced progressively but only marginally as the PPT increased, trending to a minimum char yield at 750°C. Char yields for catalysed samples showed greater reductions, essentially proportionate to catalyst loadings and increasing PPT. The impact of catalyst loading on normalised char yields was much more significant than PPT increases. Normalised char yield reductions for baseline samples were 30.4%, 30.1%, 29.9% and 29.4% for PPTs of 600°C, 650°C, 700°C and 750°C respectively while the highest catalyst loadings had yields reduced by 24%, 32%, 32% and 33% for PPTs of 600°C, 650°C, 700°C and 750°C, respectively. These results show that the catalyst has induced some secondary reactions with the char, resulting in char being consumed and product gas production increasing accordingly.

3.3.2.2 Gas yields and component distribution

Figure 3.3 shows a strong trend for gas yields to increase with increasing catalyst loading. Product gas yield (wt.%) for baseline samples were 25.4%, 26.0%, 26.9% and 27.4% for PPTs of 600°C, 650°C, 700°C and 750°C respectively and these increased for the highest catalyst loading (5.0%Fe) to 33.2%, 33.2%, 34.2% and 34.8% for PPTs of 600°C, 650°C, 700°C and 750°C, respectively.

Figure 3.4 clearly shows the hydrogen composition (%vol) of the gas increasing with both PPT and more strongly with catalyst loading; baseline yields for AR were 31.1%, 34.4%, 34.5% and 34.9% for PPTs of 600°C, 650°C, 700°C and 750°C, respectively, while for PC they were 27.3% and 32.9% at 700°C and 750°C, respectively. The results for equivalent samples with 5.0%Fe catalyst loading were 35.6%, 40.2%, 41.1% and 41.2% for AR and 38.4% and 40.9% for PC, providing increases in yield of between 15% and 40%.

The more notable differences between the two biomass types was in the components other than hydrogen with AR having CO and CH_4 contents typically between 5-10% for each with CO_2 being the balance between 45-50%. Conversely PC had CO_2 contents of around 30%, CO contents of 20%, with CH_4 at 10%. These differences in outcome are attributed to the different ligno-cellulose compositions with PC having a significantly higher cellulose content

than AR which has been demonstrated to produce higher proportions of CO and CH_4 and lower CO_2 contents than hemicellulose or lignin (Couhert C. 2009).

3.3.2.3 Liquids and tars

The combined mass of liquids and tars was very consistent across the full range of experiments with baseline samples being between 43 and 44% and catalysed samples showing a slight trend to lower values (41%) as catalyst loadings increased. The marked change however, was the proportion of tar in the combined liquid product, declining consistently with increasing pyrolysis temperature but showing little response to catalyst loading.

3.3.3 Impacts of catalyst at different pyrolysis temperatures on hydrogen yield and recovery

Hydrogen production increased due to the combined effects of higher total gas production and increased hydrogen content of the product gas as the catalyst loading increased and the PPT increased; and the overall yield of hydrogen from the biomass increased accordingly. The effect of catalyst loading was substantially greater than that of increasing PPT as shown in Figure 3.5.

Baseline AR samples produced 3.1, 3.4, 3.7 and 4.4 mmol H_2/g for PPTs from 600°C, 650°C, 700°C and 750°C respectively and baseline PC samples produced 3.1 and 3.6 mmol H_2/g for PPTs from 700°C and 750°C, respectively. With 5.0%Fe catalyst loading, with the same pyrolysis conditions production was 4.6, 5.5, 6.2 and 7.9 mmol H_2/g for AR and 5.9 and 6.6 mmol H_2/g for PC. This provided yield increases for AR of 43%, 60%, 62% and 55%, for PC of 90% and 83%. The results reflect a much stronger influence of the catalyst in increasing hydrogen production in pine chips which is possibly due to its higher contained hydrogen content and higher volatiles (Table 3.1).

Hydrogen recovery (Figure: 3.5) is an important parameter given the generally low hydrogen content of biomass. Data reported on hydrogen recovery using catalytic biomass pyrolysis at 800°C indicates recovery rates from around 5% to as high as 57%, but notably those above 25% are associated with more exotic catalysts. The highest reported recovery for iron based catalysts was 25% (Granados-Fitch et al. 2019), compared with the highest recovery in this work of 22%.

Interestingly, as shown in Figure 3.6, hydrogen production started at quite low temperatures (~300°C) and as the temperature increased above 400°C catalysed samples demonstrated a higher rate of production than the base line, and the increased rate was a function of catalyst loading. The baseline sample produced 50% of the total hydrogen as the pyrolysis temperature approached 630°C whereas the catalysed samples had produced between 75-85% of the baseline production and 65%-70% of their total production at this temperature. This illustrates the lower energy input required to release hydrogen in the presence of the catalyst, and the extent of this reflects catalyst loading.

3.3.4 Impacts of catalyst at different pyrolysis temperatures on the Hydrogen/Char production relationship

Figure 3.7 shows the relationship between hydrogen production and residual char, demonstrating the reduction in char being strongly associated with the increase in hydrogen production. This infers that as char is consumed hydrogen is one of the products and that the char supported iron catalyst enhances the process. The data for AR suggests that for every extra mole of char consumed, 0.5 mole of hydrogen is being released.

The relationship between the increase in hydrogen and loss of char, can be seen to be relatively independent of pyrolysis temperature and largely an artefact of catalyst loading alone. Baseline hydrogen production for AR at both 700°C and 750°C was 0.0083g/g biomass for baseline samples increasing to 0.0125 and 0.0130g/g biomass for 700°C and 750°C respectively for samples with 5.0%Fe loading. Similarly for PC, hydrogen production for baseline samples was 0.0063 and 0.0073g/g biomass, and for 5.0%Fe catalyst loading 0.0118 and 0.0130g/g biomass at 700°C and 750°C, respectively. While the catalyst can be seen to be highly effective in inducing these reactions there is nevertheless a trend of diminishing returns with increasing catalyst loading.

3.3.5 Impacts of catalyst at different pyrolysis temperatures on tar yield and composition

The concentration of tars in the produced gas stream is shown Figure 3.8. The pattern of tar production is similar for both biomass species with baseline

concentrations less than the reference concentration (Aigner, Wolfesberger & Hofbauer 2009) except for the result at 600°C. The broad pattern is for a significant reduction in total tar concentration as catalyst loading increases, being approximately 35-40% from baseline to maximum catalyst loading while the response to increasing PPTs is very muted.

Figure 3.9 depicts the GC-MS determined relative concentrations of PAH components differentiated between those compounds with molecular weights either above or below 200. This is based on a tar classification that classifies PAH compounds by molecular weight (MW) with light PAH compounds being those with 2-3 rings which include naphthalene and similar compounds with MW<200. These tars condense at intermediate temperatures in relatively high concentrations. Heavy PAH compounds have from 4-7 rings and include pyrene and chrysene having MW>200 which condense at high temperatures and low concentrations(Guan et al. 2016). The conclusions are that the total PAHs are essentially constant across the spectrum of PPTs and catalyst loadings irrespective of total tar reducing, and that the distribution between low and high molecular weight PAHs is also unaffected by catalyst or pyrolysis temperature.

Given the significant research into the use of char supported metal catalysts (Guo, FQ et al. 2018; Kastner, Mani & Juneja 2015; Shen, YF, Zhao, et al. 2015) for tar reduction this outcome may appear incongruous. However, the crucial differences between this experiment and most of the research is that in the latter case the process is designed for the pyrolysis vapours to be separated from the pyrolysis bed and treated either in situ or ex situ in a fixed bed of catalyst. In this experiment the catalyst is comingled with the biomass, with a high sweeping gas flow, and the pyrolysis vapours have little residence time for catalytic destruction of tars once they leave the pyrolysis bed, although some thermal cracking may occur.

3.3.6 Catalyst reduction and hydrogen production assisted by presence of carbon oxides

Carbon oxidation reactions have been studied extensively (Li, Ce & Brown, TC 2001), particularly to determine whether either or both CO and CO_2 are primary products of the process. Labile carbon atoms are considered capable of reacting directly with oxygen molecules, producing CO although the mechanism

has been debated. Experiments with powdered charcoal suggest that in a very low oxygen environment carbon oxidation commences as the temperature rises above 500°C, and at temperatures up to 700°C the rate of production of CO dominates (Li, C & Brown, TC 2001). In this temperature range iron oxides are also known to change phase, being reduced to metallic iron and become more active as a catalyst.

$$3Fe_2O_3 + CO \rightarrow 2Fe_3O_4 + CO_2 \quad (3.1)$$

$$Fe_3O_4 + CO \rightarrow 3FeO + CO_2 \quad (3.2)$$

$$FeO + CO \rightarrow Fe + CO_2 \quad (3.3)$$

$$CO + H_2O \rightarrow CO_2 + H_2 \quad (3.4)$$

In the pyrolysis process two reductants are present, CO and H_2, but reduction of Fe_2O_3 requires less energy in the presence of CO. The conversion to Fe_3O_4 occurs around 400°C (3.1), the conversion to FeO occurring between 500°C and 575°C (3.2), and the final reduction to Fe between 650°C and 700°C (3.3) depending on the concentration of CO (Abu Tahari et al. 2019). This is consistent with observations in Chapter 2 from the thermogravimetric analysis of catalytic pyrolysis.

Figure 3.10 illustrates the changes in carbon oxides and hydrogen production of samples that are baseline and those with 2.9% Fe catalyst. The notable feature is that while the pattern of production is largely the same the catalysed sample continues to have carbon oxides being produced later in the pyrolysis process (at higher temperatures) and that these include the temperature zones where the iron catalyst can be expected to be reduced in the presence of CO. It is during this time that the hydrogen production from the catalysed sample begins to reach a maximum supporting the concept that this is the period of greatest catalytic activity.

The pattern of CO and CO_2 in the produced gas stream, in the case of the catalysed sample, is one that at temperatures above 550°C, CO is in decline and ceases to be evident beyond 600°C, while CO_2 is declining slowly and develops a long tail, mirroring H_2 volumes detected in the gas stream. This could be interpreted as any produced CO being consumed by the WGS reaction (3.4) with the release of additional CO_2 and H_2 into the gas stream.

3.4 Conclusions

Catalytic pyrolysis of almond residue and pine chips was studied using a single-stage packed bed reactor. Results indicated that a mechano-chemically prepared char supported iron catalyst was effective when intimately mixed with biomass as evidenced by the conversion, yields and composition of the pyrolysis products of biomass, with particular focus on hydrogen production.

Product gas volumes increased by 27-30% as catalyst loading increased to 5.0%Fe. Hydrogen composition of the product gas from baseline samples for PPTs of 600°C, 650°C, 700°C, 750°C respectively were 31.1%, 34.4%, 34.5% and 34.9% but increased by 14%, 17%,19% and 18% for samples with 5.0%Fe catalyst loading. Consequently, hydrogen production rose from 6.4 g/kg and 8.4 g/kg (600°C and 750°C baseline) to 9.2g/kg and 13.0 g/kg (600°C and 750°C, 5.0%Fe), the latter being over a 50% increase in production, providing more than 20% recovery of hydrogen contained in biomass

The impact of catalyst loading on normalised char yields was much more significant than PPT increases, with the highest catalyst loadings producing reductions in yields by 24%, 32%, 32% and 33% for PPTs of 600°C, 650°C, 700°C, 750°C, respectively. A strong relationship was established between char and hydrogen production showing consumption of char occurred as hydrogen production increased.

With the catalyst being intimately mixed with the biomass there was little opportunity for the tars to be catalytically cracked, nevertheless there was a significant reduction in total tars but essentially no effect on the quantity and distribution of PAH tar compounds.

The higher yield of hydrogen demonstrated with this single stage pyrolysis is a major step in developing a lower cost strategy for green hydrogen production. The development of a mechano-chemically prepared catalyst offers further opportunities to simplify the overall process.

Chapter 4: : Hydrogen production from catalytic pyrolysis of almond residues, using waste iron ore tailings in char supported iron oxide catalyst.

Richard Thomson[a], Philip Kwong[b,*]

School of Chemical Engineering and Advanced Materials,
Postal Address. The University of Adelaide South Australia 5005 AUSTRALIA
[a] richard.thomson@adelaide.edu.au
[b],* Author for correspondence
P: +618 8313 0724 E:philip.kwong@adelaide.edu.au

Statement of Authorship

Title of Paper	Hydrogen production from catalytic pyrolysis of almond residues, using waste iron ore tailings in char supported iron oxide catalyst
Publication Status	☐ Published ☐ Accepted for Publication ☐ Submitted for Publication ☑ Unpublished and Unsubmitted work written in manuscript style
Publication Details	

Principal Author

Name of Principal Author (Candidate)	Richard Thomsen
Contribution to the Paper	Construction and development of the experimental apparatus. Development of the experimental methodology. Performance of experiments and interpretation of results. Responsible for drafting and revision of the paper.
Overall percentage (%)	75%
Certification:	This paper reports on original research I conducted during the period of my Higher Degree by Research candidature and is not subject to any obligations or contractual agreements with a third party that would constrain its inclusion in this thesis. I am the primary author of this paper.
Signature	Date: 20 Apr 2022

Co-Author Contributions

By signing the Statement of Authorship, each author certifies that:

i. the candidate's stated contribution to the publication is accurate (as detailed above);

ii. permission is granted for the candidate in include the publication in the thesis; and

iii. the sum of all co-author contributions is equal to 100% less the candidate's stated contribution.

Name of Co-Author	Philip Kwong
Contribution to the Paper	Corresponding author. Provided original idea of the study. Major contribution to the writing and revision of the paper.
Signature	Date: 20/4/2022

Name of Co-Author	
Contribution to the Paper	
Signature	Date:

Please cut and paste additional co-author panels here as required.

DECLARATIONS

Funding: The authors did not receive support from any organisation for the submitted work.

Conflicts of interest: The authors have no conflicts of interest to declare that are relevant to the content of this article.

Availability of data: If requested additional data associated with this research project can be accessed by contacting the authors.

Code availability: Not applicable

ABSTRACT

The performance of char supported iron catalysts using different sources of iron oxide have been assessed. Utilising low cost, waste as catalysts is a key plank in building a circular economy and so commercial iron ore (CIO) and iron ore tailings (IOT) were selected as alternative iron sources to conventionally prepared catalyst using laboratory ferric nitrate (LFN). Almond residue was catalytically pyrolysed using catalyst with iron from different sources and key parameters such as total gas production, hydrogen production and tar production and composition used to compare the performance.

At catalyst loadings of 1.6%Fe and 2.9%Fe each catalyst type produced similar quantities of hydrogen (+/-3%) at the lower pyrolysis temperatures of 600°C and 650°C. At temperatures of 700°C and 750°C hydrogen production using CIO and IOT types were 86% and 78%, and 84% and 85%, respectively, when compared to LFN. At 5.0%Fe catalyst loading a more significant divergence became apparent with production from both CIO and IOT being 70% of LFN. Importantly, however, at pyrolysis temperature of 750°C and 5.0%Fe catalyst loading LFN, CIO and IOT catalyst types produce 203%, 175% and 176%, respectively when compared to the baseline pyrolysis at 600°C.

While the performance of the catalyst types was not identical, the general pattern of outcomes in terms of the key parameters was broadly similar. It is further postulated that alkali and alkaline earth metallic (*AAEM)* species included in CIO and IOT may have contributed to variations in H_2, CO and CO_2 production by the differently sourced iron oxides.

On balance, IOT type is seen as an appropriate, effective commercial catalyst with significant benefits. In particular it provides for integration into the iron and steel industry to deliver significant decarbonisation by delivering cost effectively the twin products of green hydrogen and char, as reductant.

Key words: recycling, iron ore tailings, catalyst, steel industry, hydrogen

4.1 Introduction

Critical to establishing the sustainable use of resources is the development of waste valorisation processes. Waste-to-energy is a key pathway to achieving sustainable developments through re-use and recycling of waste products; providing a valuable alternative to incineration and landfill while providing energy recovery to meet energy demands. Nevertheless, there remain many challenges to ensure not only that the final products are market competitive but also the "gate price" is competitive with alternative disposal costs. Other aspects that need to be addressed include establishing the processes do not add significant new waste streams or environmental contamination.

Waste-to-hydrogen (WtH) can be viewed as a subset of the general Waste-to-Energy concept. Biomass conversion is viewed as having two basic conversion pathways: biochemical and thermochemical, exhibiting fundamental differences in energy requirements, operating conditions, reaction rates and yields. Thermochemical processes are generally considered to have higher reaction rates, hydrogen yields and conversion efficiencies (Huang et al. 2018; Lui et al. 2020). However, the variety of sustainable biomass species results in a broad array of physical and chemical properties, which has led to a substantial range of technologies and processes being developed for their conversion (Balat, Mustafa et al. 2009a, 2009b).

WtH through pyrolysis can either focus on production of bio-oil for subsequent catalytic reforming for hydrogen or using an in-situ catalytic process producing the hydrogen into the product gas stream. The latter approach is considered most likely to result in a lower cost process if an adequate yield can be achieved using a low cost catalyst system. Several standards have been developed for catalyst selection (Guan et al. 2016), largely focused on tar reduction, but broadly applicable to biomass processing in general. These additionally specify the need for ssuitable selectivity for product gas, resistance to de-activation, ease of preparation, and low cost; and for stationary fixed beds or fluidised beds, mechanical strength, and a capacity to be regenerated. Furthermore, the choice of catalyst needs to consider the complexities of the specific benefits achieved, any undesired side effects, and importantly environmental impacts.

For hydrogen production the catalysts of choice are primarily nickel or iron based although other metal oxides, carbonates, zeolites and more exotic combinations have been researched (Bakhtyari, Makarem & Rahimpour 2017). As with other catalytic processes the catalyst can be used in-situ either admixed with the biomass or held in fixed beds. In the former case, depending on the reactor design, it is considered that better physical contact may occur between catalyst and biomass. This allows for rapid but limited interaction of evolved vapours and the catalyst whereas for many catalysts unsuited to be mixed with the biomass, the process requires the catalyst to be held in fixed beds within the reactor. The interest in improving hydrogen yield has also resulted in a broad range of reactor configurations being proposed (Kabakcı & Hacıbektaşoğlu 2017; Uddin, Daud & Abbas 2013).

One of the major issues with catalyst systems based on fixed beds is the loss of catalytic activity and selectivity over time. Coke deposition is a significant problem with coke either blocking pores or covering active catalyst sites. This may require regeneration cycles for the catalyst and frequently this also results in a longer term decline in activity (Santamaria et al. 2021). So, a further consideration that has gained traction is the success of char and char supported metal catalysts, utilised in the in-situ mode. These are introduced continuously as fresh catalyst and not only avoid the problems of activity loss but also have been demonstrated to be particularly successful in tar reduction (Zeng et al. 2020).

Such systems are mostly amenable to mechano-chemical preparation to reduce the particle size of the metal, provide improved dispersal of metals onto solid supports and increase the activity of the catalyst due to significant size reduction and increased active surface area (Ralphs, Hardacre & James 2013). Additionally mechano-chemical synthesis is seen to provide more sustainable methods of preparation. A variety of methods have developed, such as using iron, dry milled with graphite, whereby both the iron and graphite particles are reduced in size and adhere together, (Motozuka et al. 2015); using iron oxide with different carriers (Pineda et al. 2011); and producing magnetite nano-particles supported on charcoal (Mohan, Balaji, Park, Ji Chan & Park, Kang Hyun 2016); each method is reported to provide highly active catalyst systems.

Moreover, there have been a number of attempts to incorporate the waste valorisation principle into the catalyst system with the use of nickel plating slag (Guo, D et al. 2020), naturally occurring ilmenite (Min et al. 2013), a magnesium slag/nickel catalyst (Yu et al. 2019) and sodium zirconate from dental wastes (Wang, F et al. 2019). Unfortunately, most of these systems ignore the fact that the source material itself is environmentally damaging and its re-use as a catalyst does not change this important characteristic. Nevertheless there are opportunities for pursuing this objective such as using low grade iron ore (Wicakso et al. 2016).

The steel industry across the globe is increasingly facing a decarbonisation challenge with every ton of steel produced in 2018, emitting, on average, 1.85 tons of carbon dioxide, equating to about 8 percent of global carbon dioxide emissions ('Steel's contribution to a low carbon future and climate resilient societies' 2017). while large companies and governments have announced ambitious green hydrogen expansion plans, essentially focused on electrolysis, there is some doubt about how many of these projects will actually be commissioned. Financing challenges concerning the profitability of green hydrogen projects remain and generally the cost of producing hydrogen from renewable electricity remains significantly higher than that of fossil fuels. An additional issue is the possibility that the market for hydrogen will not evolve as quickly as green hydrogen production, creating an important concern for future electrolyser expansion. (IEA 2021).

However, the use of biomass products as a both source of energy and reducing agents holds out a promising substitute to green hydrogen from electrolysis. Furthermore techno-economic studies suggest hydrogen from biomass pyrolysis will have a lower cost ($1.20- $2.60/kg$_{H2}$) than hydrogen from electrolysis ($2.35 - $4.80/kg$_{H2}$) (Lepage et al. 2021).

While biomass can be a source of green hydrogen it also has the potential to make a greater contribution to the steel industry than green hydrogen alone. Partial substitution of blast furnace coke and coal with pyrolysis char has promise, and a range of other possibilities have been identified for different areas of an integrated steelworks (Mousa et al. 2016). And the CSIRO in Australia has studied biomass utilisation in applications including sintering solid fuel, as a coke making blending component and as a tuyere injectant in blast furnace operations.

In respect of the latter it is estimated that substitution could be up to 100%, giving emission reductions of 0.41-0.55 t_{CO2}/t-crude steel or between 19 and 25% of total emissions from this source, representing the largest of the potential savings through biomass products (Mathieson 2011) other than green hydrogen.

This work reports the preparation of 3 different char supported iron oxide catalyst using different mechano-chemical production methods. The use of these components to formulate the catalyst, and the use of the mechano-chemical method, reflect the success achieved by previous researchers in this area (Bru et al. 2007; Moud et al. 2018; Richardson, Eibner, et al. 2015). A laboratory scale single-stage packed bed was used to investigate the effects of these different preparations during biomass pyrolysis. Key areas of interest were the comparative performance of the catalysts on the products of the reactions, on hydrogen production, and quantity; and, composition of tars, and normalised residual char.

4.2 Materials and Methods

4.2.1 Materials

4.2.1.1 Biomass

Biomass feedstock of almond residues was sourced from a local almond processing mill (Laragon Pty Ltd, Renmark, South Australia). Biomass was prepared by drying at 105°C for 6 hours, grinding in a DeLonghi DEDICA coffee grinder, and sieving to provide material of <500µm for experimentation. The prepared material was allowed to re-absorb moisture from the atmosphere prior to pyrolysis.

4.2.1.2 Catalyst support

Prepared biomass was pyrolysed to produce char as the support for the catalyst. Weighed quantities of biomass were pyrolysed in the packed bed reactor using a heating rate of approximately 15°C per minute, in a N_2 atmosphere to peak temperatures of 600°C, 650°C, 700°C and 750°C which were maintained for 30 minutes. The samples were cooled to ambient temperature and the yield

of char recorded. The char was subsequently ground to <500 µm for use as catalyst support.

4.2.2 Catalyst Preparation

Three different catalysts were prepared, one from laboratory sourced ferric nitrate (LFN), one from commercial iron ore (CIO) and another from commercial iron ore tailings (IOT). The preparation procedures varied for each catalyst source, with each change simplifying the preparation procedure.

LFN was prepared by making up a primary solution of 80g $Fe(NO_3)_3.9H_2O$ (Chem-Supply (Australia), AR grade: 98.0% minimum assay) in 200ml distilled water, and 2 additional solutions by diluting with distilled water, the primary solution 1:1, and another 1:3. The concentration of these solutions were determined from the volume of water required to fully wet the char. Solutions were added to chars (produced at one of the selected PPTs) at the rate of 5ml per 1g char. Each mixture was then heated to 250°C for 6 hours in air to thermally decompose the iron nitrate to Fe_2O_3. The decomposition was confirmed by measuring the weight loss (Melnikov et al. 2013; Vander Wall 1962).

The calcined product was milled in duplicate 6g batches in a Fritsch *Pulverisette 7* planetary mill at 700 rpm for 120 minutes using 70g of 3mm zirconia balls in a 45 ml zirconia grinding bowl. This produced, for each of the selected peak pyrolysis temperatures, a range of char supported catalyst samples with either 6.3%, 11.6% or 19.8% Fe (wt/wt).

CIO was supplied by the Fortescue Metals Group (FMG) and was a sub-sample of shipped iron ore. IOT was also supplied by FMG, being a sample from their tailings dam. The analysis of the samples as supplied, and their particle size distributions are shown in Table 4.1 and Figure 4.1 respectively.

The CIO was subsampled and crushed to <500 µm while the IOT was used as received. Quantities of the CIO and IOT powders that would provide Fe(wt/wt) concentrations in the prepared catalysts equal to those of the LFN preparations were added to chars (produced at one of the selected PPTs) and then thoroughly mixed prior to milling as for the LFN catalyst preparation. Given the nature of the CIO and IOT material and the sub-sampling of a non-uniform product it was expected that there would be some minor variability in the final ferric oxide concentrations of these catalysts.

4.2.3 Biomass pyrolysis

4.2.3.1 Experimental setup

A laboratory scale packed bed sample container (38.1mm dia, 225mm long) was packed with biomass or biomass/catalyst mixture (approximately 40g) and mounted inside a reactor chamber (44.5mm dia, 800mm long) which was encased by a series of separately controllable electrical heating elements (each 300mm long) forming the basis of the experimental vertical furnace. When in place the base of the sample container was located 185mm from the entry of the furnace, so that the centre of the sample container was approximately at the mid-point of the first element. Thermocouples were located at just prior to the sample container at 170mm, at 250mm (inside the sample container) and 790mm at the exit from the reactor. A small nitrogen purge (0.1 litres/min) passed through the thermocouple inlet while a larger nitrogen sweeping gas flow (2 litres/min) entered at the base of the reactor to carry the produced gas out of the reactor and through the process train (Figure 4.2). The reactor space was swept 1.6 times per minute.

The sample container was heated to one of four pyrolysis peak temperatures (PPT) controlled by the bottom and middle elements and the product gases passed through the reaction chamber to the exit line, with the upper element maintaining a temperature of 350°C to prevent condensation.

The product then immediately passed through a particle filter encased in a cylindrical heater operating at 250°C, entering a gas scrubbing train. This gas scrubbing train was set up in accordance with the CEN Technical Specification (van de Kamp W. 2006) to collect condensable vapours and tars. Non-condensable gases passed through a fine filter before being sampled for GC analysis and metered to determine production volumes. After cooling the residual mass was recovered from the packed bed.

4.2.3.2 Biomass pyrolysis

An experimental matrix was developed to examine, during pyrolysis of biomass, the effects of PPTs (600, 650, 700 and 750°C), of catalyst loading at three levels (1.6%Fe, 2.9%Fe, and 5.90%Fe) and of three different iron based catalysts (LFN, CIO and IOT).

Biomass was prepared as described in Section 4.2.1.1 above. Catalysed samples were prepared by adding 10g catalyst to 30g of biomass so that each catalysed sample had approximately the same catalyst support char loading and an Fe loading of either 1.6%, 2.9% or 5.0%. The biomass and catalyst were mixed in a DeLonghi DEDICA coffee grinder for 45 seconds.

The biomass mixture was loaded into a weighed sample carrier and inserted into the vertical furnace. The nitrogen purge and sweeping flows were used to purge the sample chamber for 15 minutes. The heating rate was set at 50°C/min up to the relevant PPT and then maintained at this temperature for 30 minutes. At the product outlet from the reactor a pre-weighed particle filter was installed within a cylindrical heater which operated at 250°C. This led the pyrolysis product to a gas scrubbing assembly. The non-condensable gases leaving the scrubbing train passed through a coalescing filter and then to a flow recorder.

4.2.4 Sampling and analysis

4.2.4.1 Gas analysis

Samples for GC analysis were delivered by a bypass line prior to the flow measurement. A three column Agilent 470 microGC was used but only columns one and two were used. Column one, MS5 mol sieve, measures major gases such as He, H_2, O_2, N_2, CH_4, and CO, and column two, PoraPLOT U (PPU), measures CO_2, C_2H_4, C_2H_6, and C_2H_2.

The data acquisition system provided recorded data from the thermocouples and the product gas flow after tar extraction, with the GC providing a sequential analysis of the gas composition. A series of trials were undertaken to establish a relationship between reactor temperature, sweeping gas flow and time difference between acquired data and microGC sampling to time align all data for processing.

4.2.4.2 Tar analysis

At the completion of the experiment the sample container and particle filter assembly were cooled in a nitrogen atmosphere and then re-weighed to determine residual mass and particle content of the product gas, respectively. Ultimate analysis of the residual mass was carried out using a CHNS elemental determinator (PerkinElmer , 2400 Series II CHNS/O). The ultimate analysis for C,

H, N, S, and O was carried out following ASTM D5373. The O content was determined by difference. The isopropanol and bio-oil mixture in the gas bubbler train was collected, mixed, weighed and sub-sampled for roto vacuum distillation to recover the tars. The tars were analysed using GC-MS. PAH analysis of the tar samples was carried out by extracting 1 mL of representative tar in 1 mL of dichloromethane and 1µl of 2mg/ml Semi-volatile Internal Standard Mix of deuterated PAHs (Supelco 4-8902) was added prior to analysis.

Analysis was conducted on an Agilent 5977B GCMS system by direct injection of 1µl of extract. Separation was conducted using a 30m, 0.25mm ID DB-5MS capillary column with helium carrier gas at a constant flow rate of 1ml/min over the temperature program from 50^{o}C, held for 1 min. ramped to 300^{o}C at 8^{o}C/min and held for 7 mins. Compounds were detected using SIM/scan mode with selected ion groups of ion mass/charge ratio being Group 1; 128, 136, Group 2; 152, 154, 166 178,188, Group 3; 202, 228, 240, Group 4; 252, 264, 276 & 278 monitored and a full scan range of ion mass/charge ratio from 45 to 400. Quantification of the EPA16 target PAHs was conducted against a calibration curve generated by injecting known quantities of PAH Mix (Sigma-Aldrich CRM47543) diluted in dichloromethane using the SIM grouping ions.

4.2.5 Mass balance

The normalised char was calculated on the basis that char formed from biomass degradation and char present as catalyst carrier were equally likely to participate in reactions involving chars, as the char carrier was originally produced in a non-catalytic environment.

As the mass of total liquids was the least reliable direct measurement it was determined by difference from the mass of all other reactants and products. The mass balance was calculated from the following:

$$M_{bt} - C_{fe} - C_{ch} - M_p - (V_{gT} \times F_i \times \rho_i) - M_{bc} = M_{liq}$$

Where:
- M_{bt} is the total mass of biomass mix loaded
- C_{fe} is the mass of iron oxide included , if any
- C_{ch} is the mass of char carrier included , if any
- M_p is the mass of particulates collected on the gas filter
- V_{gT} is the temperature corrected volume of gas

F_i is the fraction of the gas volume attributable to component *i*

ρ_i is the density of component *i*

M_{bc} is the mass of residual char attributable to the biomass, and

M_{liq} is the mass of liquids and tar

The total mass of liquids was subsequently divided into liquids other than tar (essentially bio-oil and water) and gravimetrically determined tars.

4.3 Results and Discussion

4.3.1 Characterisation of biomass and char

4.3.1.1 Biomass

The characteristics of the almond residue feedstock are shown in Table 4.2. The proximate analysis is typical of those reported for almond shells whereas almond husks show higher ash (6%) and consequently lower fixed carbon.

4.3.1.2 Characterisation of catalysts

The catalysts were characterised by particle size analysis. A selection of the catalyst samples was analysed for particle size distribution using a Malvern Mastersizer 2000 particle size analyser. In each case 0.5g of char supported catalyst was placed in 20ml water and agitated for 2 hours prior to adding to the circulating water in the analyser. Typically, the mean size was approximately 5 μm with 10% below 0.5 μm and 10% above 10 μm.

It is also important to note that LFN was produced from a laboratory “pure” product with minor impurities whereas both CIO and IOT have significant quantities of other chemicals present (Table 4.1). Both iron ore sources contain significant quantities of AAEMs, notably Al, Ca, Mg, K and Na oxides with IOT having very approximately double the concentration of most of these compounds in CIO. Numerous papers have examined the role of AAEMs within char, and their various catalytic effects (Haddad K. et al. 2016; Hu, S et al. 2015; Wang, W et al. 2022) largely reporting that AAEMs can influence the distribution of the component composition of the product gas and also PAH concentrations in tars.

In addition to variabilities in results between catalyst types that may arise from the influence of AAEMs, some variability is likely to have to arisen from the inability to ensure total uniformity of iron content when subsampling and preparing the commercial products for catalyst preparation (Section 2.1.3).

A further observation has been that AAEMs could also promote the formation of heavier PAHs in tars which has been seen in the distribution of tars across catalyst types (Section 3.2.5). The distribution of pyrolysis products may also be affected across the temperature range of 500°C to 700°C, reducing the expected increase in gas production offset by higher char production (Hu, S et al. 2015).

4.3.2 The influence catalyst type on pyrolysis products

Whilst the focus of this work is the performance of catalysts in enhancing hydrogen production it is also important to review other differences that may arise from the use of different sources of iron or preparation methods. The key areas of interest selected to determine whether there are significant differences in catalyst performance, primarily include total gas production, gas component distribution, hydrogen production, the hydrogen/char production relationship, and the distribution of the primary products, while tar composition may also contribute to understanding the overall impact of catalysts.

4.3.3 The influence of catalyst type on product gas yields and product gas compositions

4.3.3.1 Product gas yields

Figure 4.3 depicts the product gas yields generated by each catalyst type. At the lowest PPT (600°C) the baseline gas yield was 9.6 mmol/g biomass and increased by 25%, 28% and 31% as the catalyst loading increased. Over 85% of the results were within +/- 5% of the mean at each level of catalyst loading. CIO showed the greatest variability and slightly underperformed LFN and IOT but nevertheless it is clear each catalyst performed in a very similar manner. Likewise, at PPTs of 650°C and 700°C the baseline gas yields were 9.9 and 9.8 mmol/g biomass respectively and increased by 34%, 34% and 33% at 650°C and by 46%, 43% and 45% at 700°C, as the catalyst loading increased. Over 75% of

the results were within +/- 5% of the mean at each level of catalyst loading with CIO at 700°C and 5%Fe loading a major outlier (-10% from mean). CIO again showed the greatest variability and slightly underperformed LFN and IOT. At PPT of 750°C there is some divergence in performance particularly as catalyst loading increases. The baseline gas yield was 10.8 mmol/g biomass and for catalyst loadings of 1.6%Fe and 2.9%Fe the yield increased by 31% and 34% respectively with the results for each catalyst type being within +/- 6.5% of the mean for each level of catalyst loading. However, at 5%Fe catalyst loading the spread was +/- 14% with LFN outperforming IOT and CIO.

Nevertheless, from an overall perspective it is reasonable to consider that the catalysts types performed in a broadly similar manner with LFN being better at the highest PPT.

4.3.3.2 Product gas composition

Figure 4.4 provides a summary of the product gas compositions for each catalyst type across the range of PPTs and catalyst loadings. Again, it is clear that there is a common general pattern but with variability within it.

Focusing on hydrogen concentration initially it is clear that the different catalyst types have largely resulted in the same pattern and quantitative outcomes across the full spectrum of PPTs and catalyst loadings with a steady increase in hydrogen content as the PPTs increase, and a lesser increase as a response to catalyst loading. At PPT 600°C at each level of catalyst loading the hydrogen content was within +/-6% of the mean for each level of catalyst loading. As the PPT increased the performance of the catalyst types commenced diverging, at PPT 650°C CIO and LFN performed similarly being between 0% and 6% above the mean value while IOT was consistently 8% below the mean value for each level of catalyst loading. This pattern continued as the PPT increased and LFN continued to outperform and at PPT 700°C and 750°C it was 8% and 10% higher, respectively, than CIO; and 15% and 21% higher, respectively, than IOT.

The carbon dioxide concentration in product gas showed a steady downward trend with increasing PPT and this is consistent with early work predicting biomass pyrolysis products (Neves, Daniel et al. 2011) . It was also more uniform across catalyst types than hydrogen content. The maximum

variation from the mean was 9% but the results for all catalyst types at PPTs 600°C, and 650°C were generally within 4% of the mean for each level of catalyst loading and this remained so for LFN and CIO for PPTs 700°C and 750°C. The IOT type had quite variable results for PPTs 700°C and 750°C although the results were on trend with the other catalyst types. Notably AAEMs have been reported as causing CO_2 levels to drop more rapidly with some potential suppression of hydrogen production, also consistent with IOT type (Section 3.2.2.1) .

Carbon monoxide concentration in product gas was the most variable of the outcomes and was markedly higher with IOT type catalyst than CIO and LFN especially as catalyst loading increased. This is consistent with one specific effect associated with the presence of AAEMs, the yield of carbon monoxide is increased with increasing temperature which is consistent with the results in respect of IOT type. At PPT 750°C the CO concentration for IOT type catalyst was 10.2%, 13.4% and 19.3% as catalyst loadings increased, compared with 11.0%, 9.8% and 8.7% for CIO type and 6.3%, 5.6% and 8.6% for LFN type. Methane concentration across the spectrum of catalyst loading and pyrolysis temperatures were approximately 10% for LFN and CIO catalyst types but between 15%-20% for IOT type at low catalyst loadings. At higher catalyst loadings this difference moderated with IOT type falling in line with the results of the other types.

4.3.4 Hydrogen yields and hydrogen recovery

4.3.4.1 Hydrogen yields

Figure 4.4 provides hydrogen production data (mmol/g biomass) and shows that hydrogen production steadily increased across the spectrum of increasing PPTs and catalyst loadings. Notably, for the lowest catalyst loading (1.6%Fe) each catalyst type essentially demonstrated the same catalytic effectiveness (+/-2%) in respect of hydrogen production for PPTs 600°C, 650°C, and 700°C. However, for PPT 750°C the effectiveness of catalyst types CIO and IOT had fallen to 97% and 91% respectively. A similar trend emerged at the second level of catalyst loading (2.9%Fe) with each catalyst type essentially demonstrating the same catalytic effectiveness (+/-3%) in respect of hydrogen production for PPTs 600°C and 650°C but at the higher PPTs the effectiveness

of CIO and IOT fell away, being 86% and 78% at PPT 700°C and 84% and 85% at PPT 750°C, respectively. At the highest catalyst loading (5.0%Fe) the divergence in performance between catalyst type LFN and the other types had become evident even at PPT 600°C, and the gap continued to widen as PPTs increased, being 88% for both at PPT 650°C, 83% and 88% at PPT 700°C, and 70% for both at PPT 750°C.

Despite the lower levels of hydrogen production from catalyst types CIO and IOT compared with type LFN their relative effectiveness in terms of improving hydrogen yields from catalytic biomass pyrolysis remains significant as evidenced in Figure 4.5. Hydrogen production at PPT 750°C and catalyst loading of 5.0%Fe, using LFN type catalyst, increased by 203%, over baseline production at PPT 600°C. Notably, both CIO and IOT types produced increases of 175% under the same conditions.

4.3.4.2 Hydrogen recovery

Clearly the quantity of hydrogen available in the original biomass is fundamental to the quantity that can be produced. This is particularly relevant when considering the quantities of material that need to be processed to generate the desired product quantities. For many biomass the hydrogen content is between 5% and 7% so maximising the recovery of this source is critical. Figure 4.6 illustrates the increasing level of hydrogen recovery from catalytic pyrolysis from a baseline recovery at 600C of 10.8% rising to 22% for LFN catalyst type and 19% for both CIO and IOT types.

Data reported on hydrogen recovery through catalytic biomass pyrolysis at 800°C indicates recovery rates from around 5% to as high as 57%, but notably those above 25% are associated with more exotic catalysts (e.g.Re_2C, Ni/CeO2/Zro2). The highest reported recovery for iron based catalysts was 25% (Granados-Fitch et al. 2019). Those results, like those from this work, relate only to single-stage pyrolysis processes without steam gasification to ensure valid comparisons.

4.3.5 Relationship between hydrogen and char productions

The general pattern of hydrogen production and end of pyrolysis char production is the same for each catalyst type as shown in Figure 4.7. This

confirms that each catalyst supported similar reforming pathways in terms of the interaction with char to produce additional hydrogen. Research reported on using bio-char for tar reduction and char supported catalysts confirms the observation that not only is hydrogen production increased but also CO and CO_2, resulting in some consumption of char as reforming and cracking reactions proceed (Kosov, V, Kosov & Zaichenko 2014; Shen, YF, Chen, et al. 2015).

4.3.6 Distribution of primary products

Figure 4.8 shows the product distribution by primary products of normalised char, liquids including tars, and product gas. Each of the catalysts produced similar normalised char outcomes of approximately 26%(wt./wt. biomass) at PPT 600°C, reducing by approximately 1% for each 50°C rise to PPT 700C, but the outcomes were inconsistent at PPT of 750°C.

Product gas showed a broad trend of an increasing proportion of the total product yield in response to higher PPT and increased catalyst loadings, however there was significant variation between catalyst types and responses. IOT type had the highest gas proportion rising from 31% at PPT 600°C and 1.6%Fe to 39% at PPT 750°C and 5.0% Fe catalyst loading. LFN type had lower proportions than IOT type at each PPT, and an anomalous result at PPT 750C. CIO type showed the least response to increasing PPT reaching a maximum of 34% of the product mass at PPT 750C and 5%Fe catalyst loading. For the liquids product there is a slight trend to a reduced share of the total product in response to higher PPT, but increased catalyst loadings tend to increase the liquids produced. IOT type liquids content of the product was 42% at PPT 600C and 1.9%Fe catalyst loading which had reduced to 40% at PPT 750C and 5.0%Fe.

The overall scatter in results makes it difficult to draw conclusions from this data as to any specific differences in performance of the different catalyst types.

4.3.7 Effect of catalysts on tar production and component distribution

The gravimetric tar content of the product gas stream is shown in Figure 4.9 for the range of pyrolysis temperatures and catalyst loadings. Baseline results were generally around 20 g/Nm3 followed by small reductions as the catalyst loading increased to 12-15 g/Nm3. There is a high degree of scatter in the results

although across a narrow band. While it is not possible to draw specific conclusions from these results it is reasonable to presume that tar production is not strongly influenced by catalyst type.

Figure 4.10 shows the relative concentration of PAH components in the GC-MS samples of tar. At PPT of 600C the relative amounts of tar are broadly the same with high MW components (MW>200) being about 1 unit and lower MW components 2-3 units except for the CIO catalyst which had lower values. There was a barely perceptible trend to higher total PAH levels as catalyst loading increased.

At PPT of 650C the level of PAHs remained similar to those at 600C for CIO and LFN type catalysts but there was a notably change with IOT low MW PAH levels jumping almost 5-fold. At PPTs of 700C and 750C there was a more general increase in low MW tars with LFN type increasing to a steady 3-4 units and CIO type rising to 3 and then 5 units as the pyrolysis temperatures rose. IOT type continued to be an outlier with 10-14 units, and then rising to 18-20 units as the pyrolysis temperatures rose. There was little to suggest that catalyst loading had an influence rather it was an artefact of pyrolysis temperatures. This is consistent with a study on PAH formation during iron catalytic pyrolysis ((Zhao et al. 2020)). In this work it was found that the total PAHs produced increased with increasing pyrolysis temperatures, and the PAHs were distributed largely into the bio-oil and essentially less than 10% each in char and gas. In this case the iron catalyst was said to have reduced PAH formation by up to 33% from the baseline results. The latter finding is not supported by the results in this work and may reflect the difference in sweeping gas rates. A potential explanation for the significantly different result with the IOT catalyst may lie in the much higher levels of impurities in this catalyst type.

While the general trends show the catalyst types were producing essentially the same impacts, from the point-of-view of developing commercial hydrogen production using catalytic biomass pyrolysis selecting the IOT type catalyst offers significant benefits over other systems as it incorporates waste recycling, has low cost apart from transport from source, requires the simplest of preparations as it is already in “fines” form and suitable for direct ball milling with char, can be used in higher concentrations, at little cost, to offset marginal yield losses, and is reclaimable, recyclable, and environmentally benign.

4.4 Conclusions

To establish the potential for developing an effective lower cost catalyst for hydrogen production from catalytic pyrolysis this study examined alternatives to a conventional laboratory prepared ferric nitrate char supported catalyst (LFN). Commercial iron ore (CIO) and iron ore tailings (IOT) were selected, and appropriate preparation methods developed for these alternative catalysts.

Despite lower levels of hydrogen production from CIO and IOT types compared with LFN their relative effectiveness in terms of improving hydrogen yields from catalytic biomass pyrolysis remains significant with increases at pyrolysis temperature of 750C and catalyst loading of 5.0%Fe providing increases of 203% (LFN), 175% (CIO) and 176% (IOT) over baseline yields (3.0 mmol/g biomass).

Broad similarities were also found in product gas production, overall gas composition, the distribution of primary products and tar production. Variations in outcome are postulated as being a combination of the influence of potential variations in the iron contents in the catalysts made from commercial product and, by the presence of AAEMs.

Overall, it was concluded that the catalyst performed broadly in the same manner but neither CIO nor IOT was as effective as LFN. Nevertheless, it is proposed that IOT would be an appropriate choice as a commercial catalyst because of the many benefits it provides. When used in conjunction with the process developed of having the catalyst admixed with the biomass, the twin products of green hydrogen and char are amenable to integration into the iron and steel industry to deliver significant decarbonisation of the process.

.

Chapter 5: A two-stage catalytic pyrolysis process to enhance green hydrogen production

Richard Thomson[a], Philip Kwong[b,*]

School of Chemical Engineering and Advanced Materials,
Postal Address. The University of Adelaide South Australia 5005 AUSTRALIA
[a] richard.thomson@adelaide.edu.au
[b],* Author for correspondence
P: +618 8313 0724 E:philip.kwong@adelaide.edu.au

Statement of Authorship

Title of Paper	A two-stage catalytic pyrolysis process to enhance green hydrogen production
Publication Status	☐ Published ☐ Accepted for Publication ☐ Submitted for Publication ☑ Unpublished and Unsubmitted w ork w ritten in manuscript style
Publication Details	

Principal Author

Name of Principal Author (Candidate)	Richard Thomson
Contribution to the Paper	Development of the concept. Construction and development of the experimental apparatus. Development of the experimental methodology. Performance of experiments and interpretation of results. Responsible for drafting and revision of the paper.
Overall percentage (%)	80%
Certification:	This paper reports on original research I conducted during the period of my Higher Degree by Research candidature and is not subject to any obligations or contractual agreements with a third party that would constrain its inclusion in this thesis. I am the primary author of this paper.
Signature	Date: 20 Apr 2022

Co-Author Contributions

By signing the Statement of Authorship, each author certifies that:

i. the candidate's stated contribution to the publication is accurate (as detailed above);

ii. permission is granted for the candidate in include the publication in the thesis; and

iii. the sum of all co-author contributions is equal to 100% less the candidate's stated contribution.

Name of Co-Author	Philip Kwong
Contribution to the Paper	Corresponding author. Assisted with the development of the concept and experimental methodology. Major contribution to the writing and revision of the paper.
Signature	Date: 20/4/2022

Name of Co-Author	
Contribution to the Paper	
Signature	Date:

Please cut and paste additional co-author panels here as required.

DECLARATIONS

Funding: The authors did not receive support from any organisation for the submitted work.

Conflicts of interest: The authors have no conflicts of interest to declare that are relevant to the content of this article.

Availability of data: If requested additional data associated with this research project can be accessed by contacting the authors.

Code availability: Not applicable

ABSTRACT

A novel process for producing hydrogen-rich gas was developed using catalytic pyrolysis and its char product in a two-stage fixed bed reactor, with both beds at the same temperature. Almond residue was used as biomass together with two different mechano-chemically prepared, iron-based, char supported catalysts. The effects of operating temperature (600°C-750°C), catalyst type and catalyst loading were investigated in terms of yields of total gas, hydrogen, and syngas.

Total gas production increased in line with increasing pyrolysis temperatures and catalyst loadings (Baseline, 1.6%, 2.9% and 5.0%Fe), rising from 10mmol/g at 600°C, baseline to 15 mmol/g at 750°C, and 5.0%Fe loading, during one-stage pyrolysis; and increasing from 11 to 20 mmol/g at the same conditions for two-stage pyrolysis. Hydrogen production relative to baseline at 600°C operating temperature increased in one-stage processing by 100% at 750C, 5.0%Fe, whereas in two-stage processing the yield was 180% of baseline, representing a recovery of 30% of the available hydrogen in the biomass. Increases in syngas production (60%) were also pronounced due to higher CO production at higher pyrolysis temperatures, bringing improved H_2/CO ratios. These results demonstrate the major influence of catalysis, as well as the benefits of two-stage processing.

The comparative results of the two catalysts used: laboratory ferric nitrate (LFN) and commercial iron ore tailings (IOT) during two-stage processing confirmed that IOT was equally as effective as LFN when used at the same Fe_2O_3 concentrations in the prepared char supported catalyst. This further enhances the development of this process for producing green hydrogen through recycling of waste ore.

Key words: Two-stage, iron ore tailings, green hydrogen, pyrolysis, steel industry

5.1 Introduction

In 1994 the concept of a two-stage gasifier was introduced (Henriksen et al. 2003) and 10 years later, based on the Viking demonstration unit, they described the benefits they could identify from this design. Primarily these were simple operation, with a high degree of process control, allowing unattended operation; separation of the different reaction zones allowing modification of conditions for each zone, and highly consistent gas product composition and heating value, and major reductions in tar content of the produced gas.

The concept has been taken up and further developed by companies such as TARPO (Brynda et al. 2016) and Xylergy SA (SA 2022) and resulted in commercial developments which demonstrated the same benefits as those identified in the Viking unit yet with somewhat simpler designs. While these developments were focused on biomass gasification it became apparent that other thermochemical processes may benefit from the same approach. In 2013 experimental work on a laboratory reactor designed to simulate two-stage pyrolysis was reported (Kosov, V.V. et al. 2013), with a lower chamber being the pyrolysis chamber and the upper the second stage, packed with char from a previous pyrolysis and operated continuously at a higher temperature (1000°C). An increase in non-condensable gas production was observed. Further work reported in 2015 (Kosov, V. V., Kosov & Zaichenko 2015) provided insights into the proportion of char required to promote the heterogenous catalytic conversion of tars and other compounds, and the proportion of additional gas production due solely to thermal cracking. In total, the gas volume was doubled and the H_2 content of produced gas increased by 60% by using a recovered char bed of half the mass of the pyrolysis bed.

More commonly fast pyrolysis has been used to maximise liquids production as this provides great flexibility in the final products which may include H_2, syngas, fuels and chemicals. The composition and quantity of these products and the possibility of their use as a fuel have now been well studied (Bridgwater 2012). The import of the above work is that a pyrolysis-only process can also be used to produce both hydrogen and synthesis gas in significant quantities by utilising secondary thermal and heterogeneous catalytic cracking of some of the potential

liquid products of the primary pyrolysis. Several advantages accrue in such a two-stage pyrolysis compared with the air gasification process developed by Henriksen and generally used commercially. Firstly, the produced gas has a higher calorific value due to the reduced presence of nitrogen; secondly, it produces a syngas within the preferred H_2/CO ratio; and thirdly, it has a lower cost.

Considerable interest has more recently developed in two-stage pyrolysis-reforming with results suggesting that this process strongly challenges biomass gasification and bio-oil reforming for hydrogen production (Arregi, Aitor et al. 2018). In some cases the reforming is conducted in conjunction with steam injection and in most designs the reforming section is fixed bed of catalyst (Santamaria et al. 2021). Others have used spouted bed or fluidised bed systems for the reforming section but like fixed bed systems identifying catalysts that are not de-activated, largely due to coke deposition, has proven difficult (Arregi, A. et al. 2015; Singh et al. 2019). This has led to the use of char and char supported catalysts to catalyse the reforming reactions with encouraging outcomes (Wang, Y et al. 2022).

With the primary focus of biomass processing now shifted to hydrogen production the concept of two-stage pyrolysis is seen as particularly attractive; offering lower cost, which addresses one of the major impediments to many renewable hydrogen technologies (Fernyhough, James 2021). To maintain that advantage the keys are a design that remains simple; a catalyst system that is also simple and low cost, and, desirably, a second stage that operates efficiently and effectively at the same temperature as the pyrolysis temperature.

Design concepts for two-stage pyrolysis and reforming have included fixed bed pyrolysis and catalytic reactors, fluidised bed pyrolysis combined with fixed bed reforming; a screw conveyor pyrolysis reactor combined with fixed catalyst bed reforming reactor and various combinations of spouted beds and fluidised beds; many with steam addition at either stage to further increase hydrogen yields (Arregi, Aitor et al. 2018).

The objective of this work is to utilise a mechano-chemically prepared catalyst in the pyrolysis stage and to provide a second thermal and heterogeneous cracking stage where the pyrolysis gases pass through a bed of char plus catalyst recovered from an identical prior pyrolysis. The major areas of

interest are the effects of operating temperature (600°C-750°C), catalyst type and catalyst loading in terms of yields of total gas, hydrogen, and syngas compared with one-stage pyrolysis.

5.2 Materials and Methods

5.2.1 Materials

5.2.1.1 Biomass

Biomass feedstock of almond residues was sourced from a local almond processing mill (Laragon Pty Ltd, Renmark, South Australia). Biomass was prepared by drying at 105°C for 6 hours, grinding in a DeLonghi DEDICA coffee grinder, and sieving to provide material of <500µm for experimentation. The prepared material was allowed to re-absorb moisture from the atmosphere prior to pyrolysis.

5.2.1.2 Catalyst support

Prepared biomass was pyrolysed to produce char as the support for the catalyst. Weighed quantities of biomass were pyrolysed in the packed bed reactor using a heating rate of approximately 15°C per minute, in a N_2 atmosphere to peak temperatures of 600°C, 650°C, 700°C and 750°C which were maintained for 30 minutes. The samples were cooled to ambient temperature and the yield of char recorded. The char was subsequently ground to <500 µm for use as catalyst support.

5.2.2 Catalyst Preparation

5.2.2.1 Pyrolysis catalysts

Two different catalysts were prepared, one from laboratory sourced ferric nitrate (LFN), and another from commercial iron ore tailings (IOT). The preparation procedures varied for each catalyst source.

LFN was prepared by making up a primary solution of 80g $Fe(NO_3)_3.9H_2O$ (Chem-Supply (Australia), AR grade: 98.0% minimum assay) in 200ml distilled water, and 2 additional solutions by diluting with distilled water, the primary solution 1:1, and another 1:3. The concentration of these solutions were

determined from the volume of water required to fully wet the char. Solutions were added to chars (produced at one of the selected PPTs) at the rate of 5ml per 1g char. Each mixture was then heated to 250°C for 6 hours in air to thermally decompose the iron nitrate to Fe_2O_3. The decomposition was confirmed by measuring the weight loss (Melnikov et al. 2013; Vander Wall 1962).

The calcined product was milled in duplicate 6g batches in a Fritsch *Pulverisette 7* planetary mill at 700 rpm for 120 minutes using 70g of 3mm zirconia balls in a 45 ml zirconia grinding bowl. This produced, for each of the selected peak pyrolysis temperatures, a range of char supported catalyst samples with either 6.3%, 11.6% or 19.8% Fe (wt./wt.).

IOT was supplied by FMG, being a sample from their tailings dam. The analysis of the sample as supplied, and its particle size distribution are shown in Table 5.1 and Table 5.2 respectively.

Quantities of the IOT powder that would provide Fe(wt./wt.) concentrations in the prepared catalysts equal to those of the LFN preparations were added to chars (produced at one of the selected PPTs) and then thoroughly mixed prior to milling as for the LFN catalyst preparation. Given the nature of the IOT material and the sub-sampling of a non-uniform product, it was expected that there would be some minor variability in the final ferric oxide concentrations of these catalysts.

5.2.2.2 Second stage catalysts

Catalysts used in the second stage fixed bed were prepared from char recovered from the equivalent one-stage pyrolysis trials. At the completion of a one-stage pyrolysis the sample container was cooled to ambient, removed from the furnace and weighed. The char residue (also containing catalyst, if a catalytic pyrolysis) was loose and friable, and readily removed from the sample container. Char residue was stored in a sealed container until required for the two-stage experiment when it was lightly crushed in a pestle and mortar prior to loading into the SSSC.

5.2.3 Biomass pyrolysis

5.2.3.1 Experimental setup

A laboratory scale packed bed first stage sample container (FSSC)(38.1mm dia, 225mm long) was loaded with biomass or biomass/catalyst mixture

(approximately 40g) for the first stage pyrolysis. A second packed bed sample container (SSSC) (38.1mm dia, 75mm long) was loaded with recovered char or recovered char/catalyst mixture for the second stage pyrolysis. Both were mounted inside a reactor chamber (44.5mm dia, 800mm long) which was encased by a series of separately controllable electrical heating elements (each 300mm long) forming the basis of the experimental vertical furnace. When in place the base of the FSSC was located 185mm from the entry of the furnace, so that the centre of the sample container was approximately at the mid-point of the first element. The base of the SSSC was mounted 725mm from the entry, in line with the mid-point of the third element. Thermocouples were located at just prior to the FSSC at 170mm, at 250mm (inside the FSSC), at 740mm (inside the SSSC) and at 790mm at the exit from the reactor. A small nitrogen purge (0.1 litres/min) passed through the thermocouple inlet while a larger nitrogen sweeping gas flow (2 litres/min) entered at the base of the reactor to carry the produced gas out of the reactor and through the process train (Figure 5.1). The reactor space was swept 1.6 times per minute.

At commencement of a trial the heating of the SSSC was started 10 minutes prior to the heating of the FSSC to ensure the second stage was up to temperature when the pyrolysis process commenced. Then both the FSSC and SSSC were heated to one of four pyrolysis peak temperatures (PPT) controlled by all elements and the product gases passed through the reaction chamber to the exit line.

The product then immediately passed through a particle filter, encased in a cylindrical heater operating at 250°C, before entering a gas scrubbing train. This gas scrubbing train was set up in accordance with the CEN Technical Specification (van de Kamp W. 2006) to collect condensable vapours and tars. Non-condensable gases passed through a fine filter before being sampled for GC analysis and metered to determine production volumes. After cooling the residual mass was recovered from the packed bed.

Normalised char residue was calculated from the residual mass on the basis that the char formed from biomass degradation and char present as catalyst carrier were equally likely to participate in reactions involving chars, as the char carrier was originally produced in a non-catalytic environment.

5.2.3.2 Biomass pyrolysis

An experimental matrix was developed to examine the products of two-stage pyrolysis of biomass, at four PPTs (600, 650, 700 and 750°C), and using four levels of catalyst loading (Baseline, 1.6%Fe, 2.9%Fe, and 5.0%Fe) and of two different iron-based catalysts (LFN and IOT).

Biomass was prepared as described in Section 5.4.2.1.1 above. For the FSSC, baseline samples contained approximately 40g biomass while catalysed samples were prepared by adding 10g catalyst to 30g of biomass so that each catalysed sample had approximately the same catalyst support char loading and an Fe loading of either 1.6%, 2.9% or 5.0%. The biomass and catalyst were mixed in a DeLonghi DEDICA coffee grinder for 45 seconds.

Char for the SSSC was obtained from the recovered char of an equivalent one-stage pyrolysis, so baseline char had no catalyst while other chars included the catalyst from the initial pyrolysis. Approximately 7 g char was loaded into the SSSC.

The biomass mixture and char were loaded into weighed sample carriers and inserted into the vertical furnace. The nitrogen purge and sweeping flows were used to purge the sample chamber for 15 minutes. The heating rate was set at 50°C/min up to the relevant PPT and then maintained at this temperature for 30 minutes.

5.2.4 Sampling and analysis

5.2.4.1 Gas analysis

Samples for GC analysis were delivered by a bypass line prior to the flow measurement. A three column Agilent 470 microGC was used but only columns one and two were used. Column one, MS5 mol sieve, measures major gases such as He, H_2, O_2, N_2, CH_4, and CO, and column two, PoraPLOT U (PPU), measures CO_2, C_2H_4, C_2H_6, and C_2H_2.

The data acquisition system provided recorded data from the thermocouples and the product gas flow after tar extraction, with the GC providing a sequential analysis of the gas composition. A series of trials were undertaken to establish a relationship between reactor temperature, sweeping gas flow and

time difference between acquired data and microGC sampling to time align all data for processing.

5.2.4.2 Tar analysis

At the completion of the experiment the sample container and particle filter assembly were cooled in a nitrogen atmosphere and then re-weighed to determine residual mass and particle content of the product gas, respectively. Ultimate analysis of the residual mass was carried out using a CHNS elemental determinator (PerkinElmer , 2400 Series II CHNS/O). The ultimate analysis for C, H, N, S, and O was carried out following ASTM D5373. The O content was determined by difference. The isopropanol and bio-oil mixture in the gas bubbler train was collected, mixed, weighed and sub-sampled for roto vacuum distillation to recover the tars. The tars were analysed using GC-MS. PAH analysis of the tar samples was carried out by extracting 1 mL of representative tar in 1 mL of dichloromethane and 1µl of 2mg/ml Semi-volatile Internal Standard Mix of deuterated PAHs (Supelco 4-8902) was added prior to analysis.

Analysis was conducted on an Agilent 5977B GCMS system by direct injection of 1µl of extract. Separation was conducted using a 30m, 0.25mm ID DB-5MS capillary column with helium carrier gas at a constant flow rate of 1ml/min over the temperature program from 50^{o}C, held for 1 min. ramped to 300^{o}C at 8^{o}C /min and held for 7 mins. Compounds were detected using SIM/scan mode with selected ion groups of ion mass/charge ratio being Group 1; 128, 136, Group 2; 152, 154, 166 178,188, Group 3; 202, 228, 240, Group 4; 252, 264, 276 & 278 monitored and a full scan range of ion mass/charge ratio from 45 to 400. Quantification of the EPA16 target PAHs was conducted against a calibration curve generated by injecting known quantities of PAH Mix (Sigma-Aldrich CRM47543) diluted in dichloromethane using the SIM grouping ions.

5.2.5 Mass balance

The normalised char was calculated on the basis that char formed from biomass degradation and char present as catalyst carrier were equally likely to participate in reactions involving chars, as the char carrier was originally produced in a non-catalytic environment.

As the mass of total liquids was the least reliable direct measurement it was determined by difference from the mass of all other reactants and products. The mass balance was calculated from the following:

$$(M_{bt} - C_{fe1} - C_{ch})_{fsp} + (M_{rc} - C_{fe2})_{ssr} - M_p - (V_{gT} \times F_i \times \rho_i) - M_{bc} - (M_{rcr} - C_{fe2})_{ssr} = M_{liq}$$

Where: M_{bt} is the total mass of biomass mix loaded

C_{fe1} is the mass of iron oxide included , if any

C_{ch} is the mass of char carrier included , if any

$_{fsp}$ denotes First Stage Pyrolysis

M_p is the mass of particulates collected on the gas filter

V_{gT} is the temperature corrected volume of gas

F_i is the fraction of the gas volume attributable to component *i*

ρ_i is the density of component *i*

M_{bc} is the mass of residual char attributable to the biomass,

M_{rcr} is the mass of recovered char residue and

M_{liq} is the mass of liquids and tar

The total mass of liquids was subsequently divided into liquids other than tar (essentially bio-oil and water) and gravimetrically determined tars. Baseline samples were conducted in triplicate and several catalysed samples were conducted in duplicate to confirm consistency of results.

5.3 Results and Discussion

5.3.1 Characterisation of biomass and catalyst

5.3.1.1 Biomass

The characteristics of the almond residue feedstock are shown in Table 5.3. The proximate analysis is typical of those reported for almond shells whereas almond husks show higher ash (6%) and consequently lower fixed carbon.

5.3.1.2 Catalyst

The catalysts were characterised by particle size analysis. A selection of the catalyst samples was analysed for particle size distribution using a Malvern Mastersizer 2000 particle size analyser. In each case 0.5g of char supported catalyst was placed in 20ml water and agitated for 2 hours prior to adding to the circulating water in the analyser. Typically, the mean size was approximately 5 µm with 10% below 0.5 µm and 10% above 10 µm.

5.3.2 One-stage pyrolysis

As shown in Figure 5.2 the first production of gas with one-stage catalytic pyrolysis occurred around 200°C with the commencement of CO_2 evolution followed by hydrogen between 200° and 300°C with CO and CH_4 beginning to appear above 300°C. The gas composition between 300°C and 500°C is largely made up of CO_2 and CO, this being the period during which hemi-cellullose and cellulose are the primary components being degraded (Kan, Strezov & Evans 2016). Hydrogen production increased substantially from 500°C peaking at around 600°C but continued until approximately 675°C which is also the temperature range in which lignin decomposition occurs (Chapter 2) (Yang, HP et al. 2007).

Biomass undergoes thermal degradation during the pyrolysis process and in addition to the gas produced, char, bio-oil and tars are products of the reactions. Catalytic pyrolysis can improve gas yields (Figure 5.3), but tar and CO_2 content of the product stream remain high providing the potential for creating further reactions during a reforming or second stage process. It provides an opportunity to breakdown the more complex hydrocarbons produced during pyrolysis into the permanent gases thus increasing hydrogen and CO content. This can occur from a range of possible reactions:

Tar cracking reactions:

$$Tar \rightarrow C + CmHn + gases \qquad (5.1)$$

Tar dry reforming reactions:

$$CmHn + mCO2 \rightarrow 2mCO + (n/2)H2 \qquad (5.2)$$

$$CmHn + (m + n/2)CO2 \rightarrow (2m + n/2)CO + (n/2)H2O \qquad (5.3)$$

Tar steam reforming reactions:

$$C_mH_n + mH2O \rightarrow mCO + (m + n/2)H2 \quad (5.4)$$

$$C_mH_n + 2\ mH_2O \rightarrow mCO2 + 2(m + n/2)H_2 \quad (5.5)$$

And gas reactions:

$$CH_4 + H_2O \leftrightarrow CO + 3H_2 \quad (5.6)$$

$$CO + H_2O \leftrightarrow CO2 + H_2 \quad (5.7)$$

$$C + H_2O \leftrightarrow CO + H_2 \quad (5.8)$$

$$C + CO_2 \leftrightarrow 2CO \quad (5.9)$$

While the gas reactions rely on the presence of water vapour, part of which may be derived from the biomass generally it is considered that additional water vapour (steam) is required to maximise hydrogen production. This is also likely to be the case to fully exploit the tar steam cracking reactions (Wang, Y et al. 2022). These considerations have led to the development of in-line secondary processing of the pyrolysis products to improve yields of both hydrogen and syngas.

5.3.3 Impact of one vs two-stage pyrolysis on product outcomes

5.3.3.1 Product gas production

Figure 5.3 shows the total gas production for both one-stage and two-stage pyrolysis using LFN type catalyst. Clearly in every case, including baseline, the two-stage pyrolysis has resulted in increased gas production. The one-stage results showed a steady increase in gas production in response to increased catalyst loading and while this was largely mirrored in the two-stage results, the marked difference was the extent of improvement at baseline; consistent with a number of observations on the effectiveness of bio-char as a catalyst for second-stage reforming processes including tar decomposition (Buentello-Montoya et al. 2020; Sun et al. 2020; Zeng et al. 2020).

Baseline results reflected increases from 9.8, 10.0, 10.8 and 11.3 mmol/g to 11.3, 17.0, 16.8, and 16.1 mmol/g respectively, as the PPT increased from 600°C to 750°C. These changes represent substantially increased gas production of a 15%, 70%, 56% and 43%. For catalytic pyrolysis the increases using two-

stage pyrolysis compared with the equivalent one-stage result were, at 1.6%Fe LFN catalyst loading, 22%, 26%, 19%, and 41%; and at 2.9%Fe loading 15%, 34%, 6% and 35% while at 5.0%Fe loading the results were 31%, 26%, 30%, and 36% respectively, as the PPT increased from 600°C to 750°C. This illustrates that for every PPT and catalyst loading a second-stage processing has improved gas yields.

5.3.3.2 Hydrogen production

Figure 5.4 illustrates the change in hydrogen production for both one-stage and two-stage pyrolysis using LFN type catalyst. Hydrogen production in one-stage reactions increased consistently in response to increased catalyst loading and PPTs. Two-stage results showed a similar pattern and as with total gas production, hydrogen production delivered increases at all catalyst loadings except for the baseline at PPT 600°C.

One-stage pyrolysis baseline production rose from 3.1, 3.4, 3.7 and 4.1 mmol/g biomass whereas two-stage baseline production rose from 2.8, 6.9, 6.4 and 5.4 mmol/g respectively across the spectrum of PPT from 600°C to 750°C, providing increases from two-stage pyrolysis of -12%, 100%, 74% and 25%. At 1.6%Fe catalyst loading these increases were 38%, 33%, 27% and 32% while with 2.9%Fe catalyst loading hydrogen production was increased by 32%, 47%, 32% and 22% respectively as PPT rose from 600°C to 750°C. Results for the peak catalyst loading (5.0%Fe) saw one-stage productions of 4.6, 5.5, 6.2 and 6.4 mmol/g compared with two-stage outputs of 6.5, 7.3, 8.5, and 9.0 mmol/g. This provided increases in production of 43%, 34%, 37%, and 39%. This compares with results using rice husk biomass, and a second stage fixed bed char supported iron catalyst, where H_2 yields were somewhat lower at 2.75 mmol/g at 600°C and 3.1 mmol/g at 700°C (Guo, FQ et al. 2018).

The overall improvement in hydrogen yield was compared to that of the baseline one-stage at PPT 600°C in Figure 5.5 showing that even at this PPT and peak catalyst loading (5.0%Fe) one-stage production had risen by 40% and two-stage production by 100%. As the PPT progressively increased (650°C, 700°C, and 750°C) so did the yields, with one-stage achieving increases of 60%, 95% and 100% respectively and two-stage recording increases of 140%, 160%, and

180% respectively. Very importantly these results also confirmed that IOT catalyst produced results equivalent to LFN, and therefore further underwrote its selection as a potential commercial catalyst.

5.3.3.3 Syngas production

Second stage reforming not only improves hydrogen yields but also can have a significant impact on syngas yields. Figure 5.6 compares the syngas production from one and two-stage pyrolysis and clearly identifies the significant increases obtained under certain conditions.

With a PPT of 600°C one-stage results commence at 3.85 mmol/g rising steadily to 5.0 mmol/g while the two-stage results commence at a similar level of 4.0 mmol/g for the baseline and increase immediately to between 6.7 and 7.2 mmol/g for all catalyst loadings. At the peak PPT of 750C the one-stage result is between 5.4 and 7.7 mmol/g while the two-stage production has jumped to 8.3 to 11.9 mmol/g which reflects a combination of tar conversion and additional CO produced at the higher temperature, and if there is water vapour present. In the rice husk trials mentioned above, the syngas production using two-stage catalytic reforming was reported as 9.1 mmol/g at PPT 600C and 12.3 mmol/g which were 20% and 3% higher respectively than this work (Guo, FQ et al. 2018). This compares with results using rice husk biomass, and a second stage fixed bed char supported iron catalyst, where H_2 yields were somewhat lower at 2.75 mmol/g at 600°C and 3.1 mmol/g at 700°C (Guo, FQ et al. 2018). The other result based on the bimetallic K-Fe catalyst using peanut shell char, with a reforming catalyst/biomass mass ratio of 0.4, produced 5.6, 6.3 and 8.3 mmolH2/g at second stage temperatures of 600°C, 700°C and 800°C the syngas production was 15.1, 17.6 and 21.4 mmol/g respectively, (Guo, F et al. 2020) with the higher syngas being due solely to higher CO production.

5.3.3.4 H_2/CO ratio

As noted above, the two-stage process increased H_2 and CO production at higher pyrolysis temperatures (>600°C) and as a consequence brought H_2/CO ratios closer to the preferred range of 2:1 (fuels, chemicals production) to 4:1 (hydrogen production) (Thomson & Kwong 2020). Figure 5.7 shows H_2/CO ratio for one and two-stage pyrolysis gas and notably at PPT of 600C the outcomes

are similar with the ratio rising from 4 to 10 for one-stage and from 2 to 8 for two-stage with increasing catalyst loading, reflecting an almost static CO production as H_2 production increases. At PPT 650°C this effect is moderated to some extent with the range being from 2 to 6, again increasing with catalyst loading. With the temperature increasing to 700°C the one-stage ratio was 2 across the full range of catalyst loading while two-stage pyrolysis had a similar outcome to that at PPT 650°C, while at 750C both one and two-stage pyrolysis produced gas with a 2:1 ratio for all catalyst loadings.

5.3.4 Impact of different catalysts in two-stage pyrolysis product outcomes

5.3.4.1 Product gas production

As Figure 5.8 shows the two catalysts essentially produced similar levels of total gas production across the spectrum of PPTs and catalyst loadings. At the lowest PPT (600C) LFN type had lower production than IOT type at baseline (11.3 vs 14.0 mmol/g) but steadily increased to be 10% higher (16.5 mmol/g) at the highest catalyst loading. This pattern was broadly repeated as PPTs increased but the differences were less marked at the baseline and low catalyst loadings (+/-4%) with LFN outperforming IOT at the higher loadings by 5-12%. Nevertheless, these results strongly support a view that the catalyst types had very similar impacts on total gas production, across the spectrum of PPT and catalyst loading, during two-stage pyrolysis.

5.3.4.2 Hydrogen production and recovery

Hydrogen production for each of the catalyst types in two-stage pyrolysis is shown in Figure 5.9, and the outcomes for each catalyst type are very similar, with over 85% of the results being within +/-5%. These results strongly support a view that the catalyst types had very similar impacts on hydrogen production, across the full range of PPT and catalyst loading, during two-stage pyrolysis.

An important consideration in assessing the relevance of the change in yield is to examine the proportion of original hydrogen in the biomass recovered in the product gas. Figure 5.10 shows the percentage recovery achieved under the various conditions of PPT, catalyst type and catalyst loading. From the baseline level of 9.5% recovery catalytic two-stage pyrolysis rapidly improved recovery to

about 20% at PPT of 600°C, then 25% at PPT 650°C, rising to 28% and 30% respectively, at PPT of 700°C and 750°C

5.3.4.3 Syngas production

Comparing syngas production is another measure useful in assessing how comparable are the different catalysts, as it is a guide to the overall gas composition resulting from the two-stage catalytic process. Figure 5.11 clearly indicates that the quantity of syngas produced by each catalyst for each of the range of variables is very similar, with over 80% of the results being within +/-5%. Figure 5.12 shows the energy content of the syngas, increasing by 36% from a baseline at 600°C of 7.2 MJ/Nm^3 to 9.8 MJ/Nm^3 with increasing pyrolysis temperature and catalyst loading, and the energy produced per kg biomass increasing by 230% from 1.60 MJ/kg to 3.66 MJ/kg.

5.3.4.4 Tars

It has been noted that catalysts when admixed with biomass in one-stage pyrolysis have little impact on PAH tar production, particularly when sweeping gas rates are high. This is attributed to the tars and gases being moved away from the catalyst almost immediately they are formed (Chapter 3). However, with two-stage processing there is an opportunity in the second stage for catalytic cracking and reforming of tars which leads to increased gas production.

Figure 5.14 shows the relative concentration of PAHs in terms of low MW(<200MW) and higher MW for two-stage pyrolysis over the range of PPTs and catalyst loadings investigated. In addition, the results of one-stage pyrolysis using IOT type catalyst (which returned the higher levels for the different catalyst types) is provided for comparison. While the trend is the same as observed for one-stage results, that is, the concentration of PAHs increases with pyrolysis temperature, a somewhat different pattern emerges, with the IOT catalyst in two-stage mode having the lowest results, and distinctly lower than one-stage results, while LFN has returned higher relative concentrations but also lower than one-stage results.

The reason for the lower results with two-stage processing becomes apparent from Figure 5.14 which shows the distribution of PAH components for baseline samples at 650°C and 750°C and catalysed samples (5%Fe loading) at

the same PPTs following a two-stage pyrolysis. Interestingly, all the samples show primarily the same pattern of distribution which supports the previous observation that even baseline two-stage pyrolysis provides significantly superior outcomes to one-stage pyrolysis. Notably, however, nearly all high MW PAHs have been reduced to simpler components or been broken down entirely to gaseous products. In either case the impact of two-stage processing can be seen to be significant in respect of residual tars.

5.4 Conclusions

Using mechano-chemically char supported iron catalyst for pyrolysis and recovered residual pyrolysis char (which may contain residual catalyst) as reforming catalyst a novel two-stage fixed bed catalytic pyrolysis process was used for hydrogen-rich gas production.

The significant findings included that the two-stage process was clearly superior to an equivalent one-stage process yielding higher total gas production of 20 mmol/g (33% increase), higher hydrogen production of 9 mmol/g (41% increase) and higher syngas production of 12 mmol/g (52% increase). The H_2/CO ratio was in the preferred range at pyrolysis temperatures of 700°C and 750°C. Additionally tar levels were reduced and high MW tars almost totally eliminated. Notably the improvement in baseline performance was very strong at low pyrolysis temperature reflecting the role of char alone in catalysing reforming reactions.

In respect of the two catalyst types, based on total gas, hydrogen and syngas production it is reasonable to state that both catalysts were equally effective. This is despite the different preparation methods and sources of iron, which suggests the method of preparing the IOT char supported catalyst will be amenable for any source of Fe_2O_3, subject to the nature of the impurities included.

Overall, this process develops a pathway to maximise the recycling of waste materials, and further progress the two-stage catalytic pyrolysis process for producing green hydrogen.

.

Chapter 6: Contributions and Recommendations

This Chapter summarises the key contributions and recommendations of this thesis for the development of a low temperature two-stage catalytic pyrolysis process for low-cost hydrogen production. In particular, it offers a pathway to integrate green hydrogen production with iron and steel making, by recycling waste iron ore tailings.

6.1 Research Findings

6.1.1 Justification for Research

The challenge addressed in this thesis has been to develop a fundamentally lower cost approach to thermochemical conversion of biomass and yet upgrade the value of the product slate to make biomass a more competitive source of renewable energy.

Some of the critical remaining drawbacks to the widespread use of biomass as an energy source are the low energy density of many feedstocks, the difficulty to successfully scale up, and the capital cost of processing plant. On the other hand, biomass thermochemical conversion offers a product gas that has potential as both a fuel and a source of synthesis gas for processing to transport fuels, chemicals and hydrogen which are critical replacement raw materials and products as fossil fuels are phased out.

Thermochemical conversion of biomass has largely been the domain of biomass combustion and gasification. Biomass pyrolysis has, until recently, been the “poor cousin” of the thermochemical technologies but its advantages have lately been better recognised with renewed interest by several researchers. Chief of the advantages are the potential for significantly lower capital costs, simpler gas processing, lower energy requirements plus the possibility of incorporating a second stage reforming step aimed particularly at increasing the hydrogen content of the product gas.

However, to-date there has been little recognition of the importance of the cost of the catalytic processes that are required to improve product yields and reduce tars; and given the fundamental role that they play in improving the overall outcomes of pyrolysis it was important to examine this element of the process.

Much of the research to-date involves catalysts that are difficult to fabricate, use expensive materials, and operate in fixed beds with high rates of degradation; and therefore, the importance of examining alternative catalysts with a focus on commercial operations was evident.

Similarly, the two-stage processes frequently utilise fixed bed systems requiring specialised catalysts that may be subject to coking and other degradation effects that require cyclic regeneration or catalyst replacement, leading to higher operating costs. So, the second element of investigation that was evident was a process design that mitigated these impacts on operations and costs.

The final element was to examine ways to increase the value product slate by demonstrating the potential to increase the value of all product streams.

6.1.2 Catalyst selection and design

To best meet the criteria of a catalyst suited for commercial application (Chapter 1) iron was selected as the preferred metal to incorporate in a char supported catalyst. Primarily this selection was supported by ready availability, cost, and being environmentally benign but also it is well recognised as a catalyst in biomass pyrolysis and gasification (although not the best). Three sources of iron were selected reflecting increasing availability, decreasing degrees of purity and consequently lower costs (LFN, CIO and IOT respectively). Char, as catalyst carrier, would be resource generated in the process.

Traditional preparation methods of catalysts were precipitation onto the carrier or impregnation into the carrier but both methods are generally time consuming, resource use intense, and require complex processing. Impregnation of the catalyst direct into the biomass has been shown to be successful but the process remains complex. Mechano-chemical processing was adopted although the standard impregnation method was used for comparison (Chapter 2). The general mechano-chemical technique was purpose adapted for each catalyst type utilising the simplest processing that the preparation technique allowed (Chapter 4).

6.1.3 Influence of catalysts on reaction kinetics

Initially the impact of the mechano-chemically prepared LFN catalyst on reaction kinetics and the degradation of the ligno-cellulosic components was explored using thermogravimetric analyses (Chapter 2). Deconvolution of DTG data showed the major ligno-cellulose components responded to the catalyst, lowering the onset decomposition temperature, reducing the temperature at which peak rates were achieved while developing up to 40% higher decomposition rates. Total mass loss increased by 20% and the required apparent activation energy reduced for each of the components. Char yields reduced by up to 25% compared to baseline outcomes.

This provided direct evidence of the positive impacts of the catalyst on reaction kinetics.

6.1.4 Selecting the preferred catalyst

Catalysts were tested in a series of identical single-stage catalytic pyrolysis experiments using almond residue (AR) as biomass. The total gas production, hydrogen production, and other key measures across a range of pyrolysis temperatures and catalyst loadings demonstrated that at pyrolysis temperatures between 600°C and 700°C and with catalyst loadings up to 2.9%Fe(wt.% biomass) there was no significant difference in outcomes from the different catalyst types. However, at 750°C and at 5.0%Fe loading the purer form of iron (LFN) was up to 20% more effective.

It was concluded however that on balance the lowest cost catalyst type, involving the simplest processing (IOT), would be an appropriate commercial style catalyst providing the opportunity to recycle and valorise a waste product. (Chapter 4).

6.1.5 Influence of catalyst on product yields and composition

It was observed that the one-stage catalytic pyrolysis created significant differences in product yields and composition compared with baseline outcomes. Non-condensable gas yields increased both with increasing pyrolysis temperatures and with increased catalyst loadings, being approximately 25-30% higher at 600°C, 35% higher at 650°C, 45% higher at 700°C and 35% higher at 750°C than the corresponding baseline value. Normalised char yields reduced in

line with increasing hydrogen production (Chapter 2), and liquid yields decreased with increasing pyrolysis temperatures but increased with catalyst loading. Tar production is largely unaffected.

This established that the catalyst was improving the overall product yield.

6.1.6 Influence of catalysts of hydrogen production and recovery

While non-condensable gas production increased it was most important that this was accompanied by an increase in components that would enhance the value of the product stream. Previous work with other catalysts had supported this contention (Chapter 1) and the hydrogen content of the gas from catalytic pyrolysis rose strongly with increasing catalyst loading and pyrolysis temperature (Chapter 3); rising from a baseline at 600°C of 3.1 mmol/g biomass to 7.9mmol/g at 750°C and 5.0%Fe loading, an increase of over 100%. Recovery of hydrogen as a percent of that contained in the original biomass rose from less than 11% to 22%. It was further demonstrated that this benefit was not only observed with almond residue biomass but with pine chips also.

This provided the critical evidence that improved yields equate with higher valued product slate, and further, that the catalyst and process may be amenable to a broad range of agricultural biomass.

6.1.7 Influence of introducing a two-stage pyrolysis process

It is common practice to have a fixed bed catalytic reformer following the primary pyrolysis stage, which operates at significantly higher temperature; and it also common practice to inject steam at this stage to increase hydrogen output. Designing in this form has several implications; the fixed bed catalyst generally requires a regeneration or replacement cycle, and effectiveness deteriorates over time, and the energy requirements of the system increase substantially.

With the twin objectives of keeping costs dampened, and a simpler low-cost catalyst system for the whole process, both stages of the process used in this investigation operate as if they were vertical moving beds. So, as material passes through the first stage the total product (gases, liquids and solids) transfers from the first stage to the second, including the char carrier and catalyst embedded in the char remaining from the first stage pyrolysis. In the second stage the solids are formed into a loose vertical bed structure through which the pyrolysis gases

pass. This stage operates at the same temperature as the first, but the catalyst remains active and now becomes the reforming catalyst. In these experiments the reforming bed was restricted to a fixed height and was operated at the same temperature as the pyrolysis process.

Total gas production increased in line with increasing pyrolysis temperatures and catalyst loadings providing almost 50% increase from the equivalent trials with one-stage pyrolysis. Hydrogen production also responded in a similar way such that relative to baseline at 600°C, while one-stage processing at 750°C, 5.0%Fe, provided a 100% increase, with two-stage pyrolysis yield was 180% of baseline. The latter translates to a recovery of 30% of the available hydrogen in the biomass. Increases in syngas production (60%) were also pronounced due to higher CO production at higher pyrolysis temperatures, bringing improved H_2/CO ratios. Additionally, throughout the two-stage processing it was confirmed that IOT was equally as effective as LFN underwriting the selection of a waste product as the source of Fe_2O_3 for the char supported catalyst.

Overall, this two-stage process offers a significant increase in hydrogen production and syngas. It incorporates a simple catalyst system, initially the catalyst is admixed with biomass for the first stage catalysis, and then, passing to the second stage in the residual char, to act as a reforming catalyst. The whole process operates at the same moderate temperature, and the char residue may be recycled or become a coke substitute in blast furnace operations.

It provides evidence that by extending the pyrolysis process into a separate additional stage significant additional benefits can be gained by simply further processing all the pyrolysis products, and provides evidence of a potential pathway to further valorise the residual char.

6.1.8 Comparison with other work

TABLE 6.1 summarises the results of other reported research from one and two stage pyrolysis experiments. Direct comparisons are difficult because of the large number of variables involved including pyrolysis and reformer operating temperature, relative catalyst loadings, whether or not steam injection has been used and sweeping gas flow rates. Nevertheless, it is clear that catalysts using Ni provide higher hydrogen yields than those based on Fe, although the

difference is not seen to be so significant that the use of iron, based on costs and environmental considerations, remains a preferred option. Also clear is that higher operating temperatures generally deliver somewhat higher yields, although this needs to be tempered with its impact on costs and net energy requirements. Both in this work and another report (David 2020) have shown sweeping gas rates can have significant impacts on overall gas yields and hydrogen yields, both increasing with reducing sweeping gas rates. Clearly significant increases in hydrogen yields are obtained once steam reforming is included with the systems operating with S/B of 2 having over 66% of the available hydrogen provided by steam injection. And therefore this is one of the key next steps to be examined in the further development of this process.

6.1.9 Tar reduction response to catalytic pyrolysis in one or two-stages

The principal findings in respect of PAH tars were firstly, that using one-stage processing there is little difference in the component distribution whether catalysed or not. This is due to both the catalyst having been mixed with the biomass, rather than in a separate in-situ container; and also, the relatively high sweeping gas rates which carried the pyrolysis products away from the catalyst as they were formed.

With two-stage pyrolysis the notable feature was the significant reduction in high MW PAHs

6.2 Implications of the Research Findings

6.2.1 Biomass – a significant contributor to green hydrogen supply

This thesis set out to address the complexities of processing, and valorisation of the product slate, as drivers for improving the economics of thermochemical conversion of biomass, primarily to produce green hydrogen. It is clear that considerable further work is required to establish that the findings in this work can be successfully used to transform the position of utilising biomass

for hydrogen production. Nevertheless, several separate important changes have been identified, that individually, or together, may have a substantial impact on progress towards the goal.

One of the important features of this pathway is that it is a technology well suited to developing countries with high dependence on agriculture providing a natural, local source of feedstock. It offers the opportunity to substantially improve economies by reducing the need to import fuels and through increasing the overall level of economic activity.

6.2.2 Increased gas production

Generation of a higher quantity of gas may contribute to providing a higher value for the product gas stream through not only increasing hydrogen yield, important of itself, but also increasing syngas yield. A portion of the hydrogen can be removed from the product gas stream leaving a syngas stream which can be used as a fuel or further processed to synthetic natural gas (SNG) or, if within the desired H_2/CO ratio, can be utilised more broadly for transport fuels or chemicals.

6.2.3 Integrating iron ore waste, green hydrogen and char from biomass into a green steel process

As a long-term development, the elements of this work could be viewed as a step towards providing a concept for green steel manufacturing. Ideally iron ore tailings would be used to produce the catalyst system for catalytic pyrolysis of biomass. The product hydrogen could be utilised in the blast furnace for oxygen scavenging, and syngas used as a fuel within the steel works. Char from the second stage process, together with contained iron ore tailings can be used as coke replacement.

6.3 Recommendations

6.3.1 Future Work

This thesis lays the groundwork for a range of further studies and investigations to bring a simple catalytic pyrolysis process to the stage of

potentially be commercialised. Much of the continuing work is of a fundamental nature in process design and optimisation

6.3.1.1 Confirming the concepts

The next steps require the design, construction and operation of a pilot scale moving bed two-stage reactor to confirm that the general thrust of the results presented here can be produced in a moving bed system operating continuously.

6.3.1.2 Confirming the breadth of application

For the process to be accepted as having a wide application an early part of the confirmation process need be testing of broad range of biomass candidates.

6.3.1.3 Optimum operating conditions

The key operating variables examined during this work are pyrolysis temperature (which is also second stage operating temperature), catalyst preparation method, catalyst type and loading, and space velocity of sweeping gas. While the objective function in terms of optimising is generally measured in terms of product yields or energy efficiency, the objectives in this work have been a combination of product value (overall net revenue) with minimised capital cost. No specific information on these objectives have been generated, and it remains a future task.

6.3.1.4 Identifying desirable properties for final char residue

To further increase the value of the process it would be desirable to determine the preferred product criteria for char used as a coke replacement and establish how the important elements of the specification can be met by the char residue from the second stage reactor.

6.3.1.5 Further develop the "Circular industry" concept

Through engaging with industries, establish circular industry models to further broaden the capability of the technology to decarbonise industries.

References

Abu El-Rub, Z, Bramer, EA & Brem, G 2004, 'Modeling of tar reduction in biomass fuelled gasification using biomass char as a catalyst', paper presented at 2nd World Conference and Exhibition on Biomass for Energy, Industry and Climate Protection, Rome, Italy.

Abu El-Rub, Z, Bramer, EA & Brem, G 2008, 'Experimental comparison of biomass chars with other catalysts for tar reduction', *Fuel*, vol. 87, no. 10-11, 2008/08/01/, pp. 2243-2252.

Abu Tahari, MN, Salleh, F, Tengku Saharuddin, TS, Dzakaria, N, Samsuri, A, Mohamed Hisham, MW & Yarmo, MA 2019, 'Influence of hydrogen and various carbon monoxide concentrations on reduction behavior of iron oxide at low temperature', *International Journal of Hydrogen Energy*, vol. 44, no. 37, 2019/08/02/, pp. 20751-20759.

Ahmad, AA, Zawawi, NA, Kasim, FH, Inayat, A & Khasri, A 2016, 'Assessing the gasification performance of biomass: A review on biomass gasification process conditions, optimization and economic evaluation', *Renewable and Sustainable Energy Reviews*, vol. 53, Jan, pp. 1333-1347.

Aigner, I, Wolfesberger, U & Hofbauer, H 2009, 'Tar Content and Composition in Producer Gas of Fluidized Bed Gasification and Low Temperature Pyrolysis of Straw and Wood – Influence of Temperature', *ICPS 09 - Int Conf Polygeneration Strategies*, 01/01.

Al-Rahbi, AS, Onwudili, JA & Williams, PT 2016, 'Thermal decomposition and gasification of biomass pyrolysis gases using a hot bed of waste derived pyrolysis char', *Bioresource Technology*, vol. 204, Mar, pp. 71-79.

Anis, S & Zainal, ZA 2011, 'Tar reduction in biomass producer gas via mechanical, catalytic and thermal methods: A review', *Renewable and Sustainable Energy Reviews*, vol. 15, no. 5, Jun, pp. 2355-2377.

Arregi, A, Amutio, M, Lopez, G, Bilbao, J & Olazar, M 2018, 'Evaluation of thermochemical routes for hydrogen production from biomass: A review', *Energy Conversion and Management*, vol. 165, pp. 696-719.

Arregi, A, Barbarias, I, Alvarez, J & Erkiaga, A 2015, 'Hydrogen Production from Biomass Pyrolysis and In-line Catalytic Steam Reforming', *CHEMICAL ENGINEERING TRANSACTIONS*, vol. 43, pp. 547-552.

Babu, BV 2008, 'Biomass pyrolysis: a state-of-the-art review', *Biofuels Bioproducts and Biorefining-Biofpr*, vol. 2, no. 5, Sep-Oct, pp. 393-414.

Bakhtyari, A, Makarem, MA & Rahimpour, MR 2017, 'Hydrogen Production Through Pyrolysis', in RA Meyers (ed.), *Encyclopedia of Sustainability Science and Technology*, Springer New York, New York, NY, pp. 1-28.

Balat, M 2008, 'Hydrogen-Rich Gas Production from Biomass via Pyrolysis and Gasification Processes and Effects of Catalyst on Hydrogen Yield', *Energy Sources, Part A: Recovery, Utilization, and Environmental Effects*, vol. 30, no. 6, 2008/01/29, pp. 552-564.

Balat, M, Balat, M, Kırtay, E & Balat, H 2009a, 'Main routes for the thermo-conversion of biomass into fuels and chemicals. Part 1: Pyrolysis systems', vol. 50, pp. 3147-3157.

Balat, M, Balat, M, Kırtay, E & Balat, H 2009b, 'Main routes for the thermo-conversion of biomass into fuels and chemicals. Part 2: Gasification systems', vol. 50, pp. 3158-3168.

Basu, P 2010, *Biomass Gasification and Pyrolysis Practical Design and Theory*, Elsevier.

Binder, M, Kraussler, M, Kuba, M & M., L 2018, *Hydrogen from biomass gasification*, IEA Bioenergy, IEA Bioenergy.

Bridgwater, AV 2012, 'Review of fast pyrolysis of biomass and product upgrading', *Biomass and Bioenergy*, vol. 38, Mar, pp. 68-94.

Bru, K, Blin, J, Julbe, A & Volle, G 2007, 'Pyrolysis of metal impregnated biomass: An innovative catalytic way to produce gas fuel', *Journal of Analytical and Applied Pyrolysis*, vol. 78, no. 2, Mar, pp. 291-300.

Brynda, J, Skoblia, S, Beňo, Z, Pohořelý, M & Moško, J 2016, 'Application of staged biomass gasification for combined heat and power', paper presented at ICETI2016, Ho Chi Minh City, Vietnam.

Buentello-Montoya, D, Zhang, X, Li, J, Ranade, V, Marques, S & Geron, M 2020, 'Performance of biochar as a catalyst for tar steam reforming: Effect of the porous structure', *Applied Energy*, vol. 259, 2020/02/01/, p. 114176.

Cao, XF, Sun, SN & Sun, RC 2017, 'Application of biochar-based catalysts in biomass upgrading: a review', *RSC Advances*, vol. 7, no. 77, pp. 48793-48805.

Chatterjee, R, Sajjadi, B, Chen, W-Y, Mattern, DL, Hammer, N, Raman, V & Dorris, A 2020, 'Effect of Pyrolysis Temperature on PhysicoChemical Properties and Acoustic-Based Amination of Biochar for Efficient CO2 Adsorption', *Frontiers in Energy Research*, vol. 8.

Cheng, F & Li, XW 2018, 'Preparation and Application of Biochar-Based Catalysts for Biofuel Production', *Catalysts*, vol. 8, no. 9, Sep.

Collard, FX, Blin, J, Bensakhria, A & Valette, J 2012, 'Influence of impregnated metal on the pyrolysis conversion of biomass constituents', *Journal of Analytical and Applied Pyrolysis*, vol. 95, May, pp. 213-226.

Couhert C., CJ-M, Salvador S. 2009, 'Is it possible to predict gas yields of any biomass after rapid pyrolysis at high temperature from its
composition in cellulose, hemicellulose and lignin ?', *Fuel*, vol. 88, pp. 408-417.

David, E 2020, 'Evaluation of Hydrogen Yield Evolution in Gaseous Fraction and Biochar Structure Resulting from Walnut Shells Pyrolysis', *Energies*, vol. 13, no. 23.

de Lasa, H, Salaices, E, Mazumder, J & Lucky, R 2011, 'Catalytic Steam Gasification of Biomass: Catalysts, Thermodynamics and Kinetics', *Chemical Reviews*, vol. 111, no. 9, 2011/09/14, pp. 5404-5433.

Demirbas, A 2004, 'Effects of temperature and particle size on bio-char yield from pyrolysis of agricultural residues', *Journal of Analytical and Applied Pyrolysis*, vol. 72, no. 2, 2004/11/01/, pp. 243-248.

Demirbaş, A 2002, 'Gaseous products from biomass by pyrolysis and gasification: effects of catalyst on hydrogen yield', *Energy Conversion and Management*, vol. 43, no. 7, 2002/05/01/, pp. 897-909.

Derimbas, A 2001, 'Yields of hydrogen-rich gaseous products via pyrolysis from selected biomass samples', *Fuel*, vol. 80, pp. 1885-1891.

Dewayanto, N, Isha, R & Nordin, MR 2014, 'Kinetic Study on the Catalytic Pyrolysis of Decanter Cake from Palm Oil Milling Plant by using Thermogravimetry Data', *Jurnal Teknologi*, vol. 69, no. 5.

Du, H, Deng, F, Kommalapati, RR & Amarasekara, AS 2020, 'Iron based Catalysts in Biomass Processing'.

Fernyhough, J 2021, 'Australia has 38GW of green hydrogen in pipeline, but major cost falls needed', *RENEW ECONOMY*, vol. 2021, no. 11 July 2021.

Fernyhough, J 2021, *Australia has 38GW of green hydrogen in pipeline, but major cost falls needed*, RENEW ECONOMY, <https://reneweconomy.com.au/australia-has-38gw-of-green-hydrogen-in-pipeline-but-major-cost-falls-needed/>.

Fiori, L, Valbusa, M, Lorenzi, D & Fambri, L 2012, 'Modeling of the devolatilization kinetics during pyrolysis of grape residues', *Bioresource Technology*, vol. 103, no. 1, Jan, pp. 389-397.

Granados-Fitch, MG, Quintana-Melgoza, JM, Juarez-Arellano, EA & Avalos-Borja, M 2019, 'Mechanism to H2 production on rhenium carbide from pyrolysis of coconut shell', *International Journal of Hydrogen Energy*, vol. 44, no. 5, pp. 2784-2796.

Guan, GQ, Kaewpanha, M, Hao, XG & Abudula, A 2016, 'Catalytic steam reforming of biomass tar: Prospects and challenges', *Renewable and Sustainable Energy Reviews*, vol. 58, May, pp. 450-461.

Guethmundsson, A & Backvall, JE 2020, 'On the Use of Iron in Organic Chemistry', *Molecules*, vol. 25, no. 6, Mar 16.

Guo, D, Hu, M, Chen, Z, Cui, B, Zhang, Q, Liu, Y, Luo, S, Ruan, R & Liu, Y 2020, 'Catalytic pyrolysis of rain tree biomass with nano nickel oxide synthetized from nickel plating slag: A green path for treating waste by waste', *Bioresource Technology*, vol. 315, 2020/11/01/, p. 123831.

Guo, F, Li, X, Liu, Y, Peng, K, Guo, C & Rao, Z 2018, 'Catalytic cracking of biomass pyrolysis tar over char-supported catalysts', *Energy Conversion and Management*, vol. 167, 2018/07/01/, pp. 81-90.

Guo, F, Liang, S, Jia, X, Peng, K, Jiang, X & Qian, L 2020, 'One-step synthesis of biochar-supported potassium-iron catalyst for catalytic cracking of biomass pyrolysis tar', *International Journal of Hydrogen Energy*, vol. 45, no. 33, pp. 16398-16408.

Guo, FQ, Li, XL, Liu, Y, Peng, KY, Guo, CL & Rao, ZH 2018, 'Catalytic cracking of biomass pyrolysis tar over char-supported catalysts', *Energy Conversion and Management*, vol. 167, Jul 1, pp. 81-90.

Haddad K., JM, Guizani C., Jellali S. & Limousy L., AN 2016, 'Influence of Alkali and alkaline earth metallic (AAEM) species on pyrolysis process of Cypress sawdust', Mulhouse, France.

Harrison, DP 2008, 'Sorption-Enhanced Hydrogen Production: A Review', *Industrial & Engineering Chemistry Research*, vol. 47, no. 17, 2008/09/03, pp. 6486-6501.

Henriksen, U, Ahrenfeldt, J, Jensen, TK, Gøbel, B, Bentzen, JD, Hindsgaul, C & Sørensen, LH 2003, 'The Design, Construction and Operation of a 75 kW Two-Stage Gasifier', paper presented at ECOS, Copenhagen, Denmark.

Hongbo, D, Deng, F, Kommalapati, RR & Amarasekara, AS 2020, 'Iron based catalysts in biomass processing', *Renewable and Sustainable Energy Reviews*, vol. 134.

Hu, M, Cui, B, Xiao, B, Luo, S & Guo, D 2020, 'Insight into the Ex Situ Catalytic Pyrolysis of Biomass over Char Supported Metals Catalyst: Syngas Production and Tar Decomposition', *Nanomaterials*, vol. 10, no. 7.

Hu, M, Wang, X, Chen, J, Yang, P, Liu, C, Xiao, B & Guo, D 2017, 'Kinetic study and syngas production from pyrolysis of forestry waste', *Energy Conversion and Management*, vol. 135, pp. 453-462.

Hu, S, Jiang, L, Wang, Y, Su, S, Sun, L, Xu, B, He, L & Xiang, J 2015, 'Effects of inherent alkali and alkaline earth metallic species on biomass pyrolysis at different temperatures', *Bioresource Technology*, vol. 192, Sep, pp. 23-30.

Huang, Y, Chen, M, Li, Q & Xing, W 2018, 'Hydrogen-rich syngas produced from co-gasification of wet sewage sludge and torrefied biomass in self-generated steam agent', *Energy*, vol. 161, pp. 202-213.

Hydrogen Production: Biomass Gasification, Web page, Hydrogen and Fuel Cell Technologies Office, Washington DC, viewed 28 March 2022.

IEA 2019, *The Future of Hydrogen*, IEA, Paris.

IEA 2021, *Renewables 2021-Analysis and forecast to 2026*, IEA, IEA, France, <https://www.iea.org/reports/renewables-2021/renewable-heat?mode=heat&region=World&publication=2021>.

IEA Bioenergy The past, present and future of gasification 2020, I Bioenergy, 30 January 2020.

Johnsson, F, Kjärstad, J & Rootzén, J 2018, 'The threat to climate change mitigation posed by the abundance of fossil fuels', *Climate Policy*, vol. 19, no. 2, pp. 258-274.

Kabakcı, SB & Hacıbektaşoğlu, Ş 2017, 'Catalytic Pyrolysis of Biomass', in *Pyrolysis*.

Kalamaras, CM & Efstathiou, AM 2013, 'Hydrogen Production Technologies: Current State and Future Developments', *Conference Papers in Energy*, vol. 2013, pp. 1-9.

Kamitani, M 2021, *Improvements in chemical processes using iron catalysts*, Open Access Government, viewed 15 August 2022 2022, <https://www.openaccessgovernment.org/chemical-processes-using-iron-catalysts/112754/>.

Kan, T, Strezov, V & Evans, TJ 2016, 'Lignocellulosic biomass pyrolysis: A review of product properties and effects of pyrolysis parameters', *Renewable and Sustainable Energy Reviews*, vol. 57, May, pp. 1126-1140.

Kastner, JR, Mani, S & Juneja, A 2015, 'Catalytic decomposition of tar using iron supported biochar', *Fuel Processing Technology*, vol. 130, 2015/02/01/, pp. 31-37.

Kaur R., GP, Jha M.K. 2019, 'Chapter 8 Thermochemical Route for Biohydrogen Production', in *Biohydrogen*, Elsevier, pp. 187-218.

Kemper, J 2015, 'Biomass and carbon dioxide capture and storage: A review', *International Journal of Greenhouse Gas Control*, vol. 40, 2015/09/01/, pp. 401-430.

Khelfa, A, Sharypov, V, Finqueneisel, G & Weber, JV 2009, 'Catalytic pyrolysis and gasification of Miscanthus Giganteus: Haematite (Fe2O3) a versatile catalyst', *Journal of Analytical and Applied Pyrolysis*, vol. 84, no. 1, pp. 84-88.

Klinghoffer, NB, Castaldi, MJ & Nzihou, A 2012, 'Catalyst Properties and Catalytic Performance of Char from Biomass Gasification', *Industrial and Engineering Chemistry Research*, vol. 51, no. 40, Oct 10, pp. 13113-13122.

Kok, MV & Ozgur, E 2017, 'Characterization of lignocellulose biomass and model compounds by thermogravimetry', *Energy sources Part A-Recovery Utilization and Environmental Effects*, vol. 39, no. 2, pp. 134-139.

Kosov, V, Kosov, V & Zaichenko, V 2014, 'Experimental Research of Heterogeneous Cracking of Pyrolysis Tars', *Iconbm: International Conference on Biomass, Pts 1 and 2*, vol. 37, pp. 211-216.

Kosov, VV, Kosov, VF, Sinelshchikov, VA & Zaichenko, VM 2013, 'The two-stage technologyof biomass conversion into synthesis gas', in A Méndez-Vilas (ed.), *Materials and processes for energy: communicating current research and technological developments*.

Kosov, VV, Kosov, VF & Zaichenko, VM 2015, 'Investigation of a Two-stage Process of Biomass Gasification', *Icheap12: 12th International Conference on Chemical AND Process Engineering*, vol. 43, pp. 457-462.

Lepage, T, Kammoun, M, Schmetz, Q & Richel, A 2021, 'Biomass-to-hydrogen: A review of main routes production, processes evaluation and techno-economical assessment', *Biomass and Bioenergy*, vol. 144, p. 105920.

Li, C & Brown, TC 2001, 'Carbon oxidation kinetics from evolved carbon oxide analysis during temperature-programmed oxidation', *Carbon*, vol. 39, no. 5, pp. 725-732.

Li, Ce & Brown, TC 2001, 'Carbon oxidation kinetics from evolved carbon oxide analysis during temperature-programmed oxidation', *Carbon*, vol. 39, pp. 725-732.

Li, H, Dong, X, da Silva, EB, de Oliveira, LM, Chen, Y & Ma, LQ 2017, 'Mechanisms of metal sorption by biochars: Biochar characteristics and modifications', *Chemosphere*, vol. 178, Jul, pp. 466-478.

Li, X, Liu, Y, Hao, J & Wang, W 2018, 'Study of Almond Shell Characteristics', *Materials (Basel)*, vol. 11, no. 9, Sep 19.

Li, Y, Xing, B, Ding, Y, Han, X & Wang, S 2020, 'A critical review of the production and advanced utilization of biochar via selective pyrolysis of lignocellulosic biomass', *Bioresource Technology*, vol. 312, 2020/09/01/, p. 123614.

Lui, J, Chen, W-H, Tsang, DCW & You, S 2020, 'A critical review on the principles, applications, and challenges of waste-to-hydrogen technologies', *Renewable and Sustainable Energy Reviews*, vol. 134.

Malek, NH, Asadullah, M & Sauki, A 2015, 'Tar elimination from producer gas by using in-situ catalytic reforming of tar', *Advanced Material Research*, vol. 1113, pp. 459-464.

Mallick, D, Poddar, MK, Mahanta, P & Moholkar, VS 2018, 'Discernment of synergism in pyrolysis of biomass blends using thermogravimetric analysis', *Bioresource Technology*, vol. 261, Aug, pp. 294-305.

Mathieson, JR, Harold; Somerville, Michael; Ridgeway, Philip; Jahanshahi, Sharif. 27 June - 1 July 2011; 2011, 'Use of biomass in the iron and steel industry - An Australian perspective', paper presented at 1st International Conference on Energy Efficiency and CO2 Reduction in the Steel Industry (EECR Steel 2011) - incorporated in METEC InSteelCon 2011, Dusseldorf, Germany., 27 June - 1 July 2011;, <http://hdl.handle.net/102.100.100/103943?index=1>.

Melnikov, P, Nascimento, VA, Arkhangelsky, IV, Zanoni Consolo, LZ & de Oliveira, LCS 2013, 'Thermal decomposition mechanism of iron(III) nitrate and characterization of intermediate products by the technique of computerized modeling', *Journal of Thermal Analysis and Calorimetry*, vol. 115, no. 1, pp. 145-151.

Min, Z, Yimsiri, P, Zhang, S, Wang, Y, Asadullah, M & Li, CZ 2013, 'Catalytic reforming of tar during gasification. Part III. Effects of feedstock on tar reforming using ilmenite as a catalyst', *Fuel*, vol. 103, Jan, pp. 950-955.

Mohan, B, Park, JC & Park, KH 2016, 'Mechanochemical Synthesis of Active Magnetite Nanoparticles Supported on Charcoal for Facile Synthesis of Alkynyl Selenides by C-H Activation', *ChemCatChem*, vol. 8, no. 14, Jul 20, pp. 2345-2350.

Mohan, B, Park, JC & Park, KH 2016, 'Mechanochemical Synthesis of Active Magnetite Nanoparticles Supported on Charcoal for Facile Synthesis of Alkynyl Selenides by C–H Activation', *ChemCatChem*, vol. 8, no. 14, pp. 2345-2350.

Motozuka, S, Tagaya, M, Hayashi, K & Morinaga, M 2015, 'Texture formation in iron particles using mechanical milling with graphite as a milling aid', *AIP Advances*, vol. 5, no. 9, Sep.

Moud, PH, Kantarelis, E, Andersson, KJ & Engvall, K 2018, 'Biomass pyrolysis gas conditioning over an iron-based catalyst for mild deoxygenation and hydrogen production', *Fuel*, vol. 211, pp. 149-158.

Mousa, E, Wang, C, Riesbeck, J & Larsson, M 2016, 'Biomass applications in iron and steel industry: An overview of challenges and opportunities', *Renewable and Sustainable Energy Reviews*, vol. 65, pp. 1247-1266.

Neves, D, Thunman, H, Matos, A, Tarelho, L & Gomez-Barea, A 2011, 'Characterization and prediction of biomass pyrolysis products', *Progress in Energy and Combustion Science*, vol. 37, no. 5, Sep, pp. 611-630.

Neves, D, Thunman, H, Matos, A, Tarelho, L & Gómez-Barea, A 2011, 'Characterization and prediction of biomass pyrolysis products', *Progress in Energy and Combustion Science*, vol. 37, no. 5, pp. 611-630.

Nordgreen, T, Nemanova, V, Engvall, K & Sjostrom, K 2012, 'Iron-based materials as tar depletion catalysts in biomass gasification: Dependency on oxygen potential', *Fuel*, vol. 95, no. 1, May, pp. 71-78.

OECD Meeting Policy Challenges for a Sustainable Bioeconomy, 2018, O Publishing, Paris.

Pandey, B, Prajapati, YK & Sheth, PN 2019, 'Recent progress in thermochemical techniques to produce hydrogen gas from biomass: A state of the art review', *International Journal of Hydrogen Energy*, vol. 44, no. 47, Oct 4, pp. 25384-25415.

Park, HJ, Park, SH, Sohn, JM, Park, J, Jeon, JK, Kim, SS & Park, YK 2010, 'Steam reforming of biomass gasification tar using benzene as a model compound over various Ni supported metal oxide catalysts', *Bioresource Technology*, vol. 101 Suppl 1, no. 1, Supplement, Jan, pp. S101-103.

Park, J, Lee, Y & Ryu, C 2016, 'Reduction of primary tar vapor from biomass by hot char particles in fixed bed gasification', *Biomass and Bioenergy*, vol. 90, Jul, pp. 114-121.

Parthasarathy, P & Narayanan, KS 2014, 'Hydrogen production from steam gasification of biomass: Influence of process parameters on hydrogen yield – A review', *Renewable Energy*, vol. 66, pp. 570-579.

Pecha, MB, Arbelaez, JIM, Garcia-Perez, M, Chejne, F & Ciesielski, PN 2019, 'Progress in understanding the four dominant intra-particle phenomena of lignocellulose pyrolysis: chemical reactions, heat transfer, mass transfer, and phase change', *Green Chemistry*, vol. 21, no. 11, pp. 2868-2898.

Phyllis2 2020, [Database for the physico-chemical composition of (treated) lignocellulosic biomass, micro- and macroalgae, various feedstocks for biogas production and biochar], viewed 20 February 2020,<https://phyllis.nl/>.

Pineau, A, Kanari, N & Gaballah, I 2006, 'Kinetics of reduction of iron oxides by H2', *Thermochimica Acta*, vol. 447, no. 1, 2006/08/01/, pp. 89-100.

Pineda, A, Balu, AM, Campelo, JM, Romero, AA, Carmona, D, Balas, F, Santamaria, J & Luque, R 2011, 'A Dry Milling Approach for the Synthesis of Highly Active Nanoparticles Supported on Porous Materials', *ChemSusChem*, vol. 4, no. 11, 2011/11/18, pp. 1561-1565.

Pütün, E 2010, 'Catalytic pyrolysis of biomass: Effects of pyrolysis temperature, sweeping gas flow rate and MgO catalyst', *Energy*, vol. 35, no. 7, pp. 2761-2766.

Qian, KZ & Kumar, A 2017, 'Catalytic reforming of toluene and naphthalene (model tar) by char supported nickel catalyst', *Fuel*, vol. 187, Jan 1, pp. 128-136.

Qian, KZ, Kumar, A, Zhang, HL, Bellmer, D & Huhnke, R 2015, 'Recent advances in utilization of biochar', *Renewable and Sustainable Energy Reviews*, vol. 42, Feb, pp. 1055-1064.

Ralphs, K, Hardacre, C & James, SL 2013, 'Application of heterogeneous catalysts prepared by mechanochemical synthesis', *Chemical Society Review*, vol. 42, no. 18, Sep 21, pp. 7701-7718.

Richardson, Y, Blin, J & Julbe, A 2012, 'A short overview on purification and conditioning of syngas produced by biomass gasification: Catalytic strategies, process intensification and new concepts', *Progress in Energy and Combustion Science*, vol. 38, no. 6, Dec, pp. 765-781.

Richardson, Y, Blin, J, Volle, G, Motuzas, J & Julbe, A 2010, 'In situ generation of Ni metal nanoparticles as catalyst for H2-rich syngas production from biomass gasification', *Applied Catalysis A: General*, vol. 382, no. 2, pp. 220-230.

Richardson, Y, Drobek, M, Julbe, A, Blin, J & Pinta, F 2015, 'Biomass Gasification to Produce Syngas', in T Bhaskar, M Stöcker & RK Sukumaran (eds), *Recent Advances in Thermo-Chemical Conversion of Biomass*, Elsevier, Boston, pp. 213-250.

Richardson, Y, Eibner, S, Tanoh, S, Broust, F, Blin, J & Julbe, A 2015, 'The catalyst/biomass integration concept for the direct thermo-catalytic conversion of biomass into either syngas or added-value molecules', paper presented at International Symposium on Green Chemistry, La Rochelle, France, 2015-05-03 / 2015-05-07, <http://www.isgc2015.com>.

Richardson, Y, Motuzas, J, Julbe, A, Volle, G & Blin, J 2013, 'Catalytic Investigation of in Situ Generated Ni Metal Nanoparticles for Tar Conversion during Biomass Pyrolysis', *Journal of Physical Chemistry C*, vol. 117, no. 45, Nov 14, pp. 23812-23831.

SA, X 2022, *NOTAR gasifier*, viewed 12 November 2018, <https://www.xylowatt.com/notar-gasifier/>.

Sansaniwal, SK, Rosen, MA & Tyagi, SK 2017, 'Global challenges in the sustainable development of biomass gasification: An overview', *Renewable and Sustainable Energy Reviews*, vol. 80, Dec, pp. 23-43.

Santamaria, L, Lopez, G, Fernandez, E, Cortazar, M, Arregi, A, Olazar, M & Bilbao, J 2021, 'Progress on Catalyst Development for the Steam Reforming of Biomass and Waste Plastics Pyrolysis Volatiles: A Review', *Energy & Fuels*, vol. 35, no. 21, 2021/11/04, pp. 17051-17084.

Saxena, RC, Seal, D, Kumar, S & Goyal, HB 2008, 'Thermo-chemical routes for hydrogen rich gas from biomass: A review', *Renewable and Sustainable Energy Reviews*, vol. 12, no. 7, pp. 1909-1927.

Shen, Y 2015, 'Chars as carbonaceous adsorbents/catalysts for tar elimination during biomass pyrolysis or gasification', *Renewable and Sustainable Energy Reviews*, vol. 43, pp. 281-295.

Shen, YF, Chen, MD, Sun, TH & Jia, JP 2015, 'Catalytic reforming of pyrolysis tar over metallic nickel nanoparticles embedded in pyrochar', *Fuel*, vol. 159, Nov 1, pp. 570-579.

Shen, YF, Zhao, PT, Shao, QF, Ma, DC, Takahashi, F & Yoshikawa, K 2014, 'In-situ catalytic conversion of tar using rice husk char-supported nickel-iron catalysts for biomass pyrolysis/gasification', *Applied Catalysis B-Environmental*, vol. 152, Jun 25, pp. 140-151.

Shen, YF, Zhao, PT, Shao, QF, Takahashi, F & Yoshikawa, K 2015, 'In situ catalytic conversion of tar using rice husk char/ash supported nickel-iron catalysts for biomass pyrolytic gasification combined with the mixing-simulation in fluidized-bed gasifier', *Applied Energy*, vol. 160, Dec 15, pp. 808-819.

Singh, H, Yadav, R, Farooqui, SA, Dudnyk, O & Sinha, AK 2019, 'Nanoporous nickel oxide catalyst with uniform Ni dispersion for enhanced hydrogen production from organic waste', *International Journal of Hydrogen Energy*, vol. 44, no. 36, pp. 19573-19584.

Srinivasakannan, C & Balasubramanian, N 2010, 'Variations in the Design of Dual Fluidized Bed Gasifiers and the Quality of Syngas from Biomass', *Energy Sources, Part A: Recovery, Utilization, and Environmental Effects*, vol. 33, no. 4, pp. 349-359.

'Steel's contribution to a low carbon future and climate resilient societies', 2017.

Stefanidis, SD, Kalogiannis, KG, Iliopoulou, EF, Michailof, CM, Pilavachi, PA & Lappas, AA 2014, 'A study of lignocellulosic biomass pyrolysis via the pyrolysis of cellulose, hemicellulose and lignin', *Journal of Analytical and Applied Pyrolysis*, vol. 105, Jan, pp. 143-150.

Sun, H, Feng, D, Zhao, Y, Sun, S, Wu, J, Wang, P, Chang, G, Lai, X, Tan, H & Qin, Y 2020, 'Mechanism of catalytic tar reforming over biochar: Description of volatile-H2O-char interaction', *Fuel*, vol. 275, 2020/09/01/, p. 117954.

Thomson, R & Kwong, P 2020, 'Production and Applications of Synthesis Gas', in *Reference Module in Chemistry, Molecular Sciences and Chemical Engineering*.

Thomson, R, Kwong, P, Ahmad, E & Nigam, KDP 2020, 'Clean syngas from small commercial biomass gasifiers; a review of gasifier development, recent advances and performance evaluation', *International Journal of Hydrogen Energy*, vol. 45, no. 41, pp. 21087-21111.

Uddin, NM, Daud, WMAW & Abbas, HF 2013, 'Potential hydrogen and non-condensable gases production from biomass pyrolysis: Insights into the process variables', *Renewable and Sustainable Energy Reviews*, vol. 27, pp. 204-224.

UN Climate Change Conference UK 2021 2021, <https://ukcop26.org/the-conference/cop26-outcomes/>.

van de Kamp W., dWP, Knoef H., Neeft J., Kiel J. 2006, *Tar measurement in biomass gasification, standardisation and supporting R&D*, ECN.

Vander Wall, EM 1962, *Thermal decomposition of hydrated iron, chromium and nickel nitrates and their mixtures*, AEC Research and Development
Report, Atomic Energy Commission, Idaho.

Wang, F, Wang, P, Raheem, A, Ji, G, Memon, MZ, Song, Y & Zhao, M 2019, 'Enhancing hydrogen production from biomass pyrolysis by dental-wastes-derived sodium zirconate', *International Journal of Hydrogen Energy*, vol. 44, no. 43, 2019/09/06/, pp. 23846-23855.

Wang, W, Lemaire, R, Bensakhria, A & Luart, D 2022, 'Review on the catalytic effects of alkali and alkaline earth metals (AAEMs) including sodium, potassium, calcium and magnesium on the pyrolysis of lignocellulosic biomass and on the co-pyrolysis of coal with biomass', *Journal of Analytical and Applied Pyrolysis*, vol. 163.

Wang, Y, Hu, X, Song, Y, Min, ZH, Mourant, D, Li, TT, Gunawan, R & Li, CZ 2013, 'Catalytic steam reforming of cellulose-derived compounds using a char-supported iron catalyst', *Fuel Processing Technology*, vol. 116, Dec, pp. 234-240.

Wang, Y, Huang, L, Zhang, T & Wang, Q 2022, 'Hydrogen-rich syngas production from biomass pyrolysis and catalytic reforming using biochar-based catalysts', *Fuel*, vol. 313.

White, JE, Catallo, WJ & Legendre, BL 2011, 'Biomass pyrolysis kinetics: A comparative critical review with relevant agricultural residue case studies', *Journal of Analytical and Applied Pyrolysis*, vol. 91, no. 1, May, pp. 1-33.

Wicakso, DR, Sutijan, Rochmadi & Budiman, A 2016, 'Catalytic decomposition of tar derived from wood waste pyrolysis using Indonesian low grade iron ore as catalyst'.

Woolcock, PJ & Brown, RC 2013, 'A review of cleaning technologies for biomass-derived syngas', *Biomass and Bioenergy*, vol. 52, May, pp. 54-84.

World Energy Resources | 2016, World Energy Council, WE Council, London.

World Energy Resources Waste to Energy | 2016, World Energy Council.

Xia, S, Li, K, Xiao, H, Cai, N, Dong, Z, Xu, C, Chen, Y, Yang, H, Tu, X & Chen, H 2019, 'Pyrolysis of Chinese chestnut shells: Effects of temperature and Fe presence on product composition', *Bioresource Technology*, vol. 287, Sep, p. 121444.

Xiong, X, Yu, IKM, Cao, L, Tsang, DCW, Zhang, S & Ok, YS 2017, 'A review of biochar-based catalysts for chemical synthesis, biofuel production, and pollution control', *Bioresource Technology*, vol. 246, Dec, pp. 254-270.

Xu, C, De, S, Balu, AM, Ojeda, M & Luque, R 2015, 'Mechanochemical synthesis of advanced nanomaterials for catalytic applications', *Chem Commun (Camb)*, vol. 51, no. 31, Apr 21, pp. 6698-6713.

Yang, H & Chen, H 2015, '11 - Biomass gasification for synthetic liquid fuel production', in R Luque & JG Speight (eds), *Gasification for Synthetic Fuel Production*, Woodhead Publishing, pp. 241-275.

Yang, HP, Yan, R, Chen, HP, Lee, DH & Zheng, CG 2007, 'Characteristics of hemicellulose, cellulose and lignin pyrolysis', *Fuel*, vol. 86, no. 12-13, Aug, pp. 1781-1788.

Yao, D, Hu, Q, Wang, D, Yang, H, Wu, C, Wang, X & Chen, H 2016, 'Hydrogen production from biomass gasification using biochar as a catalyst/support', *Bioresource Technology*, vol. 216, Sep, pp. 159-164.

Yao, J, Kraussler, M, Benedikt, F & Hofbauer, H 2017, 'Techno-economic assessment of hydrogen production based on dual fluidized bed biomass steam gasification, biogas steam reforming, and alkaline water electrolysis processes', *Energy Conversion and Management*, vol. 145, 2017/08/01/, pp. 278-292.

Yu, H, Liu, Y, Liu, J & Chen, D 2019, 'High catalytic performance of an innovative Ni/magnesium slag catalyst for the syngas production and tar removal from biomass pyrolysis', *Fuel*, vol. 254, 2019/10/15/, p. 115622.

Zeng, X, Ueki, Y, Yoshiie, R, Naruse, I, Wang, F, Han, Z & Xu, G 2020, 'Recent progress in tar removal by char and the applications: A comprehensive analysis', *Carbon Resources Conversion*, vol. 3, 2020/01/01/, pp. 1-18.

Zhang, S, Dong, Q, Zhang, L & Xiong, Y 2015, 'High quality syngas production from microwave pyrolysis of rice husk with char-supported metallic catalysts', *Bioresource Technology*, vol. 191, Sep, pp. 17-23.

Zhang, YL, Luo, YH, Wu, WG, Zhao, SH & Long, YF 2014, 'Heterogeneous Cracking Reaction of Tar over Biomass Char, Using Naphthalene as Model Biomass Tar', *Energy AND Fuels*, vol. 28, no. 5, May, pp. 3129-3137.

Zhao, L, Zhao, Y, Nan, H, Yang, F, Qiu, H, Xu, X & Cao, X 2020, 'Suppressed formation of polycyclic aromatic hydrocarbons (PAHs) during pyrolytic production of Fe-enriched composite biochar', *Journal of Hazardous Materials*, vol. 382, 2020/01/15/, p. 121033.

Zieliński, J, Zglinicka, I, Znak, L & Kaszkur, Z 2010, 'Reduction of Fe2O3 with hydrogen', *Applied Catalysis A: General*, vol. 381, no. 1-2, pp. 191-196.

TABLES

CHAPTER 1

Table 2.1: Sample nomenclature

Peak pyrolysis and char carrier preparation temperature (°C)	Sample descriptions of baseline samples			Sample descriptions of mechano- chemically prepared samples			Sample descriptions of incipient wetness impregnation prepared samples		
450	450-B	450-010		450-2	450-4	450-6	450-2-IWI	450-4-IWI	450-6-IWI
550	550-B	550-010		550-2	550-4	550-6	550-2-IWI	550-4-IWI	550-6-IWI
650	650-B	650-010	650-050	650-2	650-4	650-6	650-2-IWI	650-4-IWI	650-6-IWI
750	750-B	750-010	750-050	750-2	750-4	750-6	750-2-IWI	750-4-IWI	750-6-IWI
Catalyst support, % biomass (wt./wt.)	0	10%	50%	14.7%	29.4%	44.1%	14.7%	29.4%	44.1%
Catalyst loading, Fe (%wt./wt.)	0	0%	0%	1.96%	3.87%	5.82%	1.96%	3.87%	5.82%

Table 2.2: Ultimate analysis, Proximate analysis of almond residue on dry basis, and Ligno-cellulose composition of almond residue determined from graphical analysis

Ultimate analysis					Proximate analysis			Ligno-cellulose composition		
C	H	O*	N	S	Volatile matter	Fixed carbon	Ash	Hemi-cellulose	Cellulose	Lignin
42.6%	5.9%	49.9%	1.2%	<0.4%	73.4%	23.4%	3.2%	30.4%	38.6%	31.0%

*By difference

Table 2.3: Char yield; catalyst mass constant and Normalised Char Yields

Char yield catalyst mass constant wt.% biomass	*Sample*	*Char*	*Sample*	*Char*	*Sample*	*Char*	*Sample*	*Char*	*Sample*	*Char*
	450-B	37.6%	450-0	35.8%	450-2	34.5%	450-4	29.2%	450-6	19.0%
	550-B	35.2%	550-0	33.2%	550-2	32.4%	550-4	28.2%	550-6	23.3%
	650-B	33.5%	650-0	32.8%	650-2	28.6%	650-4	22.8%	650-6	14.6%
	750-B	32.7%	750-0	30.7%	750-2	27.7%	750-4	19.1%	750-6	7.2%
Normalised Char yield wt.% biomass	Sample	Char	Sample	Char	Sample	Char	Sample	Char	Sample	Char
	450-B	37.6%	450-0	36.5%	450-2	36.0%	450-4	33.1%	450-6	31.9%
	550-B	35.2%	550-0	33.6%	550-2	33.2%	550-4	32.2%	550-6	32.1%
	650-B	33.5%	650-0	32.9%	650-2	30.1%	650-4	28.7%	650-6	27.8%
	750-B	32.7%	750-0	31.2%	750-2	29.3%	750-4	26.7%	750-6	25.5%

Table 2.4 Analysis of char from pyrolysed almond residue at various temperatures (dry basis)

Elemental analysis (wt. %)				
Sample	Carbon	Hydrogen	Nitrogen	Oxygen*
450-B	55.7%	3.3%	1.0%	40.0%
550-B	56.7%	2.1%	1.2%	40.0%
650-B	61.5%	1.0%	1.0%	35.8%
750-B	62.3%	1.2%	1.3%	35.3%

Table 2.5: Temperatures of initiation and completion of mass loss, and Temperature at peak loss rate by stage, for almond residue pyrolysis heated at 15°C/min to 750 °C

Sample	T_o (°C)	T_{p1} (°C)	T_{p2}(°C)	T_{p3} (°C)	T_{p4}(°C)	T_{p5}(°C)	T_{p6}°C)	T_f (°C)
750-B	179	205	265	315	446	657		682
750-2	174	202	263	310	427	643	688	714
750-4	171	202	259	306	425	643	669	720
750-6	169	202	254	308	428	633	686	734

Table 3.1: Ultimate analysis and Proximate analysis of almond residue, and of pine chips, on dry basis

Biomass type	Ultimate analysis					Proximate analysis		
	C	H	O*	N	S	Volatile matter	Fixed carbon	Ash
Almond residue (AR)	42.6%	5.9%	49.9%	1.2%	<0.4%	73.4%	23.4%	3.2%
Pine chips (PC)	46.4%	6.5%	46.5%	0.2%	<0.4%	74.6%	24.0%	1.4%

*By difference

Table 4.1: Iron ore analysis as supplied by FMG (%wt)

Component	Fe	SiO_2	Al_2O_3	TiO_2	Mn	CaO	P	S	MgO
CIO	57.94	5.77	2.53	0.14	0.59	0.04	0.058	0.030	0.08
IOT	47.82	12.23	7.28	0.31	1.21	0.07	0.07	0.05	0.23

Component	K_2O	Na_2O	Zn	As	Cl	Cu	Pb	Ba	V
CIO	0.034	0.039	0.006	0.001	0.028	0.001	-	0.010	0.002
IOT	0.20	0.08	0.06	0.00	0.05	0.00	0.00	0.01	0.002

Component	Cr	Ni	Co	Sn	Sr	Zr		LOI	Total
CIO	0.003	0.002	0.002	-	0.005	0.002		7.43	99.99
IOT	0.003	0.002	0.002	-	0.005	0.002		9.19	99.99

Table 4.2: Ultimate analysis and Proximate analysis of almond residue on dry basis

Ultimate analysis					Proximate analysis		
C	H	O*	N	S	Volatile matter	Fixed carbon	Ash
42.6%	5.9%	49.9%	1.2%	<0.4%	73.4%	23.4%	3.2%

*By difference

CHAPTER 5

Table 5.1: Iron ore tailings (IOT) analysis as supplied by FMG (%wt./wt.)

Component	Fe	SiO_2	Al_2O_3	TiO_2	Mn	CaO	P	S	MgO
IOT	47.82	12.23	7.28	0.31	1.21	0.07	0.07	0.05	0.23

Component	K_2O	Na_2O	Zn	As	Cl	Cu	Pb	Ba	V
IOT	0.20	0.08	0.06	0.00	0.05	0.00	0.00	0.01	0.002

Component	Cr	Ni	Co	Sn	Sr	Zr		LOI	Total
IOT	0.003	0.002	0.002	-	0.005	0.002		9.19	99.99

Table 5.2: Iron ore tailings screen sizing - cumulative %wt. passing

Aperture size mm	0.025	0.038	0.053	0.075	0.106	0.150	0.212	0.300	0.425	0.600	0.850	1.00
Percent passing	67.1	72.6	76.7	82.8	87.2	90.8	93.6	95.6	97.0	98.3	99.4	99.8

Table 5.3: Ultimate analysis and Proximate analysis of almond residue on dry basis

Ultimate analysis					Proximate analysis		
C	H	O*	N	S	Volatile matter	Fixed carbon	Ash
42.6%	5.9%	49.9%	1.2%	<0.4%	73.4%	23.4%	3.2%

*By difference

TABLE 6.1 Summary of one and two stage pyrolysis with and without steam reforming

Reference	Reactor configuration	Biomass and elemental hydrogen content (%)	Catalyst details	Operating conditions	Details of study	Reported hydrogen production (g/100g biomass)
1	Two stage fixed bed. First stage: biomass pyrolysis Second Stage: Catalytic reforming	Rice husk (7.2%)	Char, Char supported K (5.8%) Char supported Cu (7.5%) Char supported Fe (8.9%)	Pyrolysis reactor 600°C Reforming reactor 700°C and 800°C	Thermal only 700°C Thermal only 800°C Char only 700°C Char only 800°C K 700°C K 800°C Cu 700°C Cu 800°C Fe 700°C Fe 800°C	0.13 0.29 0.36 0.61 0.47 0.72 0.43 0.68 0.63 0.88
2	Two stage fixed bed. First stage: biomass pyrolysis Second Stage: Catalytic reforming	Pine sawdust (5.75%)	No catalyst, Char only, Char supported iron (~5%)	Pyrolysis reactor 800°C Reforming reactor 800°C	No catalyst Char only Char supported Fe	0.97 1.6 3.6
3	Single bed TGA	Methyl cellulose (MC)(7.6%), Spirlina (SP) (6.2%), Sludge (SL)(4.2%)	No catalyst Catalyst (50% Na_2ZrO_3)	Catalytic pyrolysis reactor 900°C	MC – No catalyst MC – sod. zirconate SP – no catalyst SP – sod. zirconate SL – no catalyst SL – sod. zirconate	0.8 1.7 0.8 1.9 0.6 1.3

Reference	Reactor configuration	Biomass and elemental hydrogen content (%)	Catalyst details	Operating conditions	Details of study	Reported hydrogen production (g/100g biomass)
4	Two stage fixed bed. First stage: biomass pyrolysis Second Stage: Catalytic reforming	Wood sawdust (5.75%)	Char only, Char supported Fe (~6%) /Ni(~6%)	Pyrolysis reactor 800°C Reforming reactor 800°C	Char only Char supported Fe/Ni	1.6 2.8
5	Single stage separated biomass and catalyst beds Two stage fixed bed. First stage: biomass pyrolysis Second Stage: Catalytic reforming	Bagasse (5.76%) Wood sawdust (5.75%)	Ni/NiO Ni/Al/Ca/Mg Steam S/B = 2	Pyrolysis reactor 500°C 600°C Pyrolysis 500°C/600°C Steam reform 800°C 850°C	Uncalcined Ni/NiO Reduced Ni/NiO Ni/Al_2O_3 Ni/Al_2O_3 Ni/Al_2O_3 $Ni/CaAlO_x$ $Ni\text{-}Mg\text{-}AlO_x$ Nio/MgO	2.0 2.6 1.0 3.2 2.2 3.1 4.3 7.0

References: 1:(Guo, F et al. 2018)

2:(Hu, M et al. 2017)

3:(Wang, F et al. 2019)

4:(Hu, M et al. 2020)

5:(Singh et al. 2019)

FIGURES

CHAPTER 1

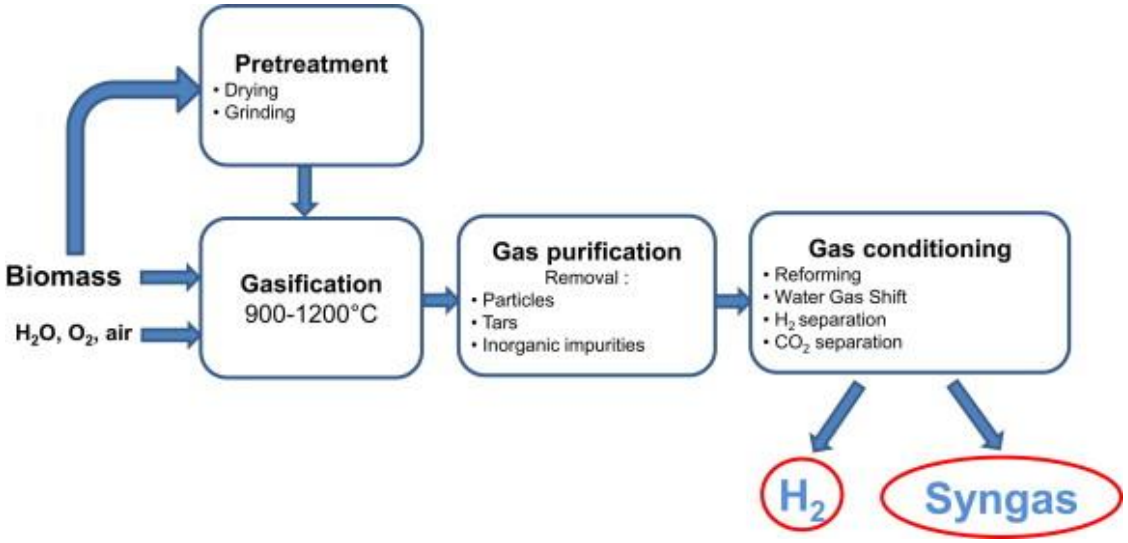

Figure 1.1: Processes involved in classical biomass gasification for syngas (Richardson, Blin & Julbe 2012)

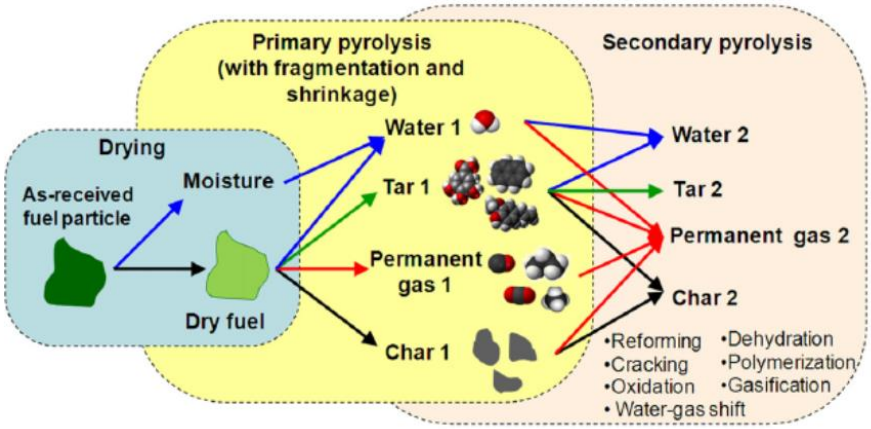

Figure 1.2: Depiction of thermal degradation of a biomass particle in an inert atmosphere (Neves, D. et al. 2011)

Figure 1.3: Moving from reactants to products with mechanical impact energy (Xu et al. 2015)

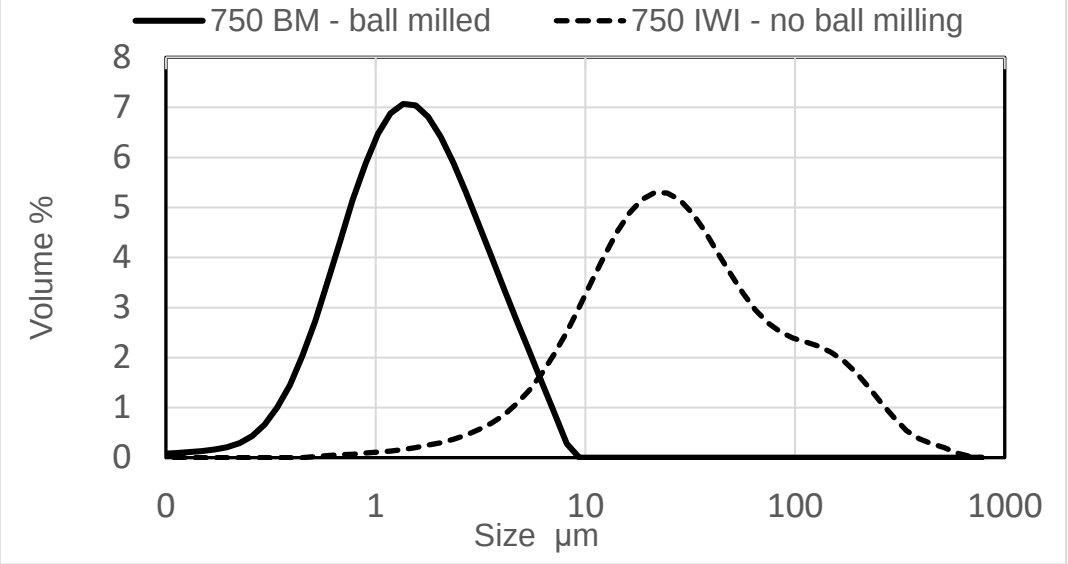

Figure 2.1: Catalyst particle size distribution determined using Malvern Mastersizer 2000 particle size analyser. **Ball milling method**: 6g catalyst with 50g of 3mm zirconia balls milled at 700 rpm for 120 minutes.

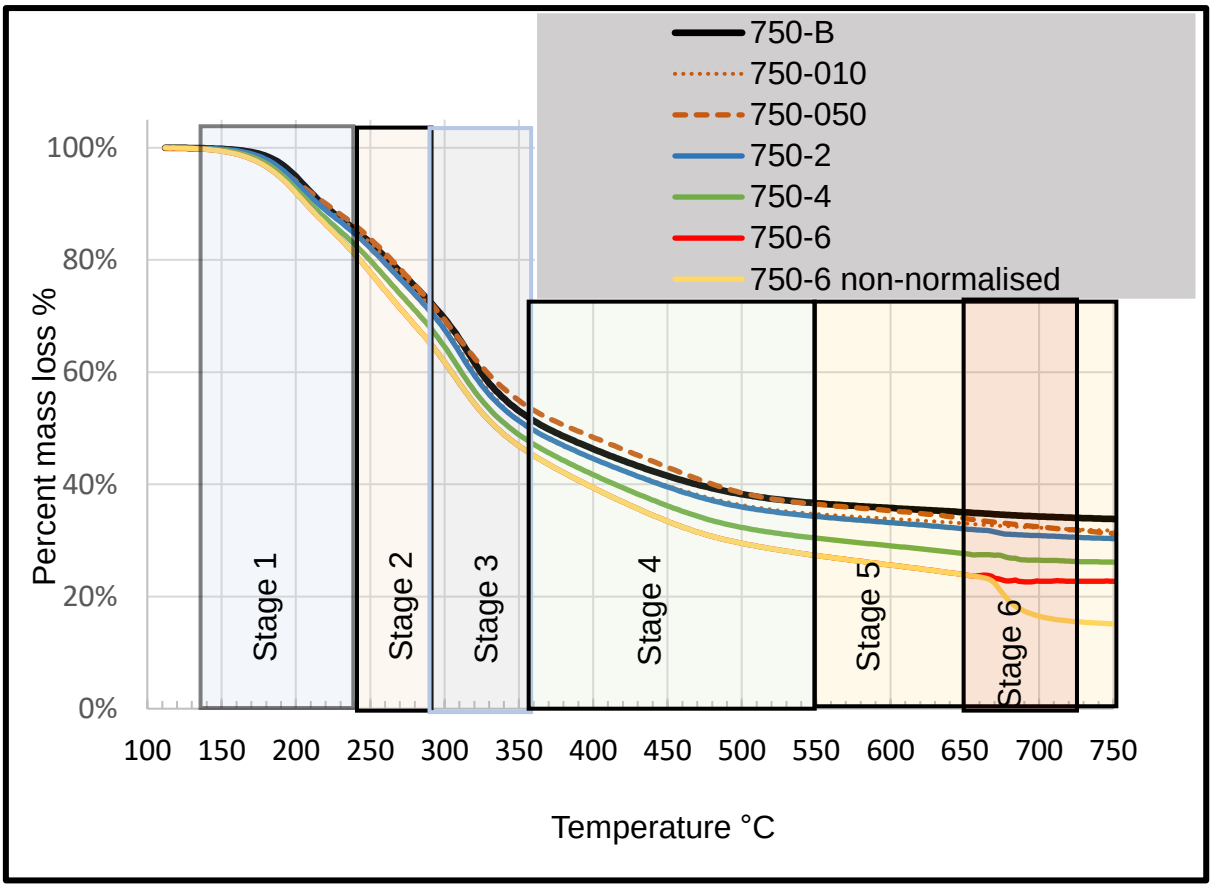

Figure 2.2: (a) The TG curves produced during the pyrolysis of almond residues at peak pyrolysis temperature of 750°C with different catalyst loadings. **Experimental conditions**: In a Mettler Toledo TGA/DSC2 each sample was heated from room temperature at 15°C/minute, using nitrogen as carrier gas (50mL/min), to 105°C, then held for 10 minutes, after which heating continued to the PPT of 750°C which was maintained for 30 minutes. The carrier gas was then switched to oxygen to oxidise the sample over a period of 30 minutes.

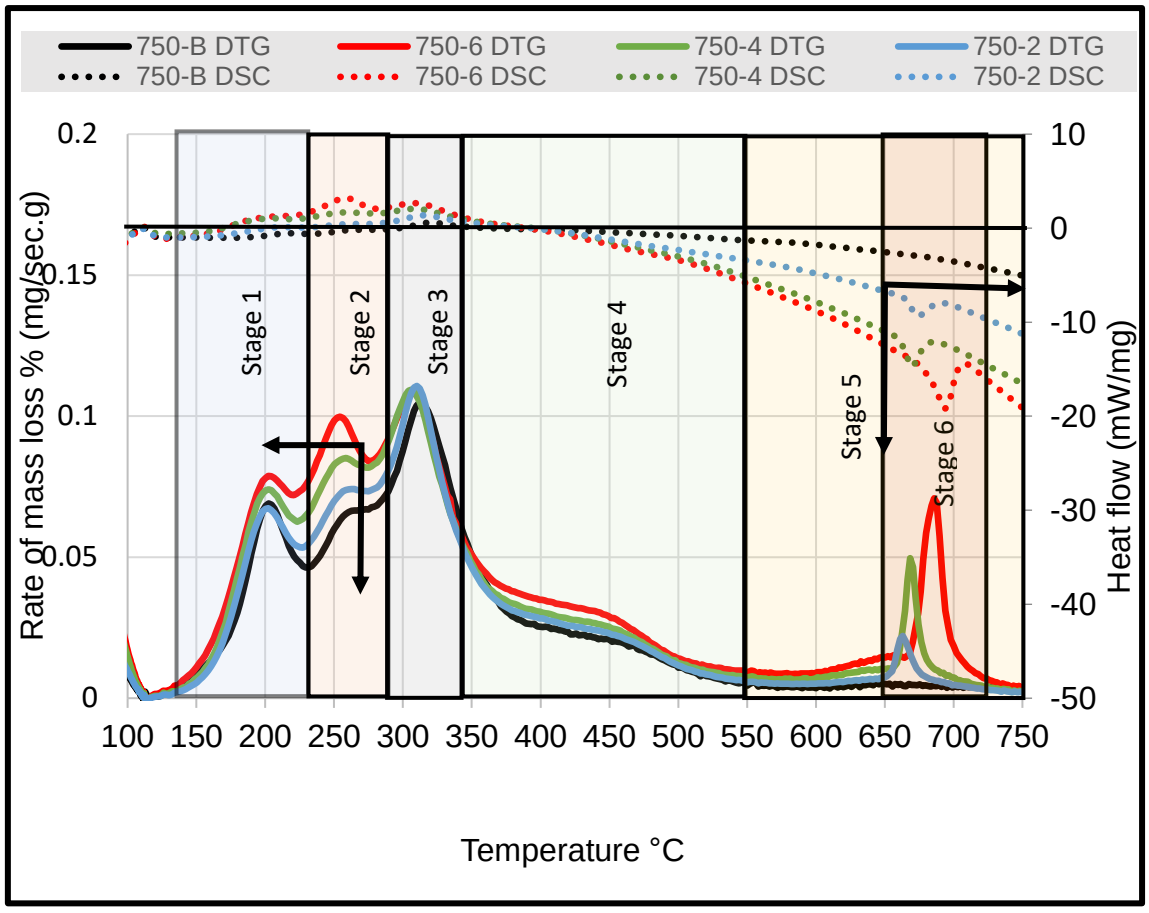

Figure 2.2: (b) DTG curves produced during the pyrolysis of almond residues at peak pyrolysis temperature of 750°C with different catalyst loadings. **Experimental conditions**: In a Mettler Toledo TGA/DSC2 each sample was heated from room temperature at 15°C/minute, using nitrogen as carrier gas (50mL/min), to 105°C, then held for 10 minutes, after which heating continued to the PPT of 750°C which was maintained for 30 minutes. The carrier gas was then switched to oxygen to oxidise the sample over a period of 30 minutes.

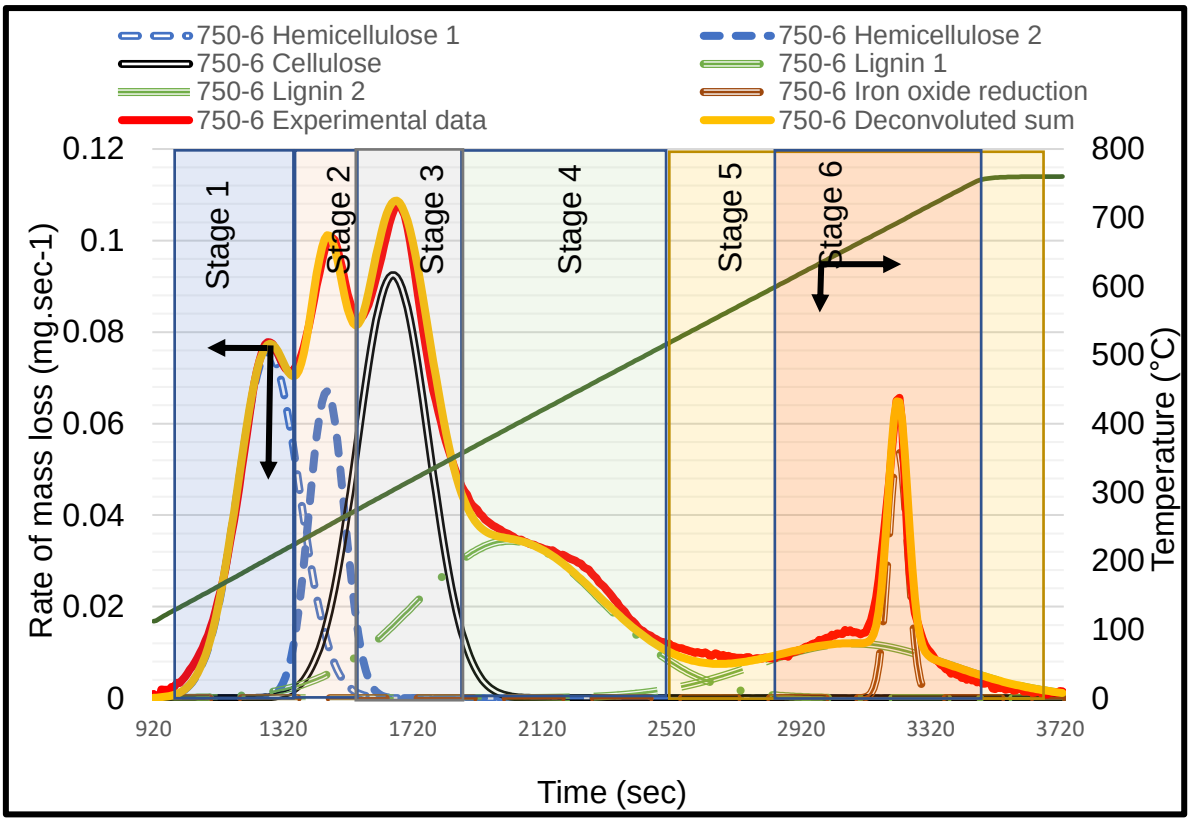

Figure 2.3 a): Degradation of the ligno-cellulosic species as determined from deconvolution of DTG data for the pyrolysis of catalysed almond residue sample 750-6. **Experimental conditions**: In a Mettler Toledo TGA/DSC2 each sample was heated from room temperature at 15°C/minute, using nitrogen as carrier gas (50mL/min), to 105°C, then held for 10 minutes, after which heating continued to the PPT of 750°C which was maintained for 30 minutes. The carrier gas was then switched to oxygen to oxidise the sample over a period of 30 minutes.

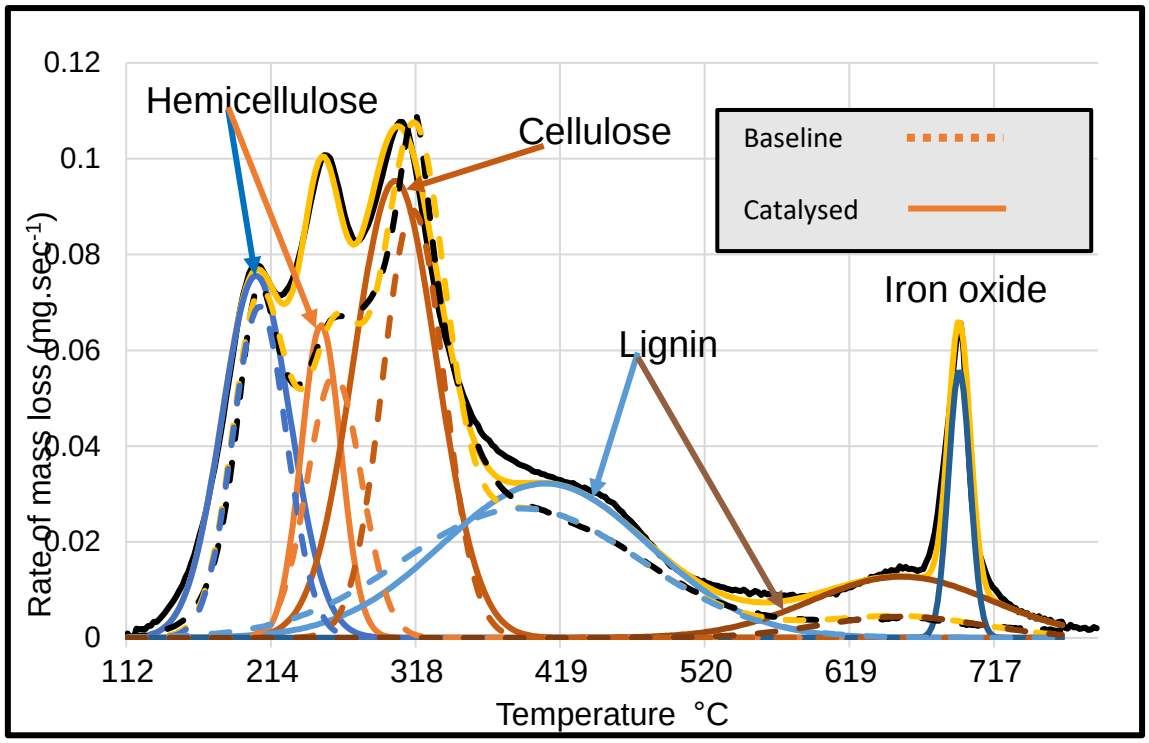

Figure 2.3 b): Degradation of the ligno-cellulosic species as determined from deconvolution of DTG data, for the pyrolysis of catalysed almond residue samples 750-B and 750-6. **Experimental conditions**: In a Mettler Toledo TGA/DSC2 the sample was heated from room temperature at 15°C/minute, using nitrogen as carrier gas (50mL/min), to 105°C, then held for 10 minutes, after which heating continued to the PPT of 750°C which was maintained for 30 minutes. The carrier gas was then switched to oxygen to oxidise the sample over a period of 30 minutes.

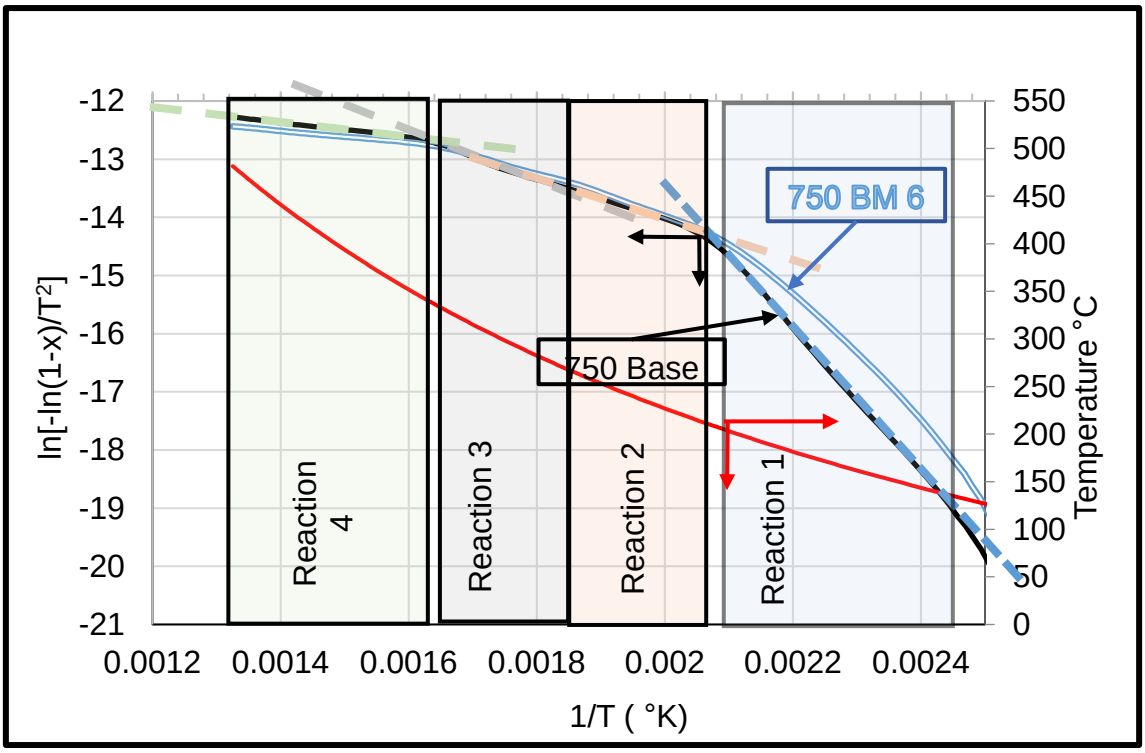

Figure 2.4: Four first order reactions were identified as occurring during pyrolysis of almond residue (AR) at 750°C. **Experimental conditions**: In a Mettler Toledo TGA/DSC2 the samples were heated from room temperature at 15°C/minute, using nitrogen as carrier gas (50mL/min), to 105°C, then held for 10 minutes, after which heating continued to the PPT of 750°C which was maintained for 30 minutes. The carrier gas was then switched to oxygen to oxidise the sample over a period of 30 minutes.

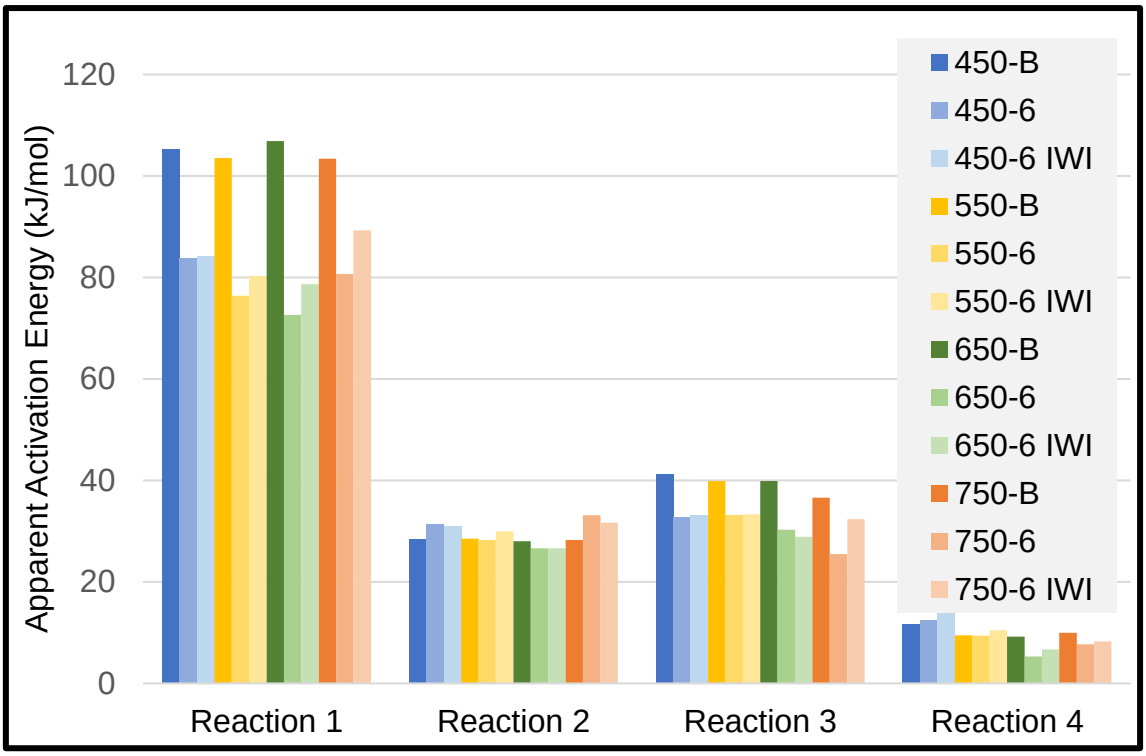

Figure 2.5: Apparent Activation Energies (kJ/mol) derived from reaction kinetic data for each reaction for each PPT and catalyst loading. **Experimental conditions**: In a Mettler Toledo TGA/DSC2 the samples were heated from room temperature at 15°C/minute, using nitrogen as carrier gas (50mL/min), to 105°C, then held for 10 minutes, after which heating continued to the PPT of 750°C which was maintained for 30 minutes. The carrier gas was then switched to oxygen to oxidise the sample over a period of 30 minutes.

CHAPTER 3

VERTICAL FURNACE - EQUIPMENT DETAIL AND LAYOUT

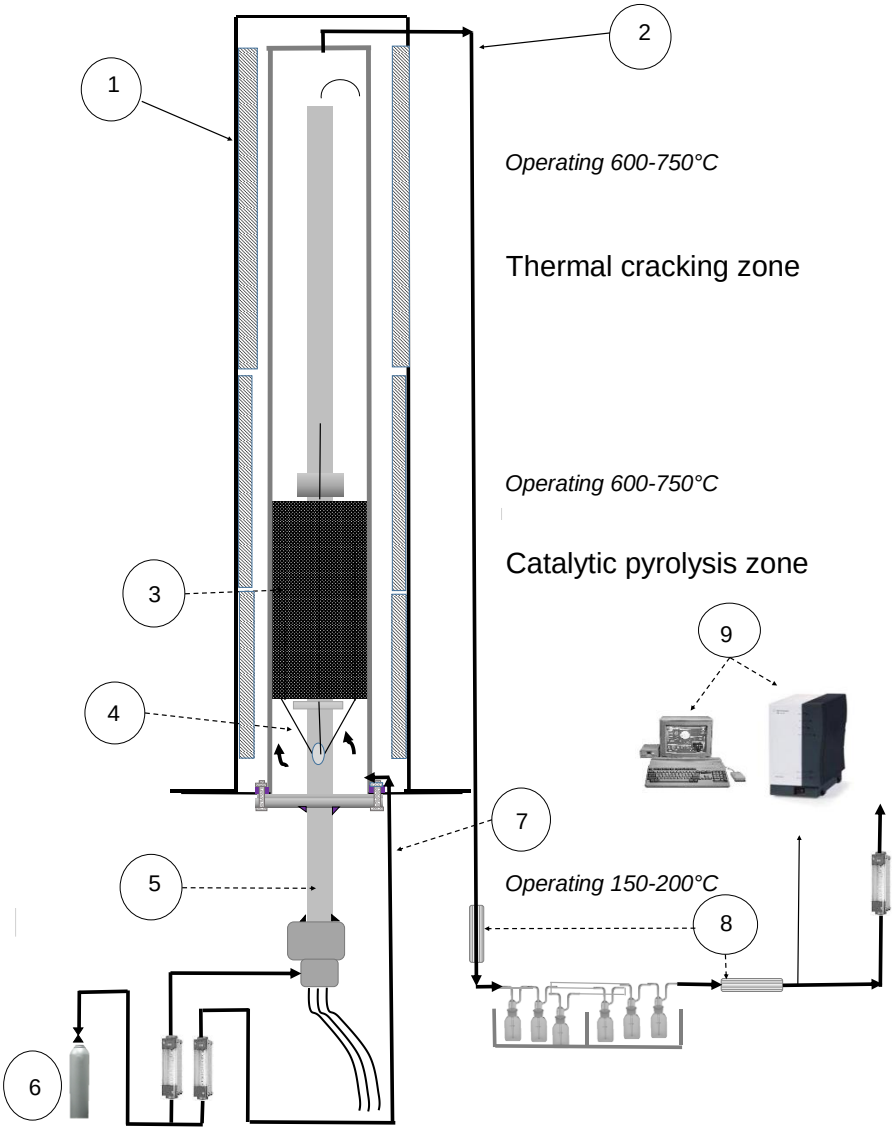

Figure 3.1: Schematic diagram of the experimental setup

1:Carbolite three element furnace, 2: Pyrolysis gas product outlet, 3: Biomass sample with co-mingled char supported catalyst, 4: Thermocouples, 5: Sample tube carrier,6: Nitrogen sweeping gas supply, 7: Sweeping gas inlet, 8: Fine filters to remove particulates, 9: Gas chromatograph for gas analysis and data acquisition

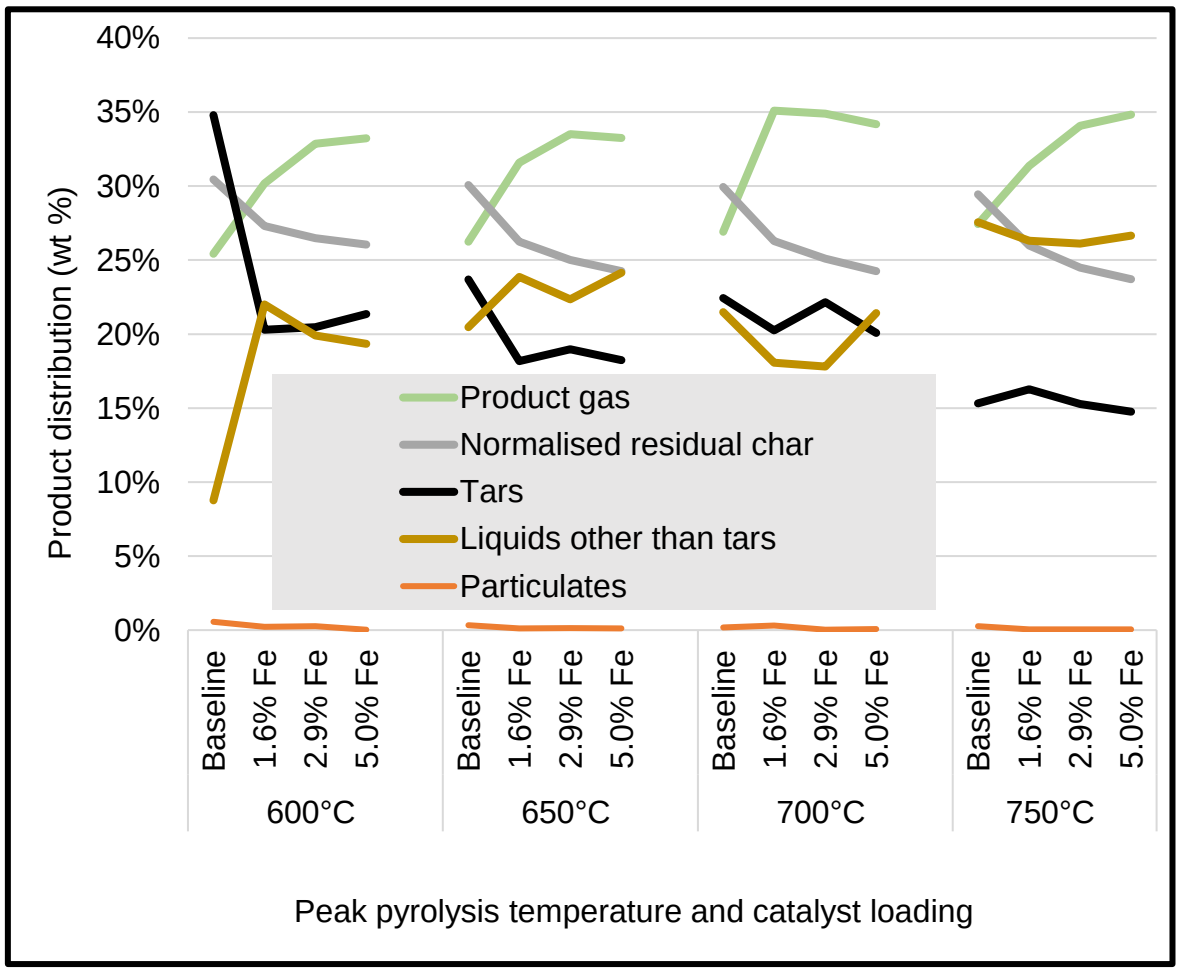

Figure 3.2: Changes in product distribution over a range of pyrolysis temperature and catalyst loading, for pyrolysis of almond residues (AR). **Experimental conditions**: Heating rate 50°C/min to peak pyrolysis temperature 600°C-750°C in 50°C increments, held for 30 min. Sweeping gas N_2 at a space velocity of 1.6min^{-1}. Catalyst loadings of 0%, 1.6%, 2.9% and 5.0%Fe.

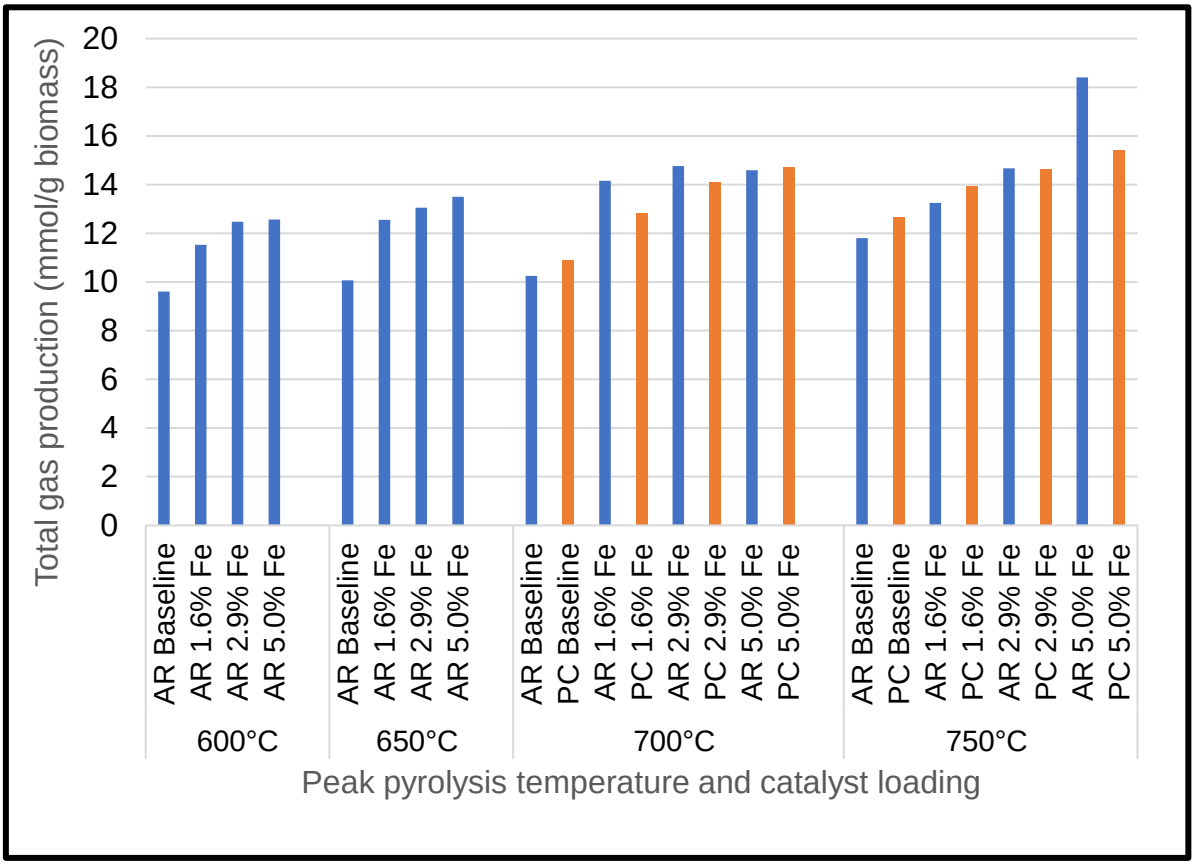

Figure 3.3: Changes in total gas production over a range of pyrolysis temperature and catalyst loading, for pyrolysis of almond residues (AR) and of pine chips (PC). **Experimental conditions**: Heating rate 50°C/min to peak pyrolysis temperature 600°C-750°C in 50°C increments, held for 30 min. Sweeping gas N_2 at a space velocity of 1.6min^{-1}. Catalyst loadings of 0%, 1.6%, 2.9% and 5.0%Fe.

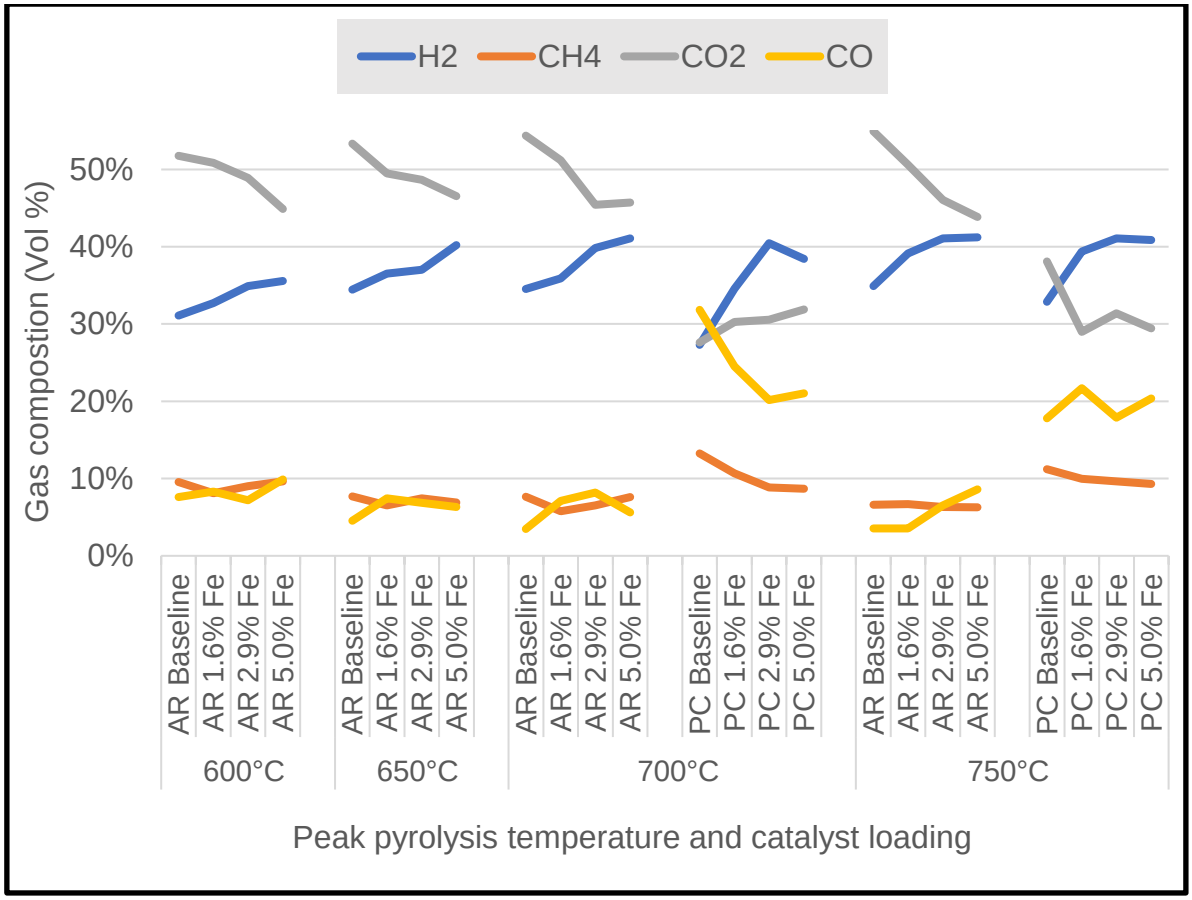

Figure 3.4: Changes in gas component distribution with temperature and catalyst loading for pyrolysis of biomass almond residues (AR) and pine chips (PC). **Experimental conditions**: Heating rate 50°C/min to peak pyrolysis temperature 600°C-750°C in 50°C increments, held for 30 min. Sweeping gas N_2 at a space velocity of 1.6min^{-1}. Catalyst loadings of 0%, 1.6%, 2.9% and 5.0%Fe.

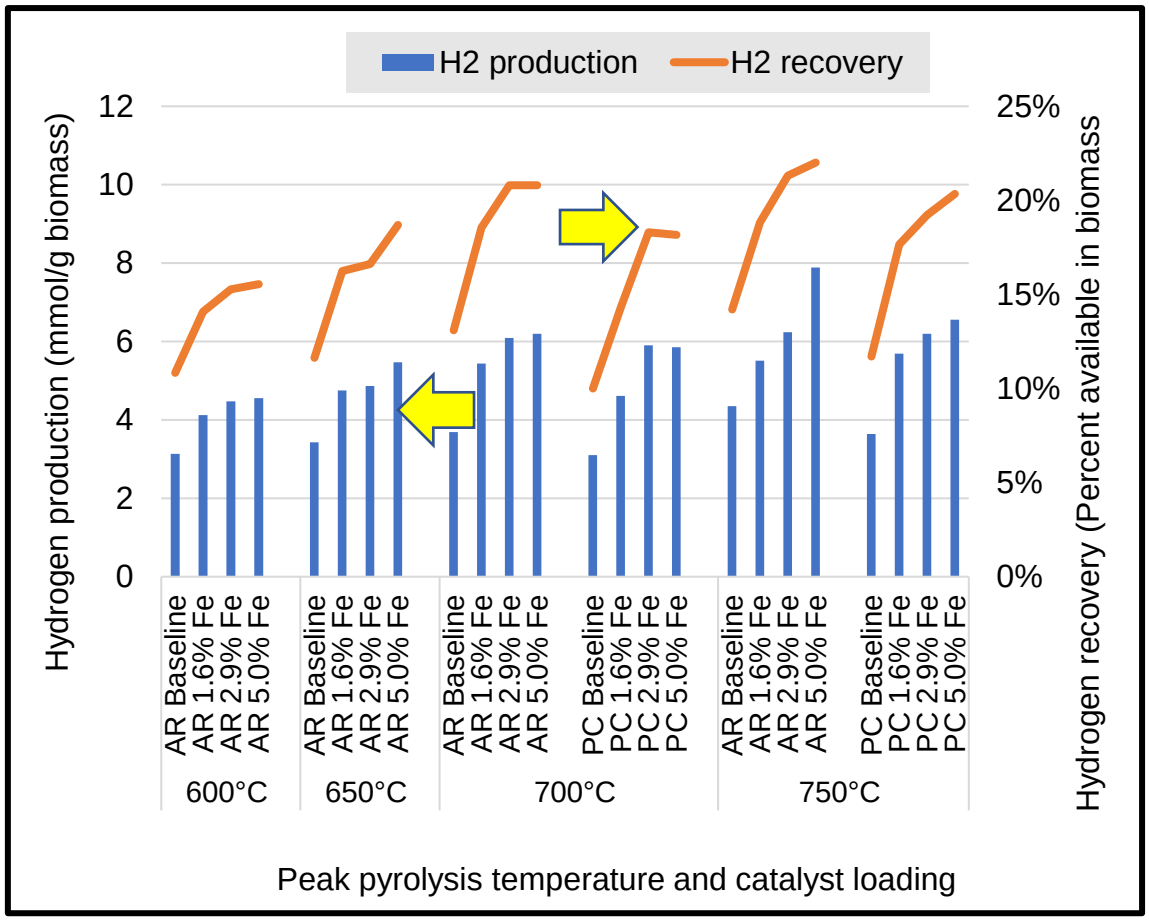

Figure 3.5: Changes in hydrogen production and hydrogen recovery (as a % of hydrogen in biomass) for pyrolysis of almond residues (AR) and pine chip (PC) biomass. **Experimental conditions**: Heating rate 50°C/min to peak pyrolysis temperature 600°C-750°C in 50°C increments, held for 30 min. Sweeping gas N_2 at a space velocity of 1.6min^{-1}. Catalyst loadings of 0%, 1.6%, 2.9% and 5.0%Fe.

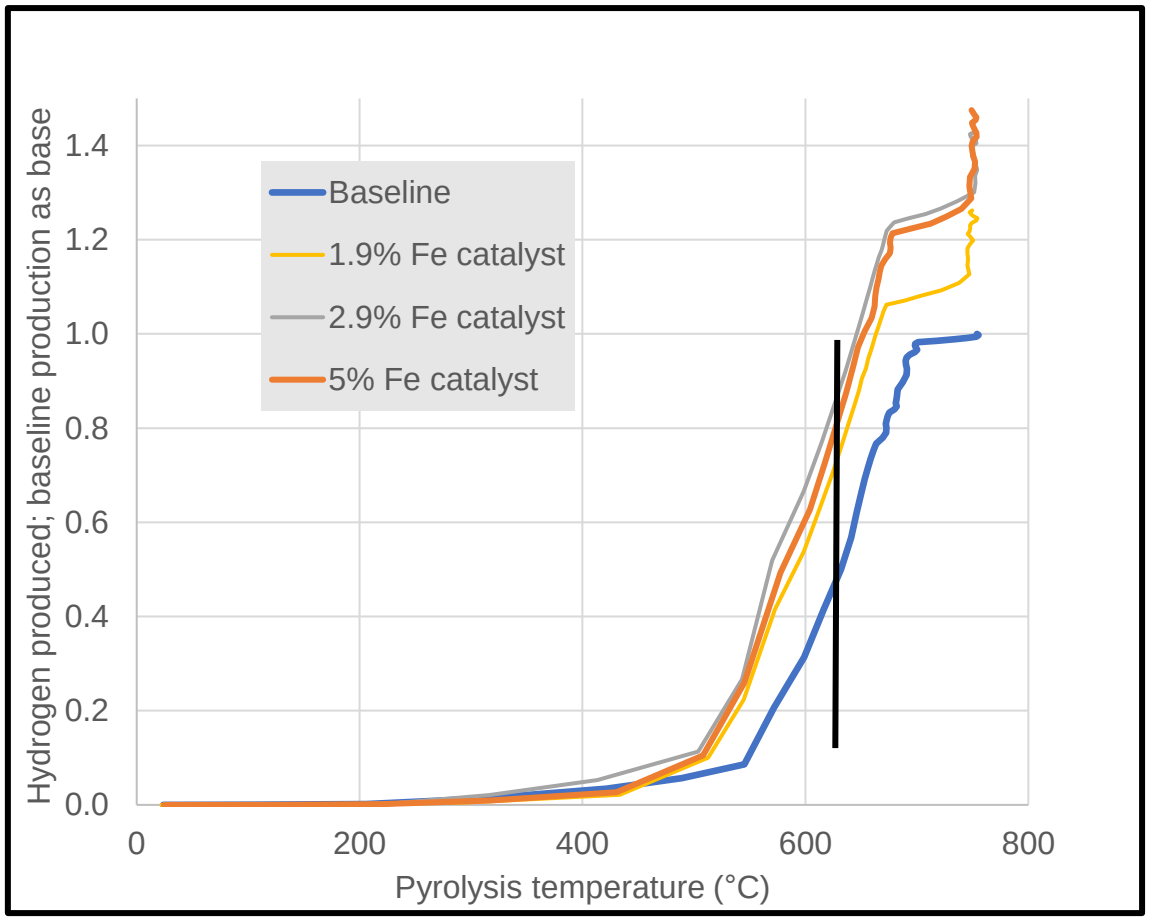

Figure 3.6: Changes in the rate of hydrogen production with catalyst loading during pyrolysis to a peak pyrolysis temperature of 750°C. **Experimental conditions**: Heating rate 50°C/min to peak pyrolysis temperature 750°C, held for 30 mi n. Sweeping gas N_2 at a space velocity of 1.6min^{-1}. Catalyst loadings of 0%, 1.6%, 2.9% and 5.0%Fe.

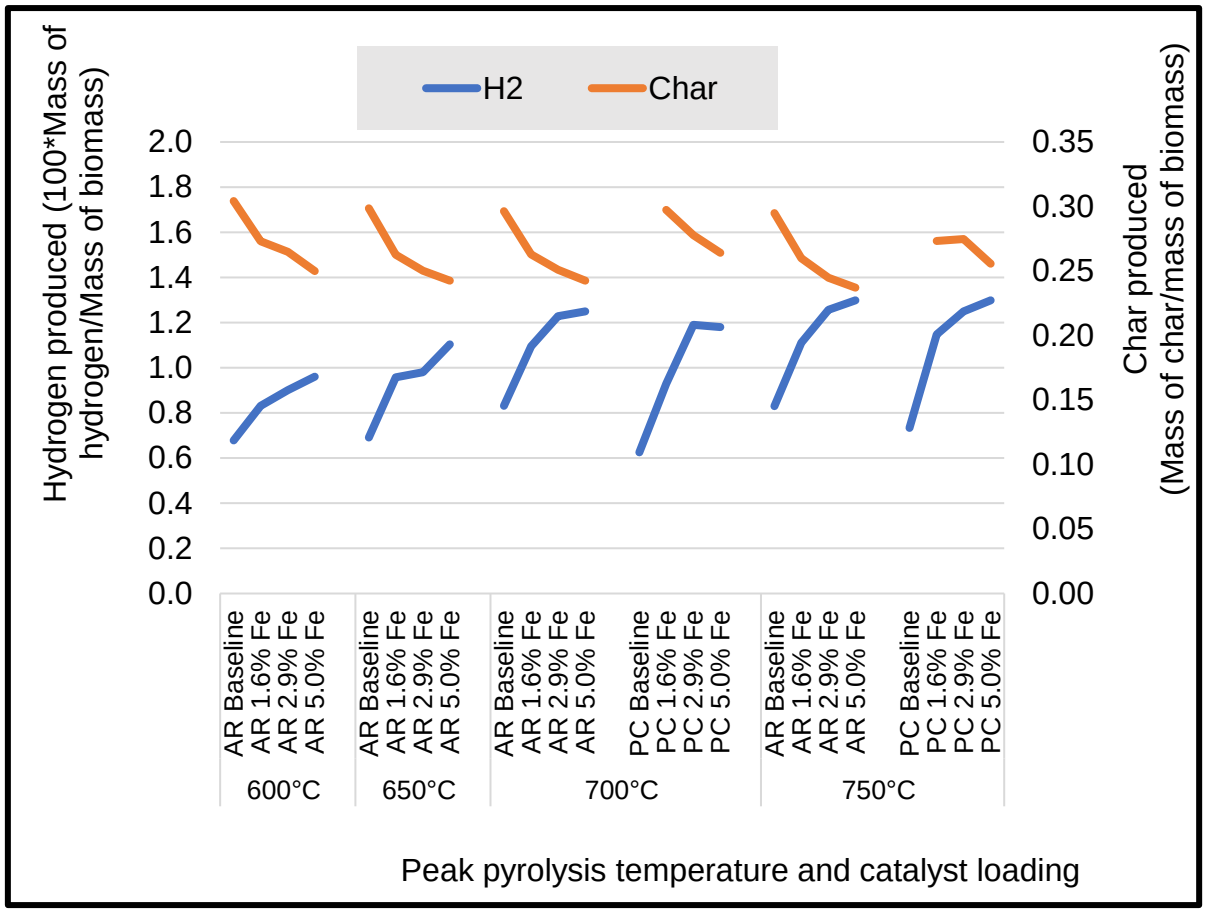

Figure 3.7: The mass of hydrogen and char produced over the course of pyrolysis depict an inverse relationship. **Experimental conditions**: Heating rate 50°C/min to peak pyrolysis temperature 700°C-750°C in 50°C increments, held for 30 min. Sweeping gas N_2 at a space velocity of 1.6min^{-1}. Catalyst loadings of 0%, 1.6%, 2.9% and 5.0%Fe.

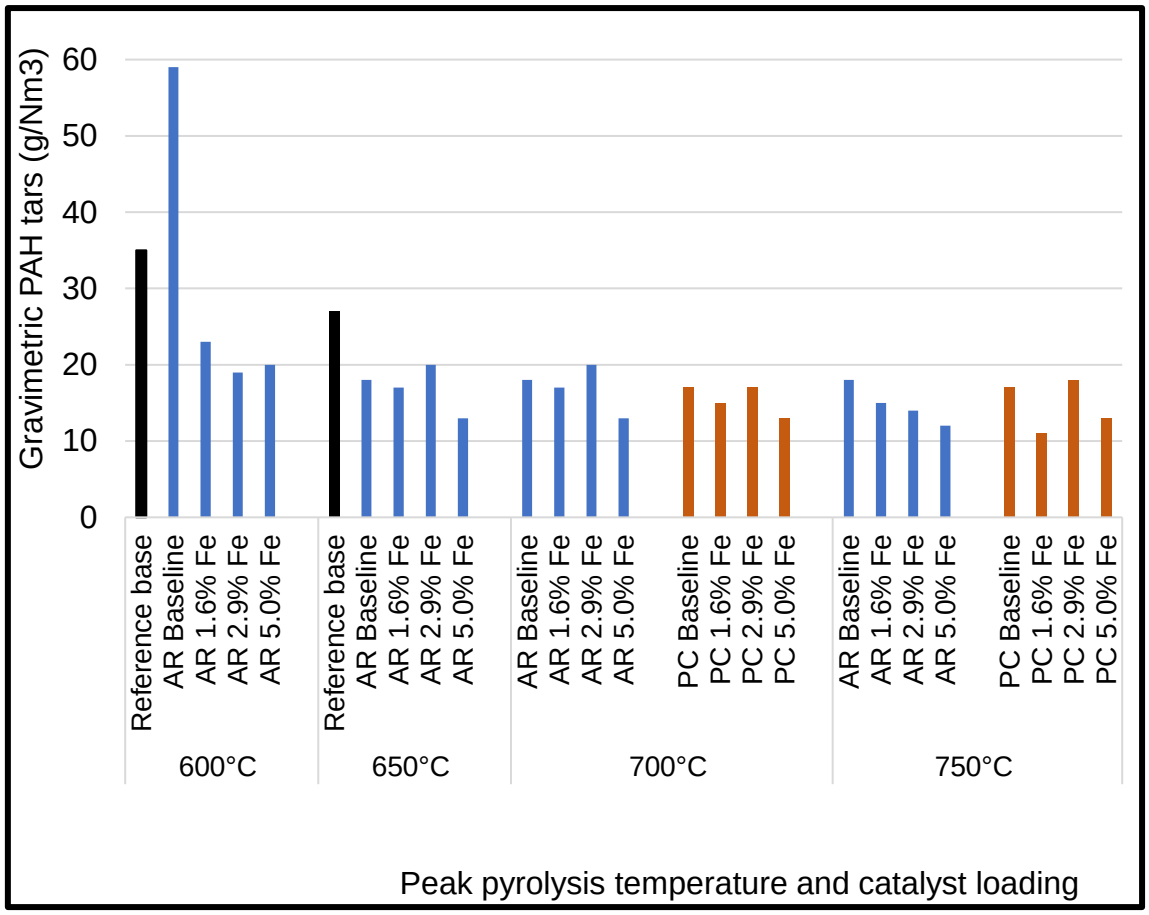

Figure 3.8: Gravimetric PAH tars contained in the pyrolysis product gas streams of almond residue (AR) and pine chips (PC) biomass were determined across a range of pyrolysis temperatures and catalyst loadings. **Experimental conditions**: Heating rate 50°C/min to peak pyrolysis temperature 600°C-750°C in 50°C increments, held for 30 min. Sweeping gas N_2 at a space velocity of 1.6min^{-1}. Catalyst loadings of 0%, 1.6%, 2.9% and 5.0%Fe.

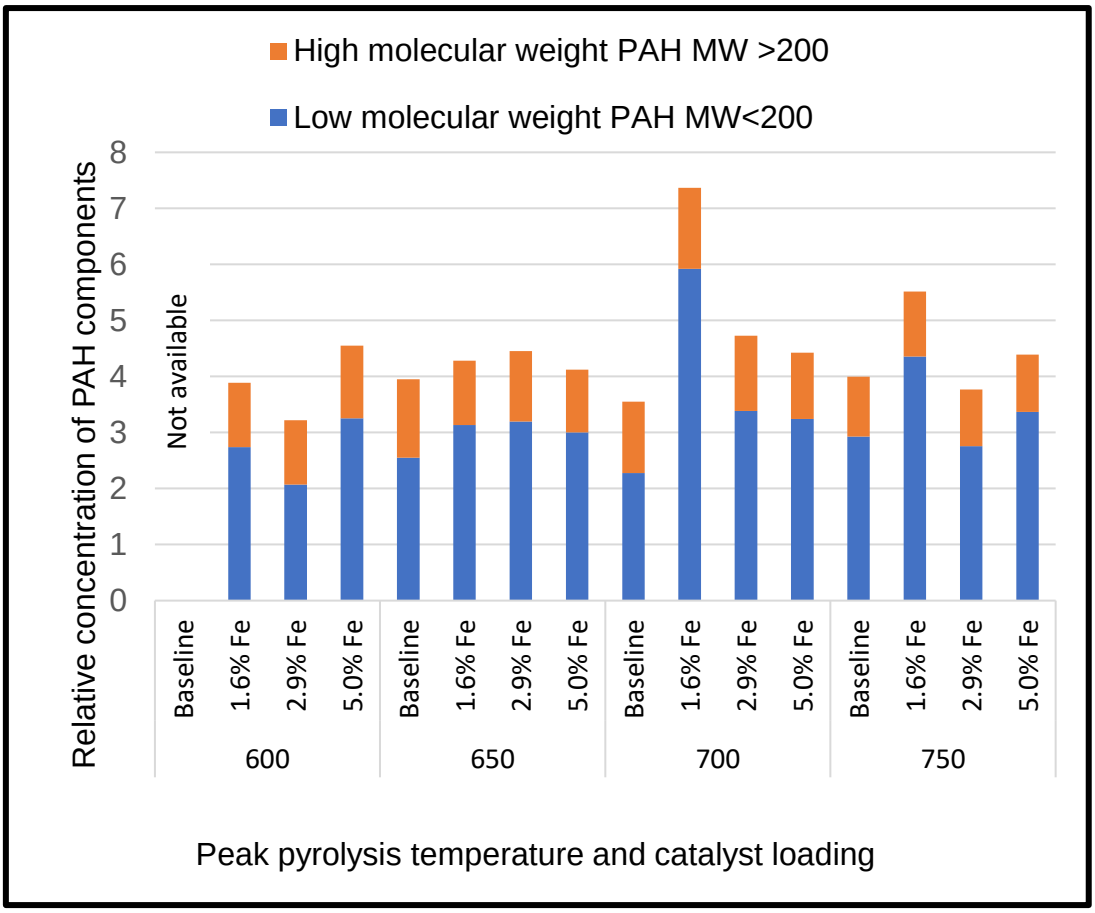

Figure 3.9: The distribution of gravimetric PAH tars for pyrolysis of almond residue (AR) biomass for a range of pyrolysis temperatures and catalyst loadings. **Experimental conditions**: Heating rate 50°C/min to peak pyrolysis temperature 600°C-750°C in 50°C increments, held for 30 min. Sweeping gas N_2 at a space velocity of 1.6min^{-1}. Catalyst loadings of 0%, 1.6%, 2.9% and 5.0%Fe.

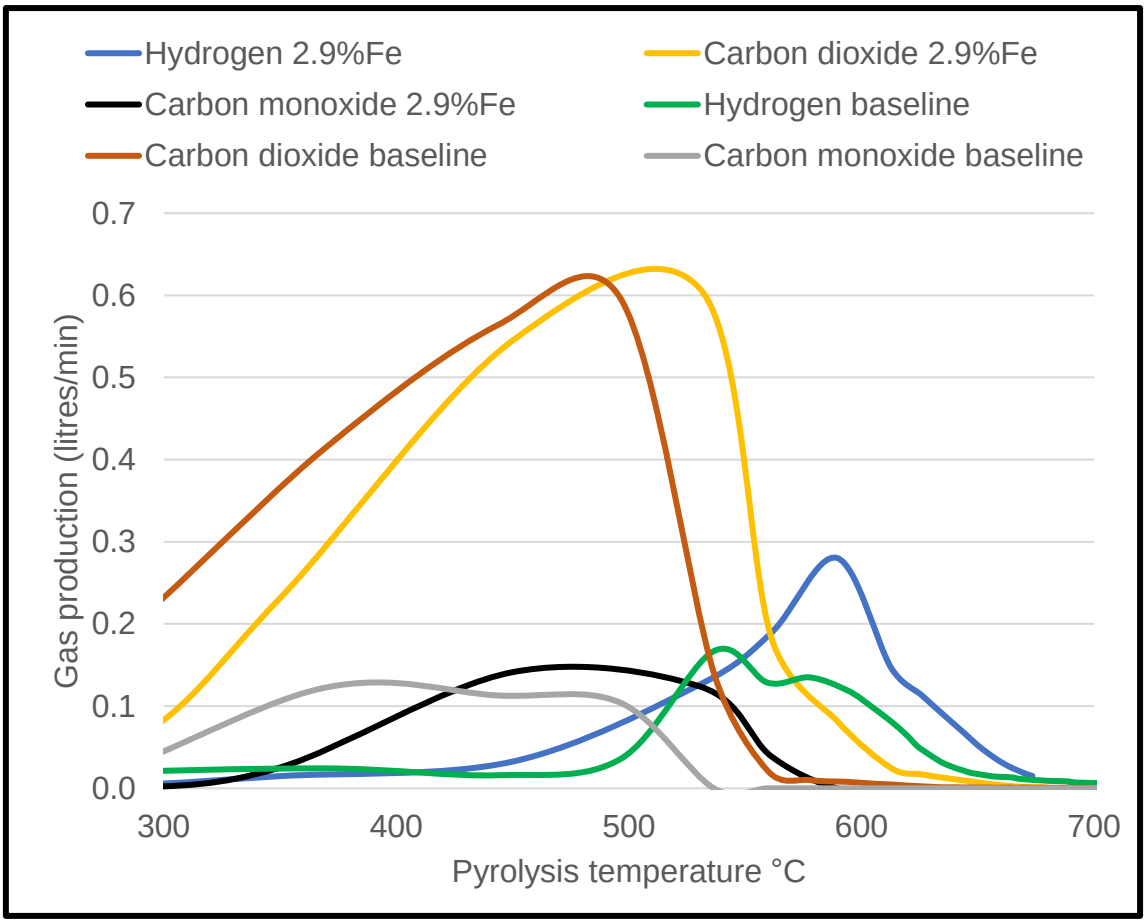

Figure 3.10: The production of carbon oxides and hydrogen during the progress of pyrolysis of almond residue (AR) biomass to a peak pyrolysis temperature of 700°C, for catalyst loadings of 0% and 2.9%Fe. **Experimental conditions**: Heating rate 50°C/min to peak pyrolysis temperature 700°C, held for 30 min. Sweeping gas N_2 at a space velocity of 1.6min^{-1}. Catalyst loadings of 0%, and 2.9%Fe.

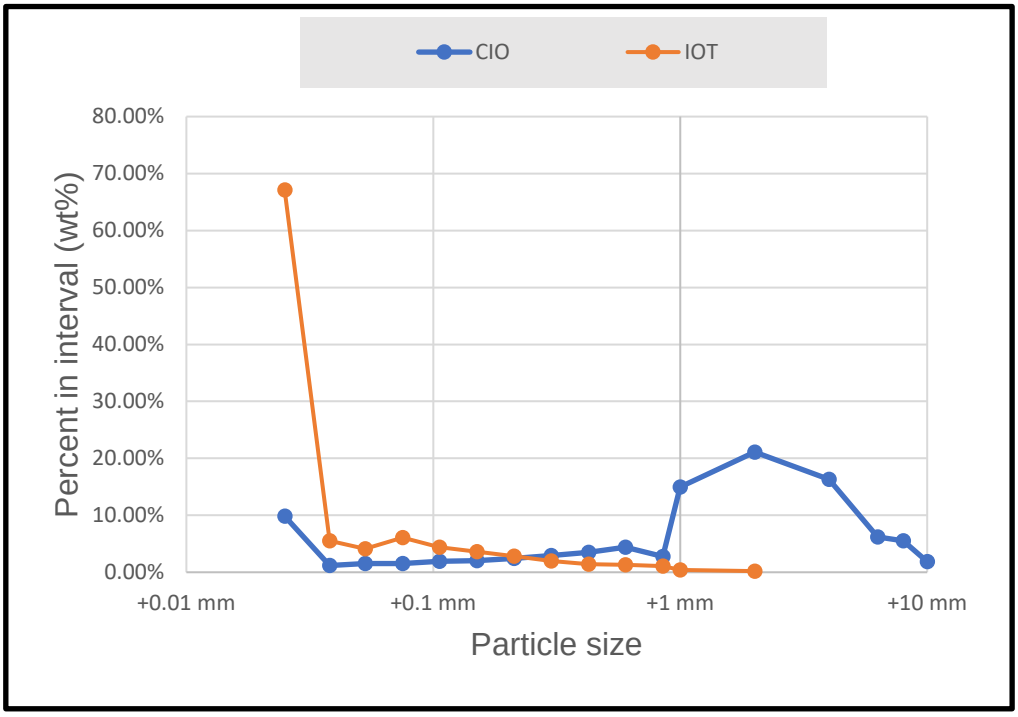

Figure 4.1: Size distribution of CIO and IOT samples, as received

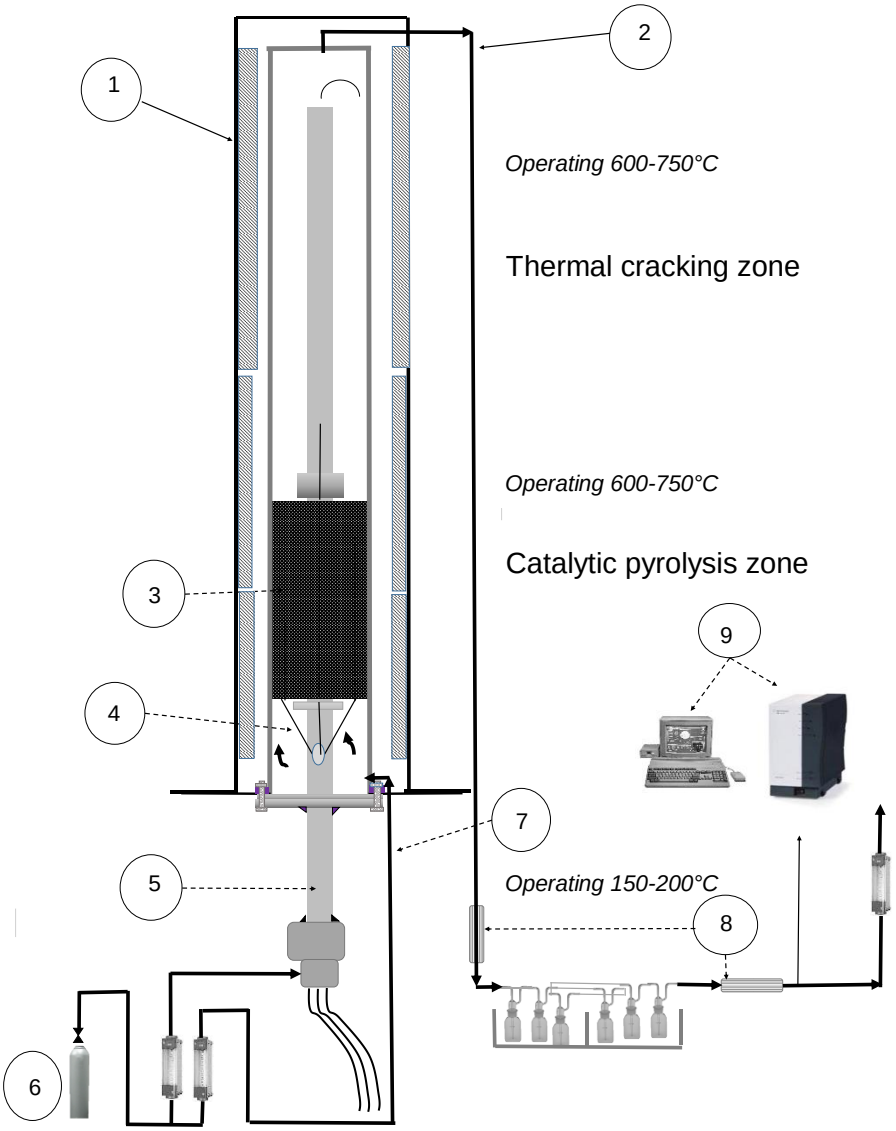

Figure 4.2: Schematic diagram of the experimental setup

1:Carbolite three element furnace, 2: Pyrolysis gas product outlet, 3: Biomass sample with co-mingled char supported catalyst, 4: Thermocouples, 5: Sample tube carrier,6: Nitrogen sweeping gas supply, 7: Sweeping gas inlet, 8: Fine filters to remove particulates, 9: Gas chromatograph for gas analysis and data acquisition

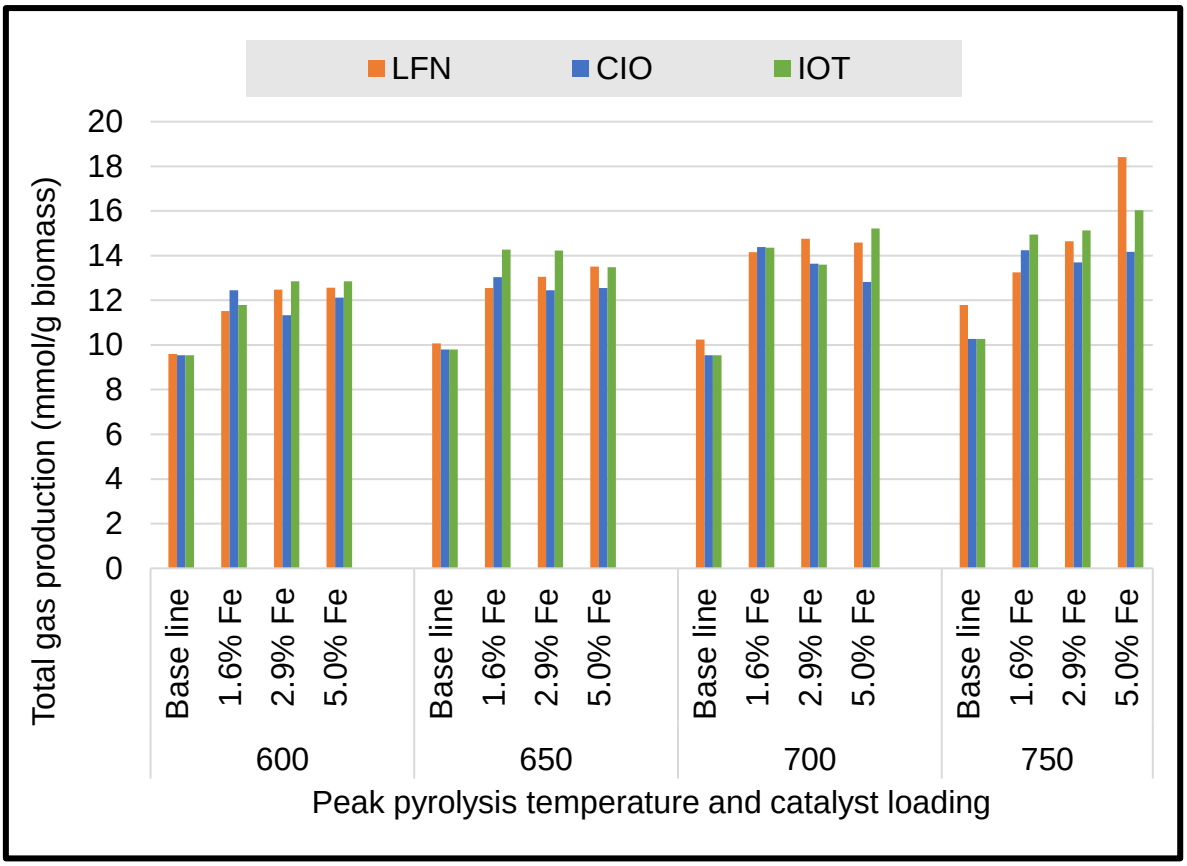

Figure 4.3: Changes in total gas production for the three catalyst types LFN, CIO and IOT, for catalytic pyrolysis of almond residues (AR). **Experimental conditions**: Heating rate 50°C/min to peak pyrolysis temperature 600°C-750°C in 50°C increments, held for 30 min. Sweeping gas N_2 at a space velocity of 1.6min^{-1}. Catalyst loadings of 0%, 1.6%, 2.9% and 5.0%Fe.

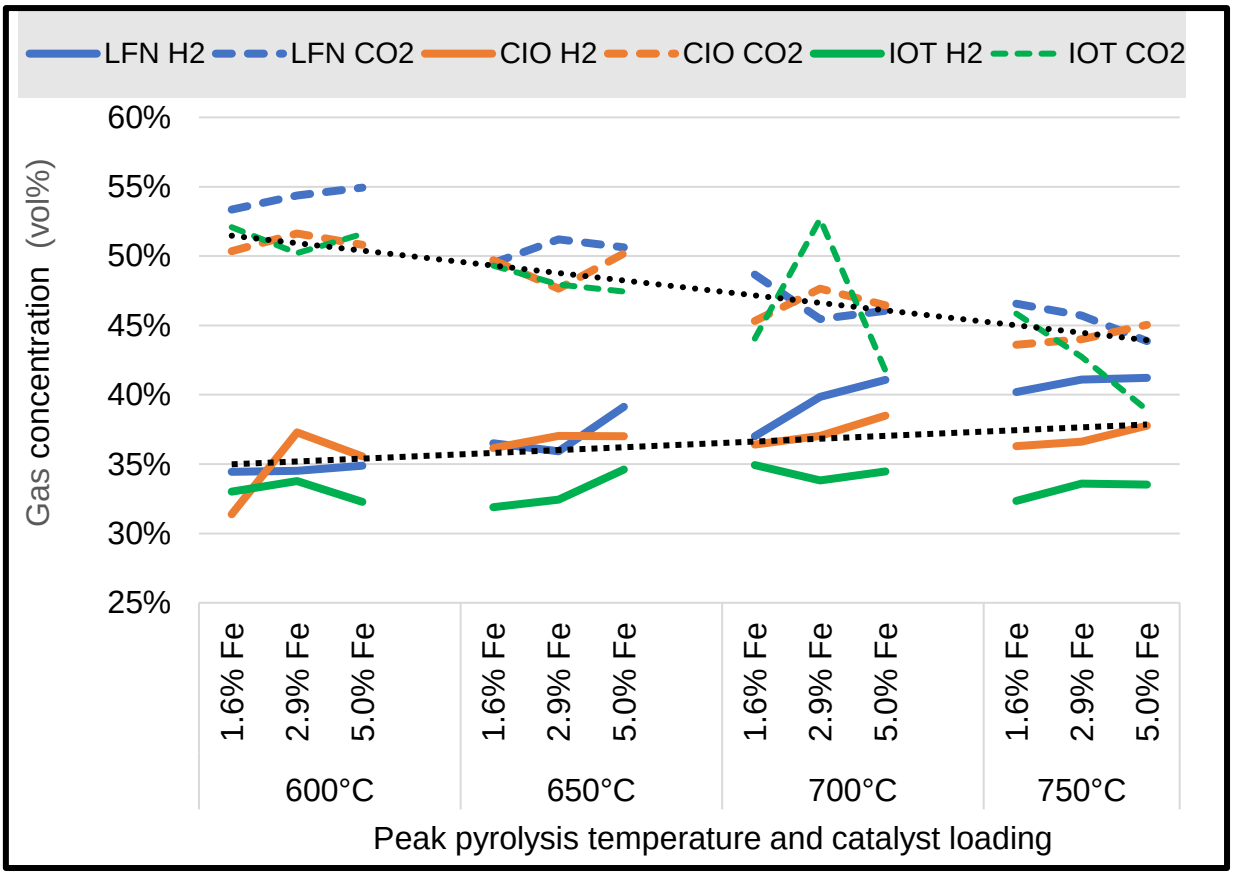

Figure 4.4: Changes in gas component distribution for the three catalyst types LFN, CIO and IOT, for catalytic pyrolysis of almond residues (AR). **Experimental conditions**: Heating rate 50°C/min to peak pyrolysis temperature 600°C-750°C in 50°C increments, held for 30 min. Sweeping gas N_2 at a space velocity of 1.6min^{-1}. Catalyst loadings of 1.6%, 2.9% and 5.0%Fe.

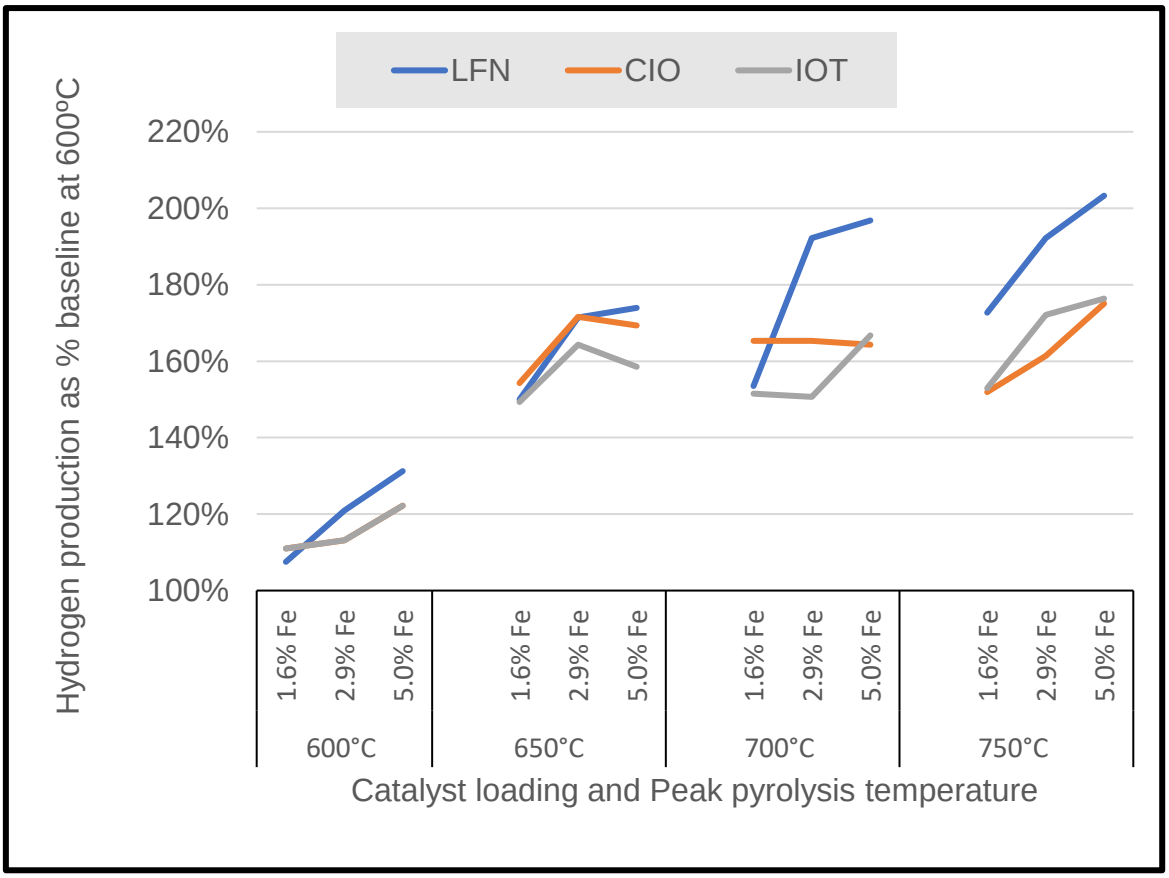

Figure 4.5: Changes in hydrogen production relative to baseline production at 600°C for the three catalyst type LFN, CIO and IOT, for catalytic pyrolysis of almond residues (AR). **Experimental conditions**: Heating rate 50°C/min to peak pyrolysis temperature 600°C-750°C in 50°C increments, held for 30 min. Sweeping gas N_2 at a space velocity of 1.6min^{-1}. Catalyst loadings of 1.6%, 2.9% and 5.0%Fe.

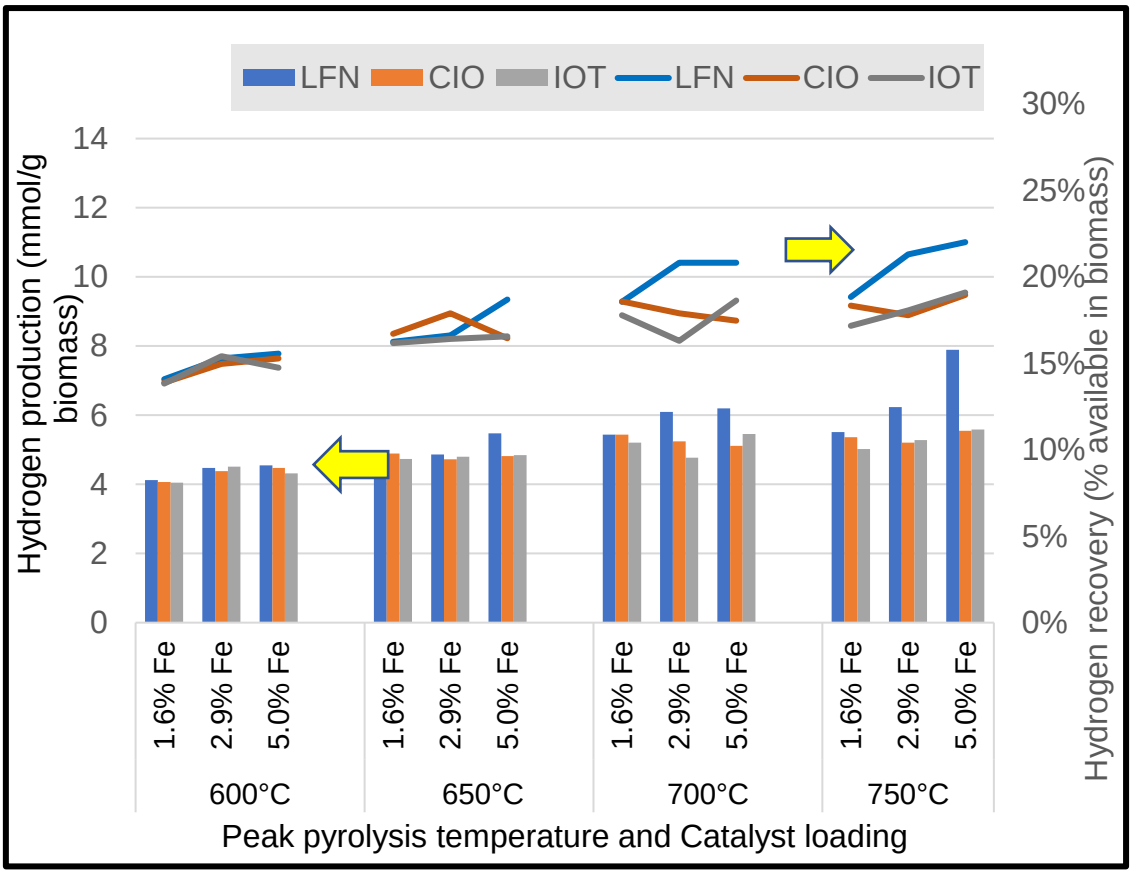

Figure 4.6: Changes in hydrogen production and hydrogen recovery (as a % of hydrogen in biomass) for the three catalyst type LFN, CIO and IOT, for catalytic pyrolysis of almond residues (AR). **Experimental conditions**: Heating rate 50°C/min to peak pyrolysis temperature 600°C-750°C in 50°C increments, held for 30 min. Sweeping gas N_2 at a space velocity of 1.6min^{-1}. Catalyst loadings of 1.6%, 2.9% and 5.0%Fe.

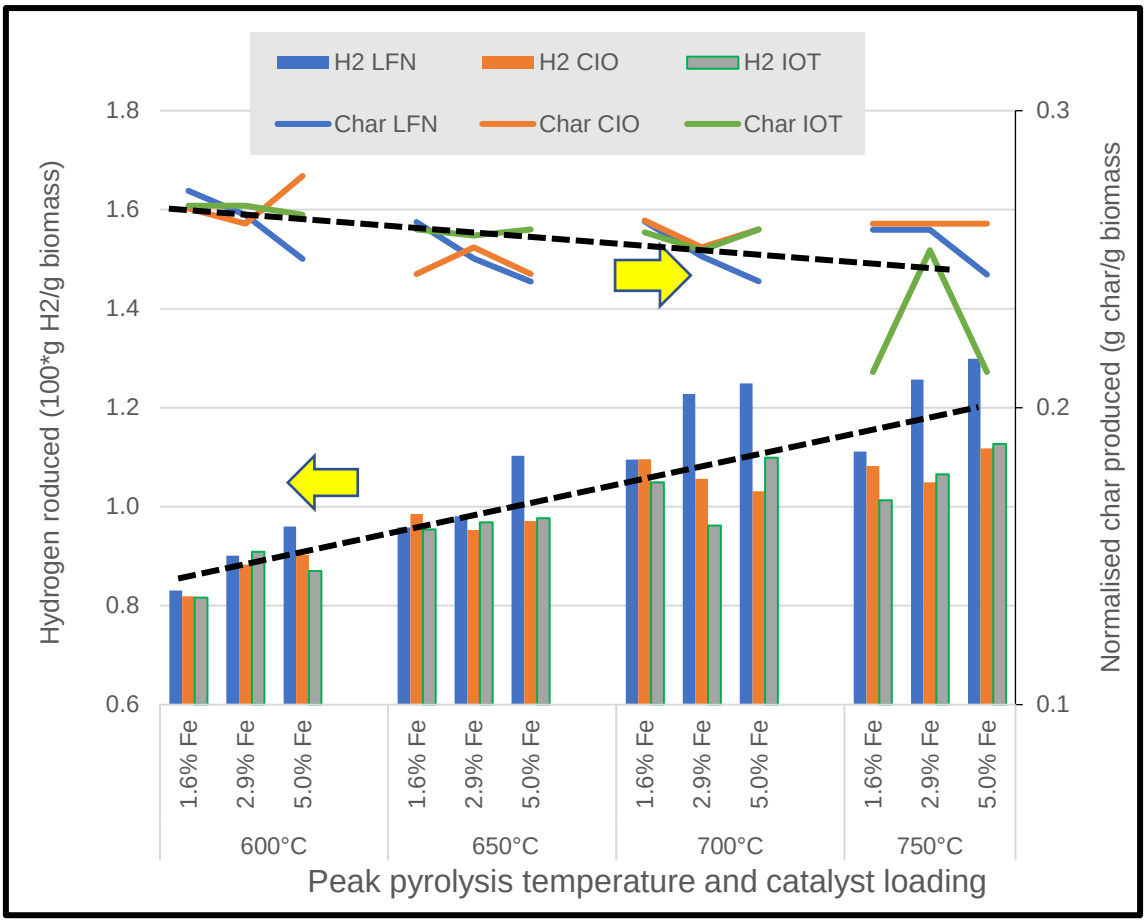

Figure 4.7: Changes in the mass of hydrogen produced and the mass of char produced for the three catalyst types LFN, CIO and IOT, for catalytic pyrolysis of almond residues (AR). **Experimental conditions**: Heating rate 50°C/min to peak pyrolysis temperature 600°C-750°C in 50°C increments, held for 30 min. Sweeping gas N_2 at a space velocity of 1.6min^{-1}. Catalyst loadings of 1.6%, 2.9% and 5.0%Fe.

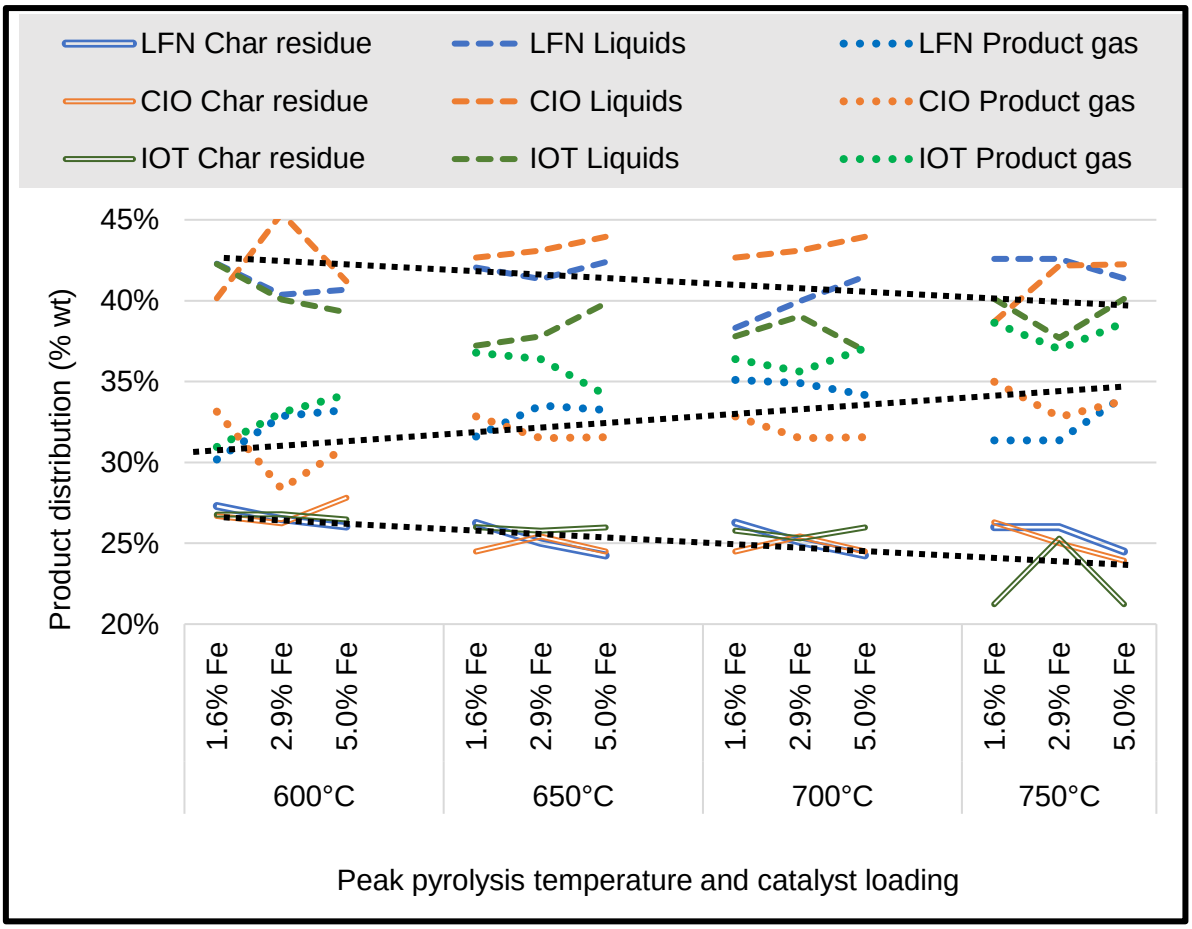

Figure 4.8: Distribution of primary products of normalised char, liquids including tars, and product gas are shown for the three catalyst types LFN, CIO and IOT, for catalytic pyrolysis of almond residues (AR). **Experimental conditions**: Heating rate 50°C/min to peak pyrolysis temperature 600°C-750°C in 50°C increments, held for 30 min. Sweeping gas N_2 at a space velocity of 1.6min^{-1}. Catalyst loadings of 1.6%, 2.9% and 5.0%Fe.

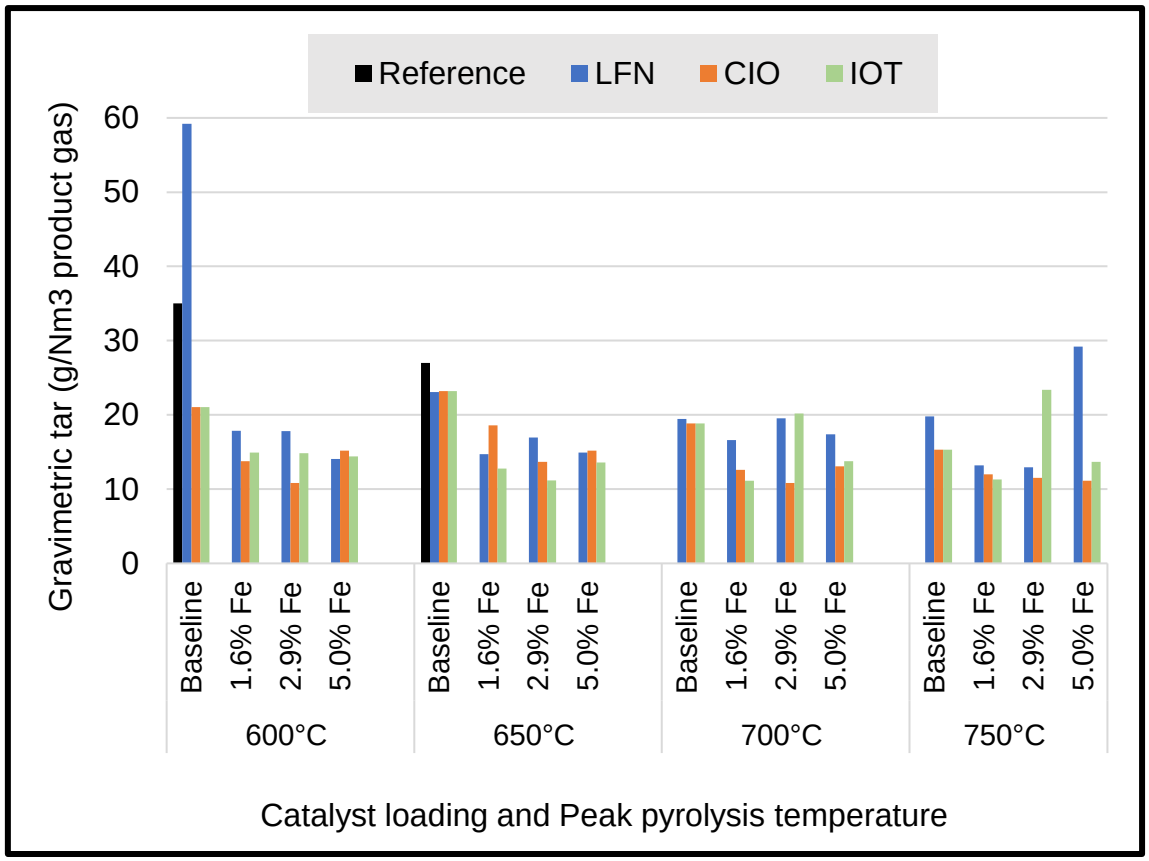

Figure 4.9: The quantity of gravimetric tar in product gas the three catalyst types LFN, CIO and IOT. **Experimental conditions**: Heating rate 50°C/min to peak pyrolysis temperature 600°C-750°C in 50°C increments, held for 30 min. Sweeping gas N_2 at a space velocity of 1.6min^{-1}. Catalyst loadings of 0%, 1.6%, 2.9% and 5.0%Fe.

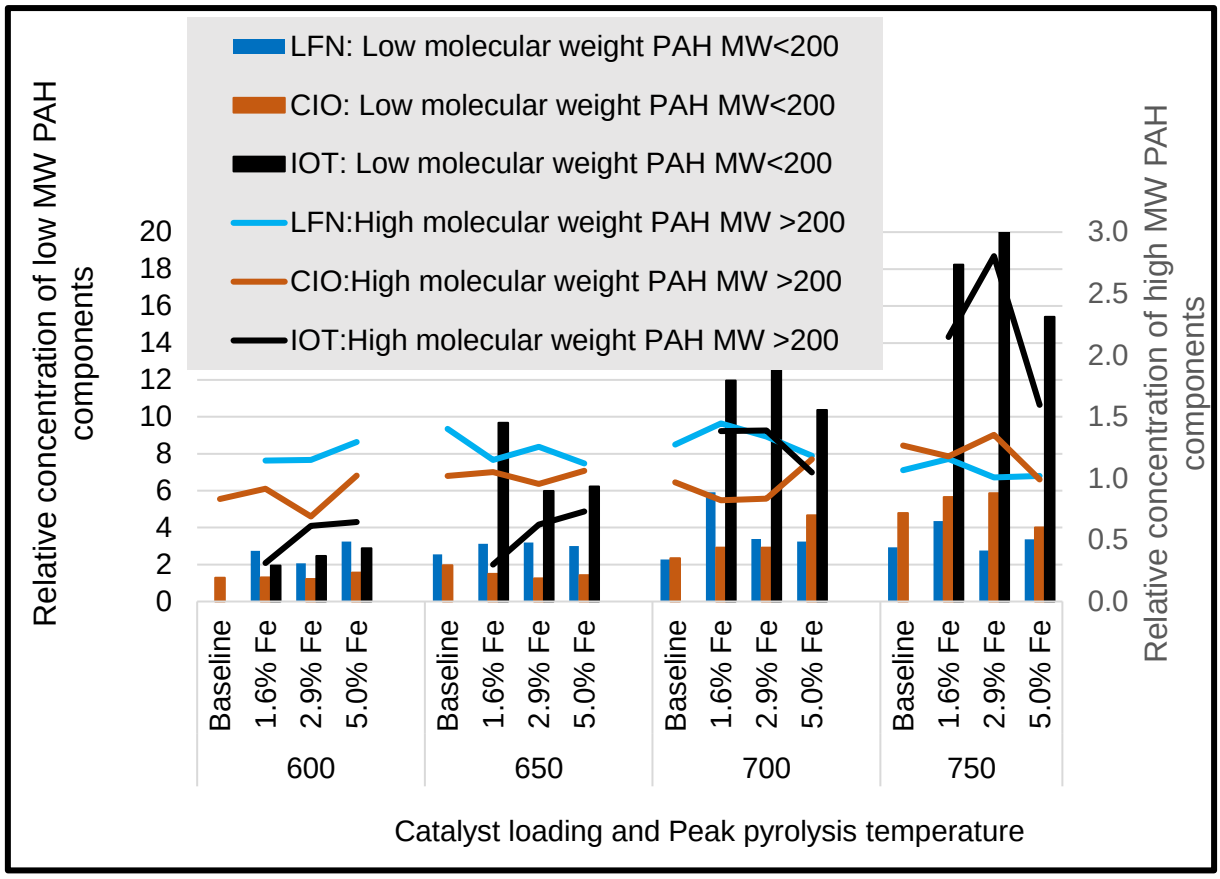

Figure 4.10: The relative concentrations (determined by GC-MS) of PAH tars for the three catalyst types LFN, CIO and IOT. **Experimental conditions**: Heating rate 50°C/min to peak pyrolysis temperature 600°C-750°C in 50°C increments, held for 30 min. Sweeping gas N_2 at a space velocity of 1.6min^{-1}. Catalyst loadings of 0%, 1.6%, 2.9% and 5.0%Fe.

CHAPTER 5

VERTICAL FURNACE - EQUIPMENT DETAIL AND LAYOUT

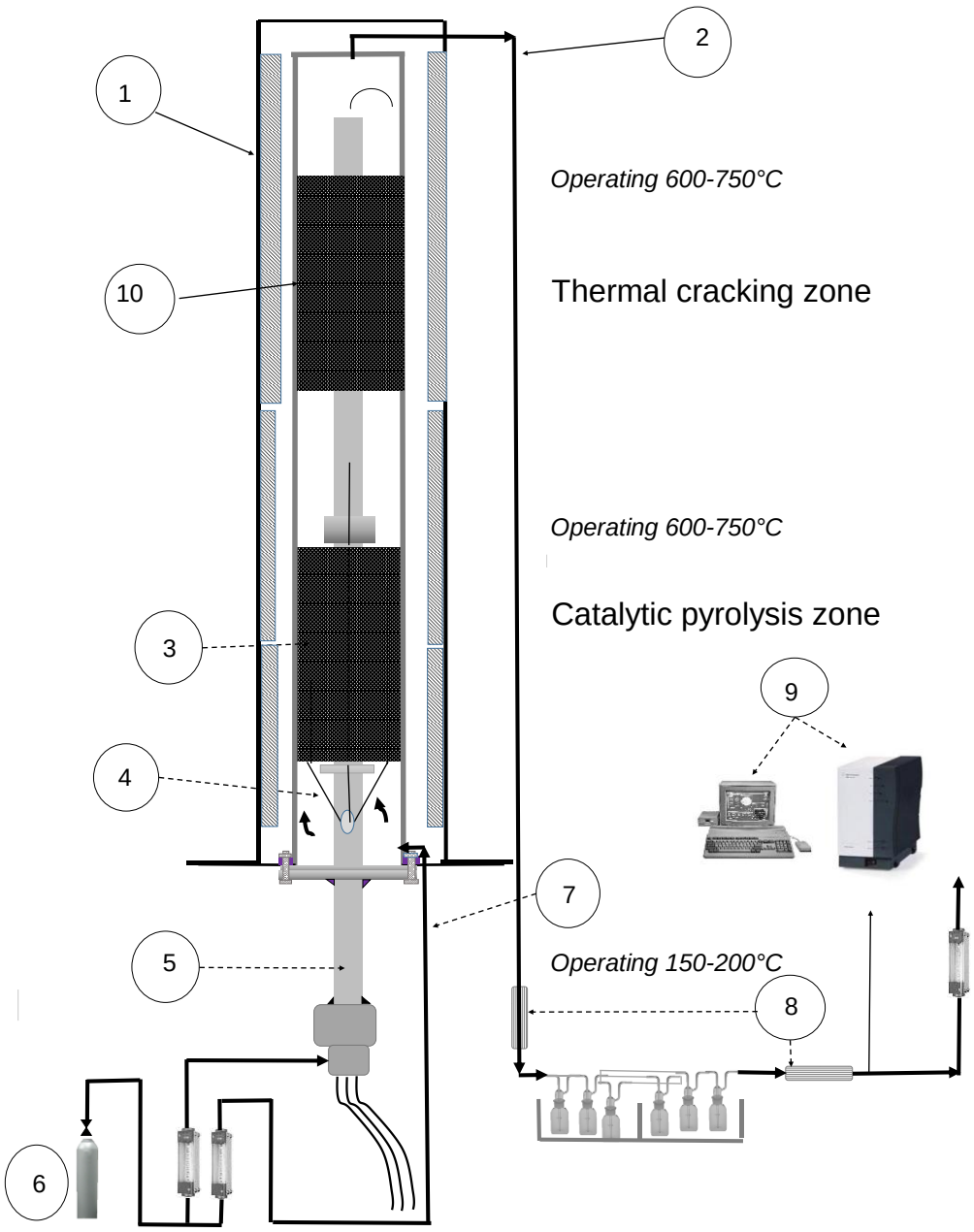

Figure 5.1: Schematic diagram of the experimental setup

1:Carbolite three element furnace, 2: Pyrolysis gas product outlet, 3: Biomass sample with co-mingled char supported catalyst, 4: Thermocouples, 5: Sample tube carrier,6: Nitrogen sweeping gas supply, 7: Sweeping gas inlet, 8: Fine filters to remove particulates, 9: Gas chromatograph for gas analysis and data acquisition

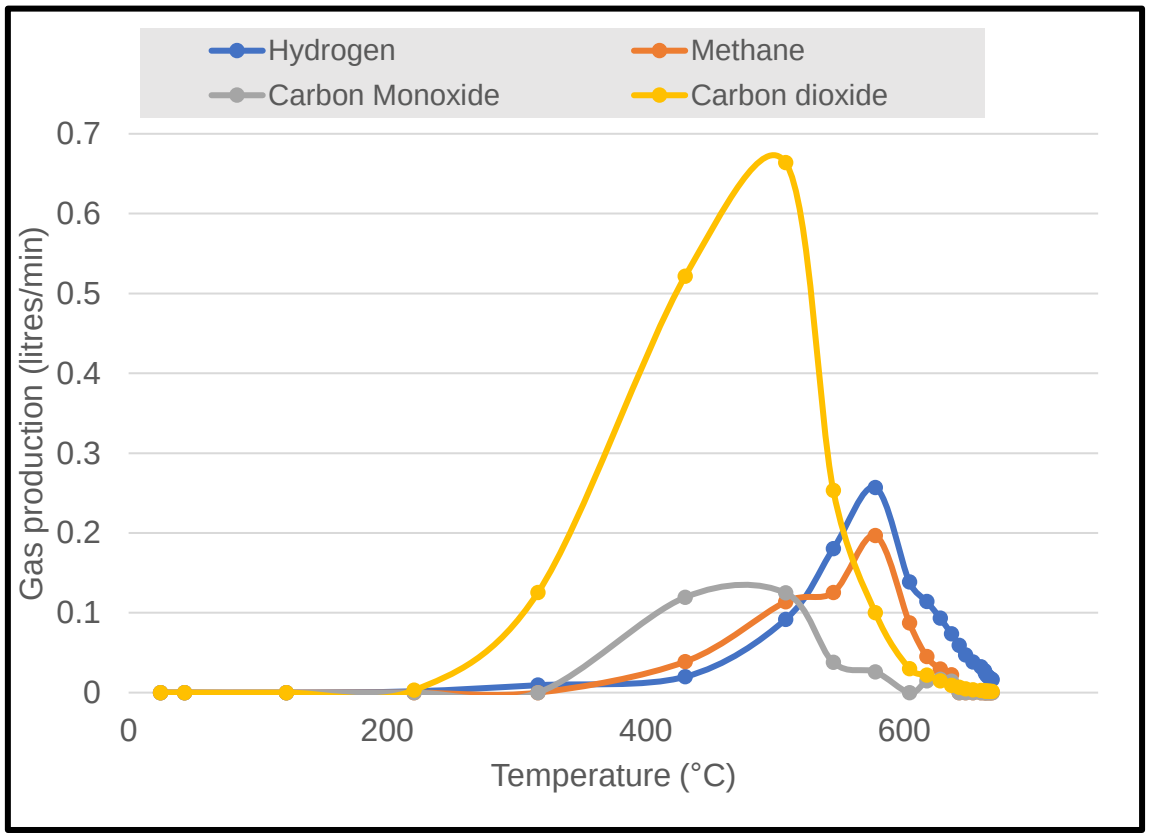

Figure 5.2: Gas production during one-stage pyrolysis. **Experimental conditions**: Heating rate 50°C/min to peak pyrolysis temperature 750°C, held for 30 min. Sweeping gas N_2 at a space velocity of 1.6min^{-1}. LFN catalyst loadings of 5.0%Fe.

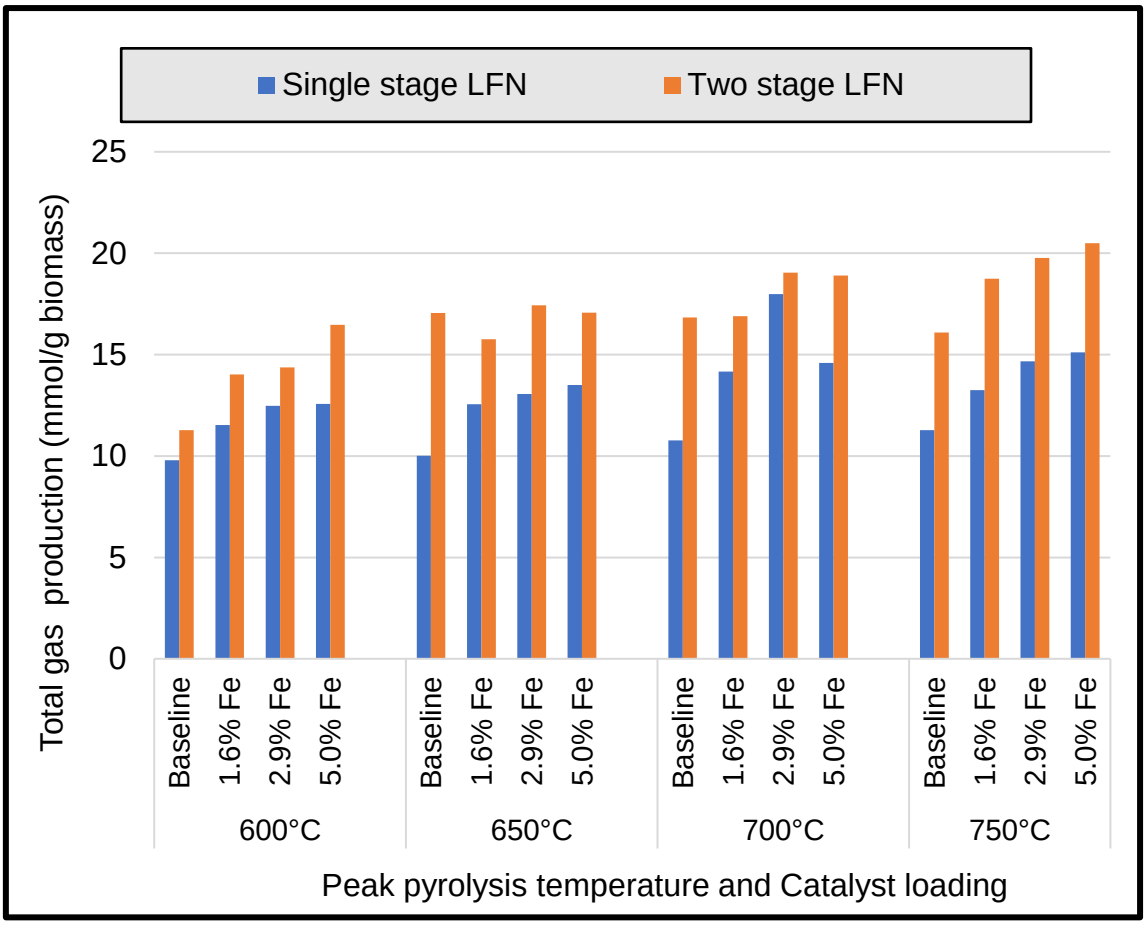

Figure 5.3: Total gas production from one and two-stage pyrolysis for a range of pyrolysis temperatures and catalyst loadings. **Experimental conditions**: *One-stage*: Heating rate 50°C/min to peak pyrolysis temperature 600°C-750°C in 50°C increments, held for 30 min. Sweeping gas N_2 at a space velocity of 1.6min^{-1}. Catalyst loadings of 0%, 1.6%, 2.9% and 5.0%Fe. *Two-stage*: Pre-heat second stage at 75°C/min for 10 minutes to pyrolysis temperature, then heat first stage at 50°C/min to peak pyrolysis temperature 600°C-750°C in 50°C increments, held for 30 min. Sweeping gas N_2 at a space velocity of 1.6min^{-1}. First stage catalyst loadings of 0%, 1.6%, 2.9% and 5.0%Fe; second stage catalyst loadings of 0%, ~6%, ~11%, and ~19%Fe.

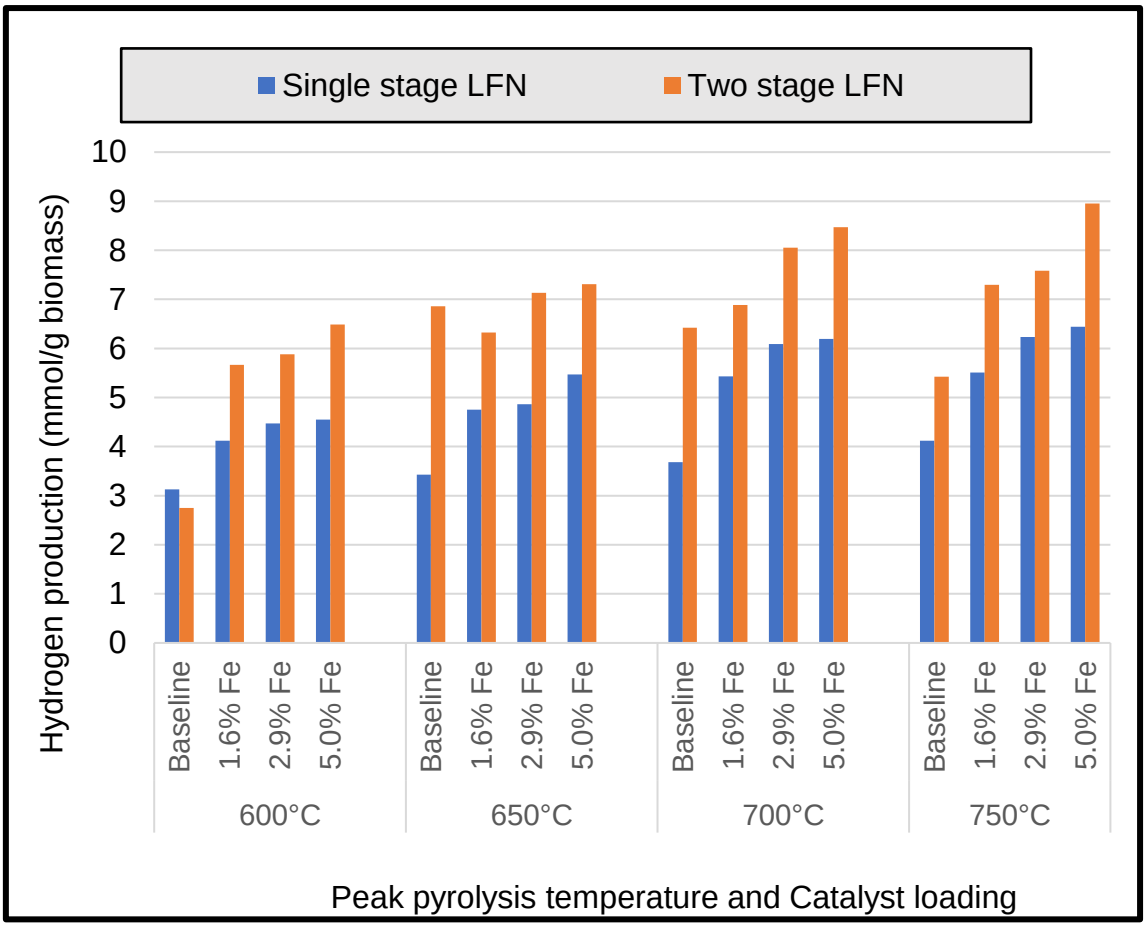

Figure 5.4 Total hydrogen production from one- and two-stage pyrolysis for a range of pyrolysis temperatures and catalyst loadings. **Experimental conditions**: *One-stage*: Heating rate 50°C/min to peak pyrolysis temperature 600°C-750°C in 50°C increments, held for 30 min. Sweeping gas N_2 at a space velocity of 1.6min^{-1}. Catalyst loadings of 0%, 1.6%, 2.9% and 5.0%Fe. *Two-stage*: Pre-heat second stage at 75°C/min for 10 minutes to pyrolysis temperature, then heat first stage at 50°C/min to peak pyrolysis temperature 600°C-750°C in 50°C increments, held for 30 min. Sweeping gas N_2 at a space velocity of 1.6min^{-1}. First stage catalyst loadings of 0%, 1.6%, 2.9% and 5.0%Fe; second stage catalyst loadings of 0%, ~6%, ~11%, and ~19%Fe.

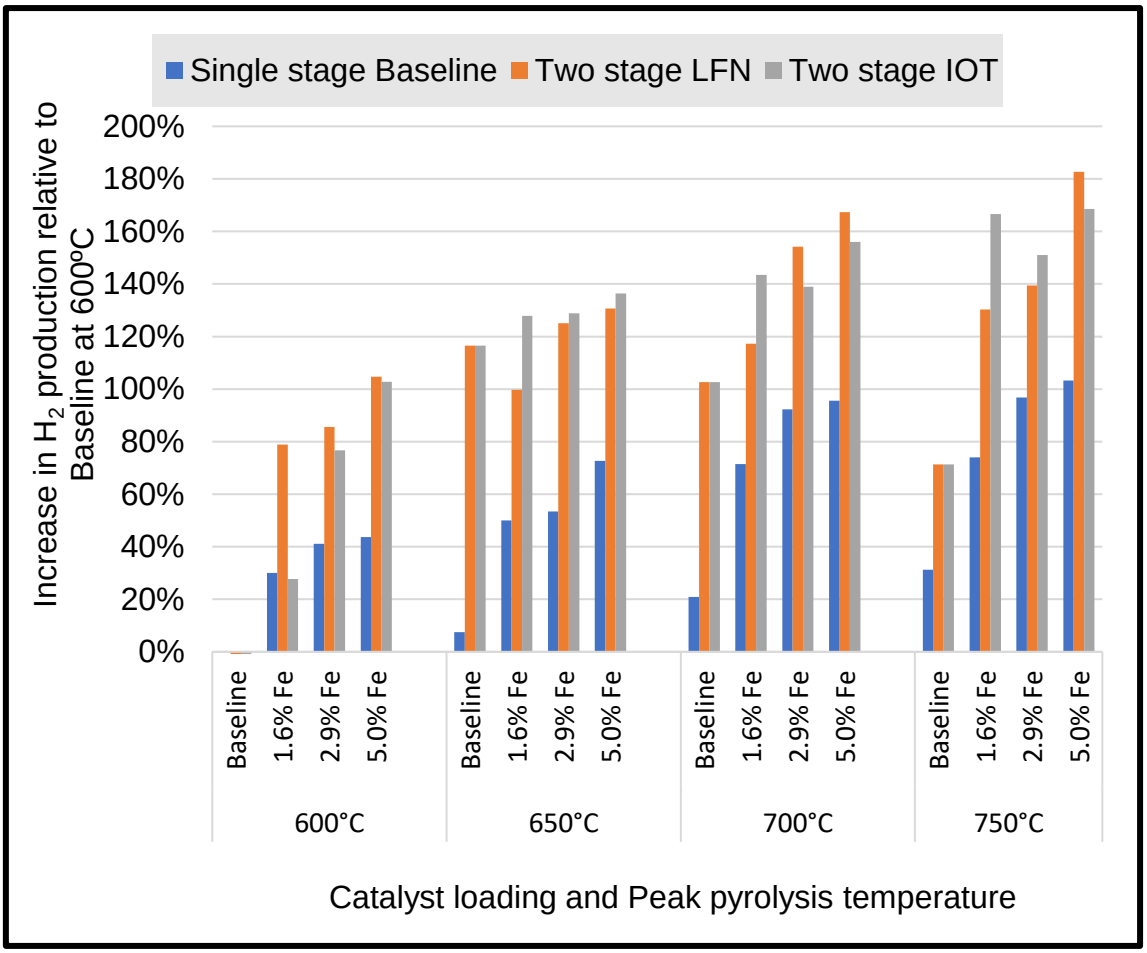

Figure 5.5: Increases in H_2 production from one- and two-stage pyrolysis using baseline at 600°C as reference for a range of pyrolysis temperatures and catalyst loadings. **Experimental conditions**: *One-stage*: Heating rate 50°C/min to peak pyrolysis temperature 600°C-750°C in 50°C increments, held for 30 min. Sweeping gas N_2 at a space velocity of 1.6min^{-1}. Catalyst loadings of 0%, 1.6%, 2.9% and 5.0%Fe. *Two-stage*: Pre-heat second stage at 75°C/min for 10 minutes to pyrolysis temperature, then heat first stage at 50°C/min to peak pyrolysis temperature 600°C-750°C in 50°C increments, held for 30 min. Sweeping gas N_2 at a space velocity of 1.6min^{-1}. First stage catalyst loadings of 0%, 1.6%, 2.9% and 5.0%Fe; second stage catalyst loadings of 0%, ~6%, ~11%, and ~19%Fe.

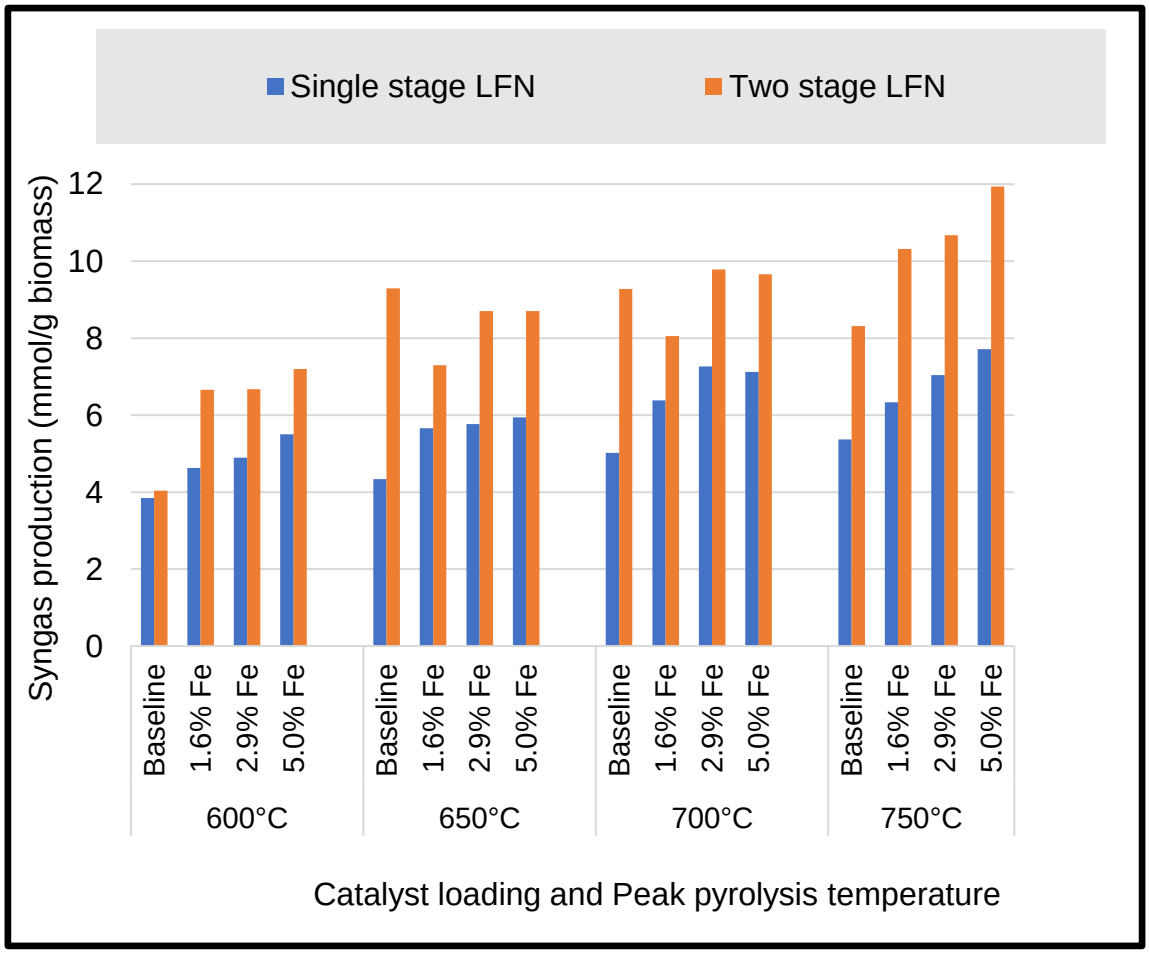

Figure 5.6: Total syngas production from one-stage and two-stage pyrolysis for a range of pyrolysis temperatures and catalyst loadings. **Experimental conditions**: *One-stage*: Heating rate 50°C/min to peak pyrolysis temperature 600°C-750°C in 50°C increments, held for 30 min. Sweeping gas N_2 at a space velocity of 1.6min^{-1}. Catalyst loadings of 0%, 1.6%, 2.9% and 5.0%Fe. *Two-stage*: Pre-heat second stage at 75°C/min for 10 minutes to pyrolysis temperature, then heat first stage at 50°C/min to peak pyrolysis temperature 600°C-750°C in 50°C increments, held for 30 min. Sweeping gas N_2 at a space velocity of 1.6min^{-1}. First stage catalyst loadings of 0%, 1.6%, 2.9% and 5.0%Fe; second stage catalyst loadings of 0%, ~6%, ~11%, and ~19%Fe.

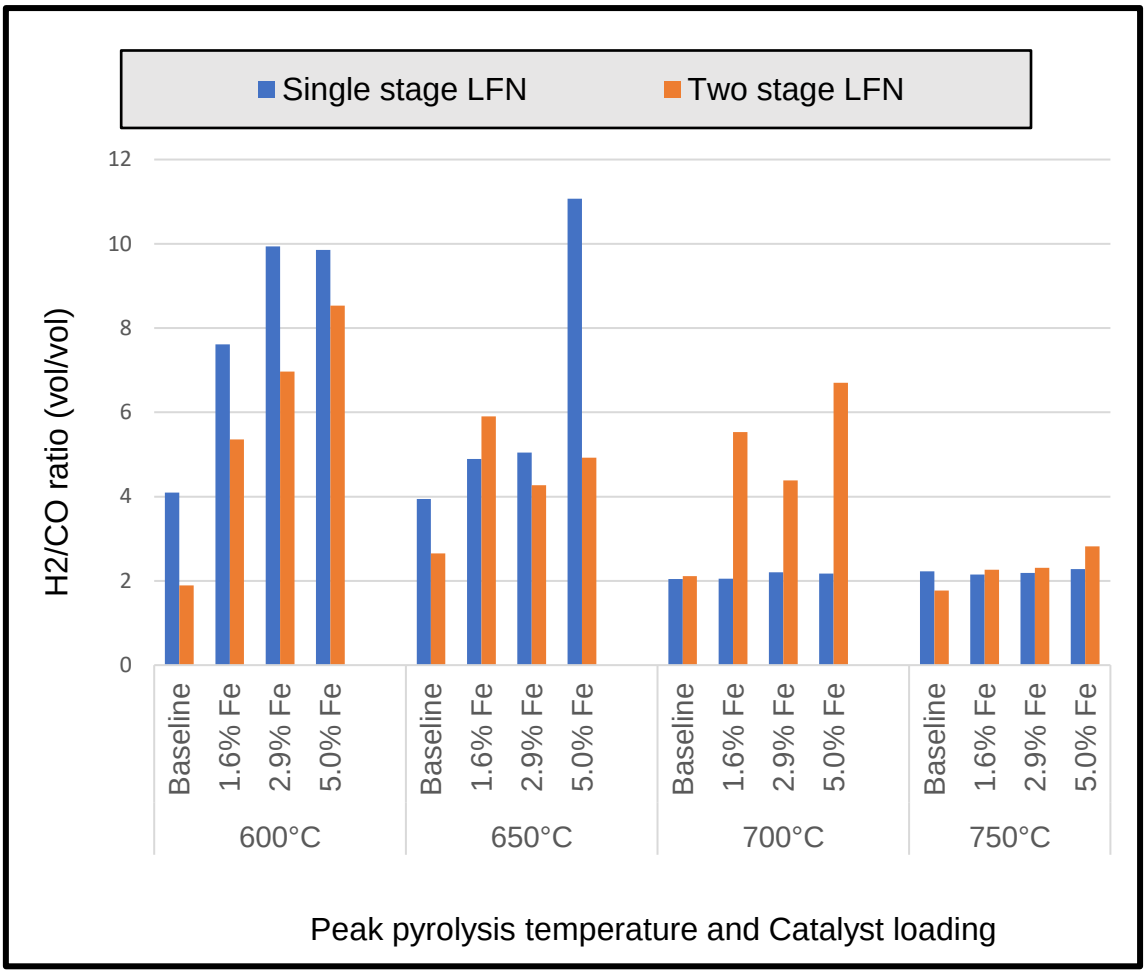

Figure 5.7: H_2/CO ratios resulting from one-stage and two-stage pyrolysis for a range of pyrolysis temperatures and catalyst loadings. **Experimental conditions**: *One-stage*: Heating rate 50°C/min to peak pyrolysis temperature 600°C-750°C in 50°C increments, held for 30 min. Sweeping gas N_2 at a space velocity of 1.6min^{-1}. Catalyst loadings of 0%, 1.6%, 2.9% and 5.0%Fe. *Two-stage*: Pre-heat second stage at 75°C/min for 10 minutes to pyrolysis temperature, then heat first stage at 50°C/min to peak pyrolysis temperature 600°C-750°C in 50°C increments, held for 30 min. Sweeping gas N_2 at a space velocity of 1.6min^{-1}. First stage catalyst loadings of 0%, 1.6%, 2.9% and 5.0%Fe; second stage catalyst loadings of 0%, ~6%, ~11%, and ~19%Fe.

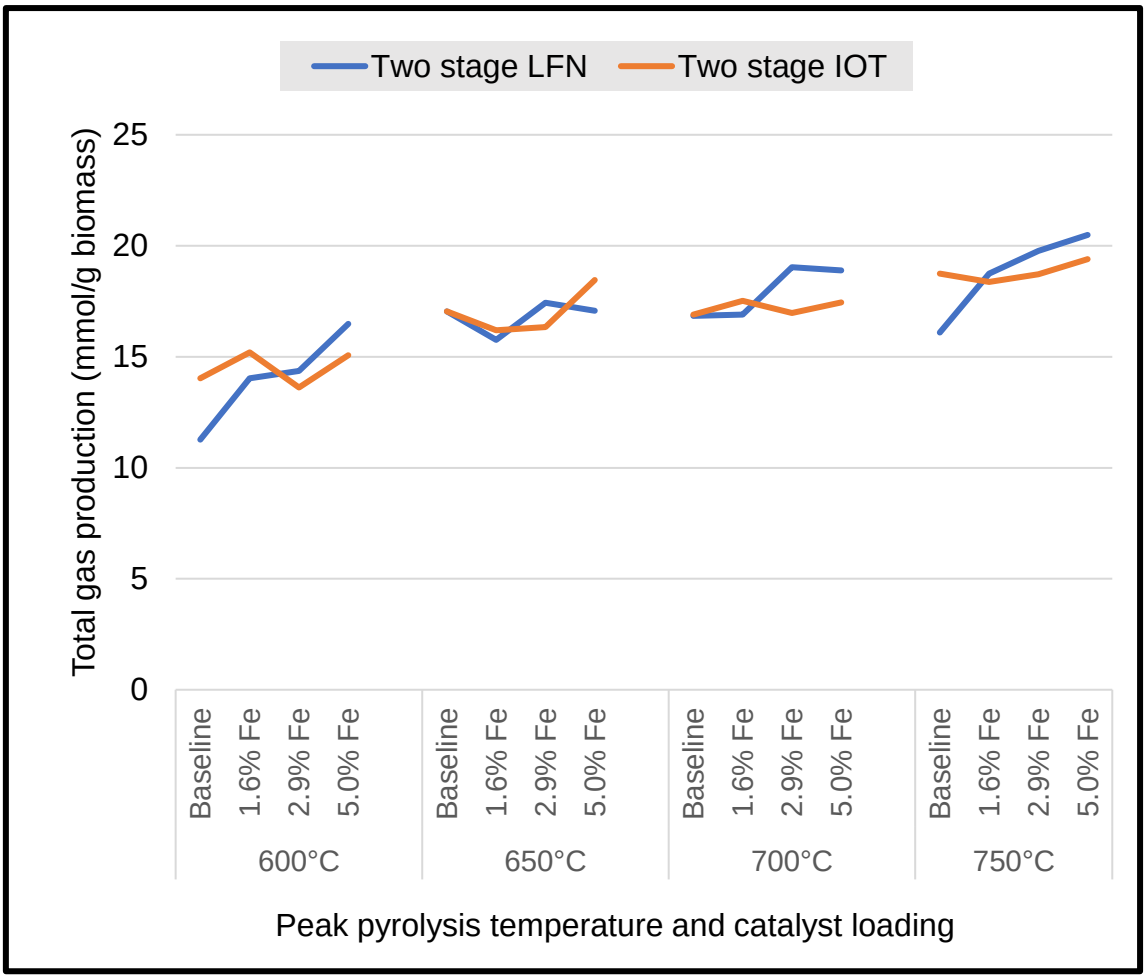

Figure 5.8: Total gas production from two-stage pyrolysis across the spectrum of pyrolysis temperatures and catalyst loadings using either LFN and IOT catalysts. **Experimental conditions:** *Two-stage*: Pre-heat second stage at 75°C/min for 10 minutes to pyrolysis temperature, then heat first stage at 50°C/min to peak pyrolysis temperature 600°C-750°C in 50°C increments, held for 30 min. Sweeping gas N_2 at a space velocity of 1.6min^{-1}. First stage catalyst loadings of 0%, 1.6%, 2.9% and 5.0%Fe; second stage catalyst loadings of 0%, ~6%, ~11%, and ~19%Fe.

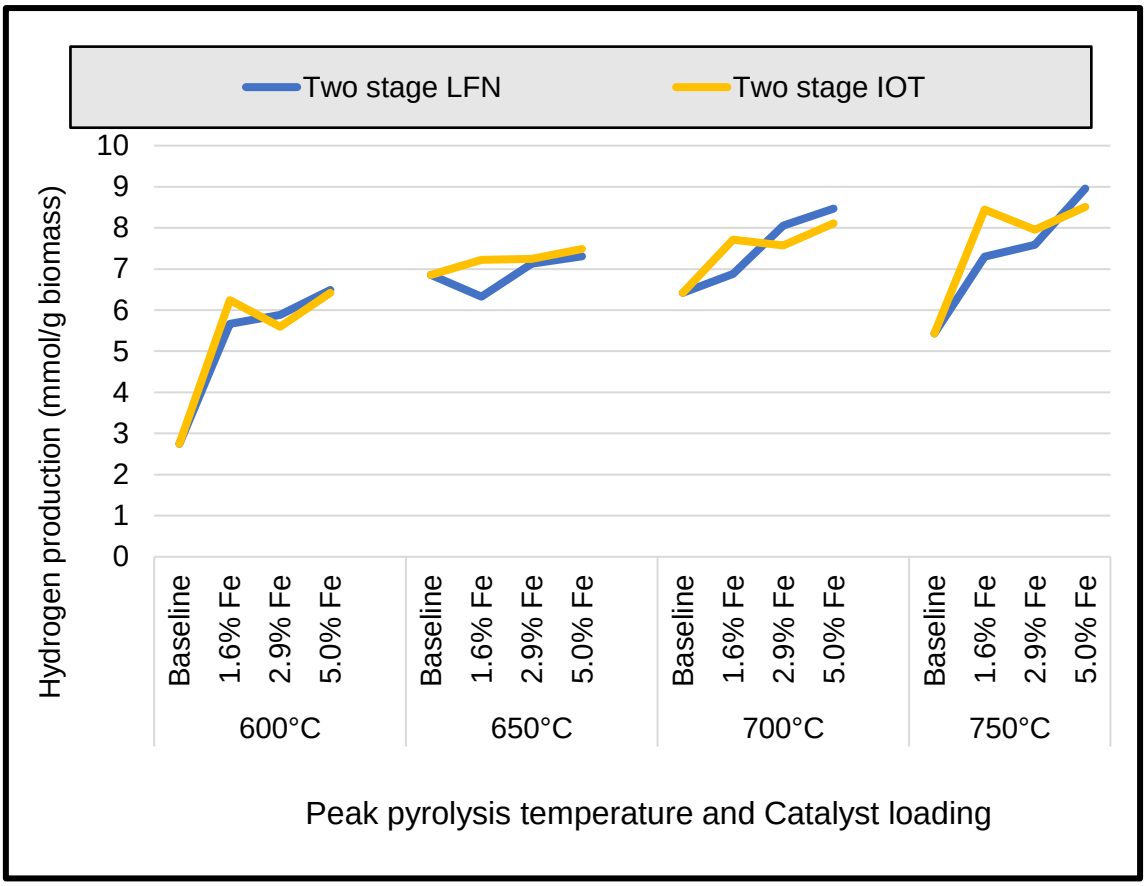

Figure 5.9: Hydrogen production from two-stage pyrolysis across the spectrum of pyrolysis temperatures and catalyst loadings using either LFN or IOT catalyst. **Experimental conditions:** *Two-stage*: Pre-heat second stage at 75°C/min for 10 minutes to pyrolysis temperature, then heat first stage at 50°C/min to peak pyrolysis temperature 600°C-750°C in 50°C increments, held for 30 min. Sweeping gas N_2 at a space velocity of 1.6min^{-1}. First stage catalyst loadings of 0%, 1.6%, 2.9% and 5.0%Fe; second stage catalyst loadings of 0%, ~6%, ~11%, and ~19%Fe.

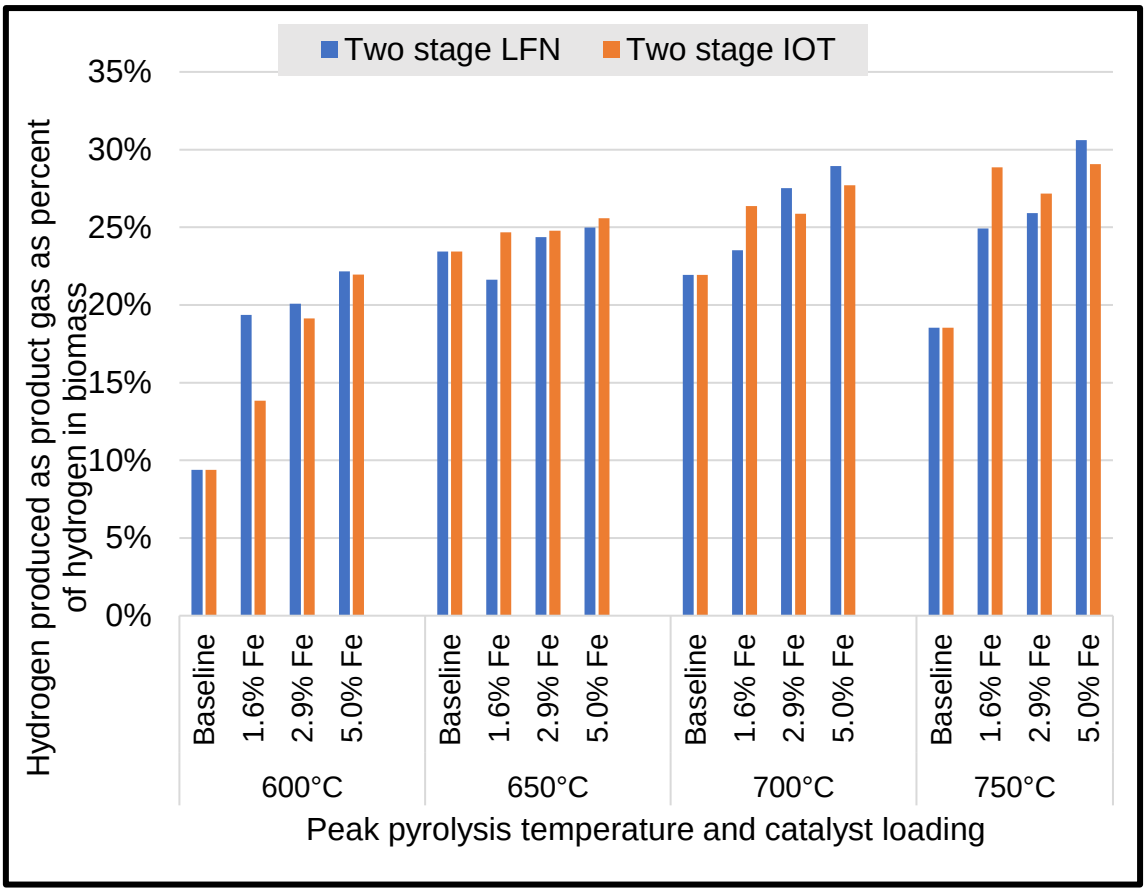

Figure: 5.10: Hydrogen produced as product gas as percent of elemental hydrogen in biomass; using two-stage pyrolysis across the spectrum of pyrolysis temperatures and catalyst loadings with either LFN or IOT catalyst. **Experimental conditions:** *Two-stage*: Pre-heat second stage at 75°C/min for 10 minutes to pyrolysis temperature, then heat first stage at 50°C/min to peak pyrolysis temperature 600°C-750°C in 50°C increments, held for 30 min. Sweeping gas N_2 at a space velocity of 1.6min^{-1}. First stage catalyst loadings of 0%, 1.6%, 2.9% and 5.0%Fe; second stage catalyst loadings of 0%, ~6%, ~11%, and ~19%Fe.

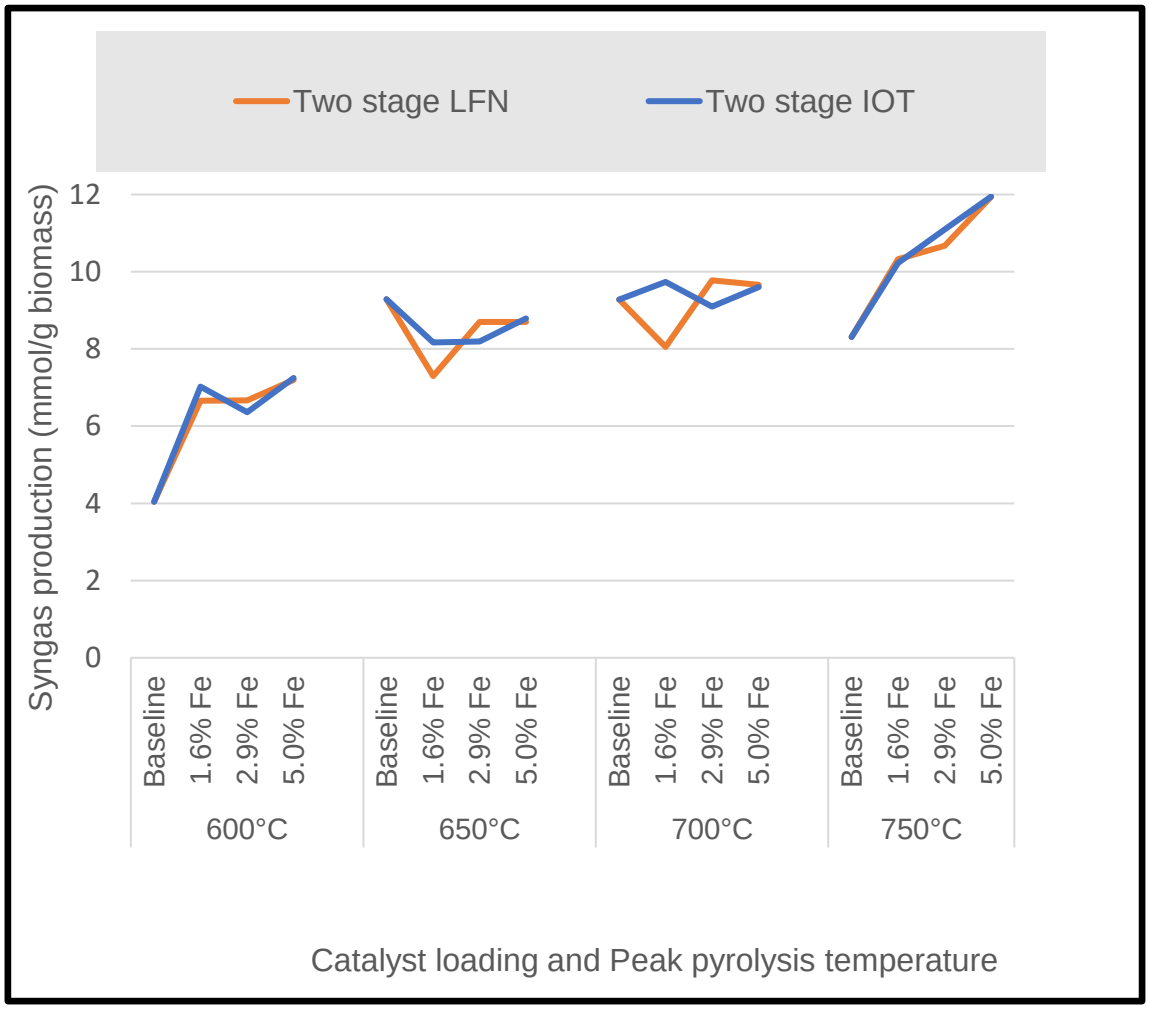

Figure 5.11: Syngas production from two-stage pyrolysis across the spectrum of pyrolysis temperatures and catalyst loadings using either LFN or IOT catalyst. production comparing catalysts during two-stage pyrolysis. **Experimental conditions:** *Two-stage*: Pre-heat second stage at 75°C/min for 10 minutes to pyrolysis temperature, then heat first stage at 50°C/min to peak pyrolysis temperature 600°C-750°C in 50°C increments, held for 30 min. Sweeping gas N_2 at a space velocity of 1.6min^{-1}. First stage catalyst loadings of 0%, 1.6%, 2.9% and 5.0%Fe; second stage catalyst loadings of 0%, ~6%, ~11%, and ~19%Fe.

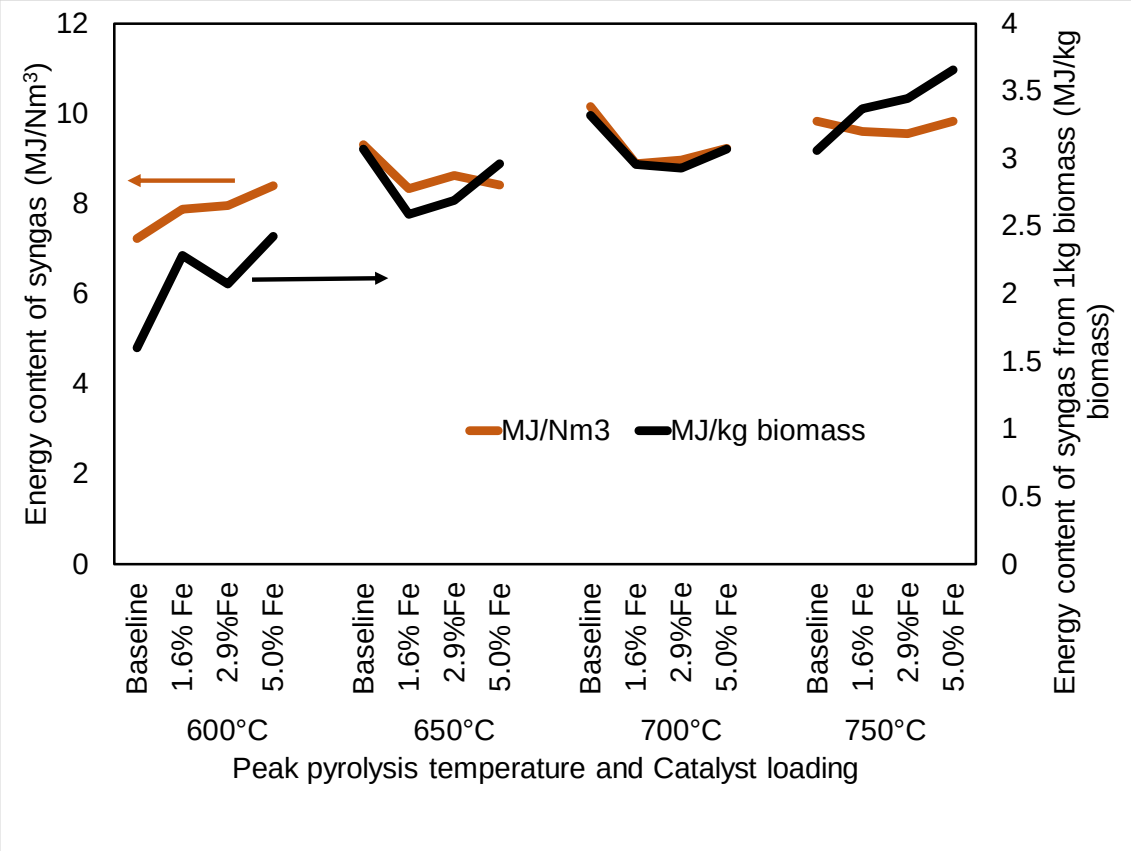

Figure 5.12: Energy content of syngas production from two-stage pyrolysis across the spectrum of pyrolysis temperatures and catalyst loadings using IOT catalyst. **Experimental conditions:** *Two-stage*: Pre-heat second stage at 75°C/min for 10 minutes to pyrolysis temperature, then heat first stage at 50°C/min to peak pyrolysis temperature 600°C-750°C in 50°C increments, held for 30 min. Sweeping gas N_2 at a space velocity of 1.6min^{-1}. First stage catalyst loadings of 0%, 1.6%, 2.9% and 5.0%Fe; second stage catalyst loadings of 0%, ~6%, ~11%, and ~19%Fe.

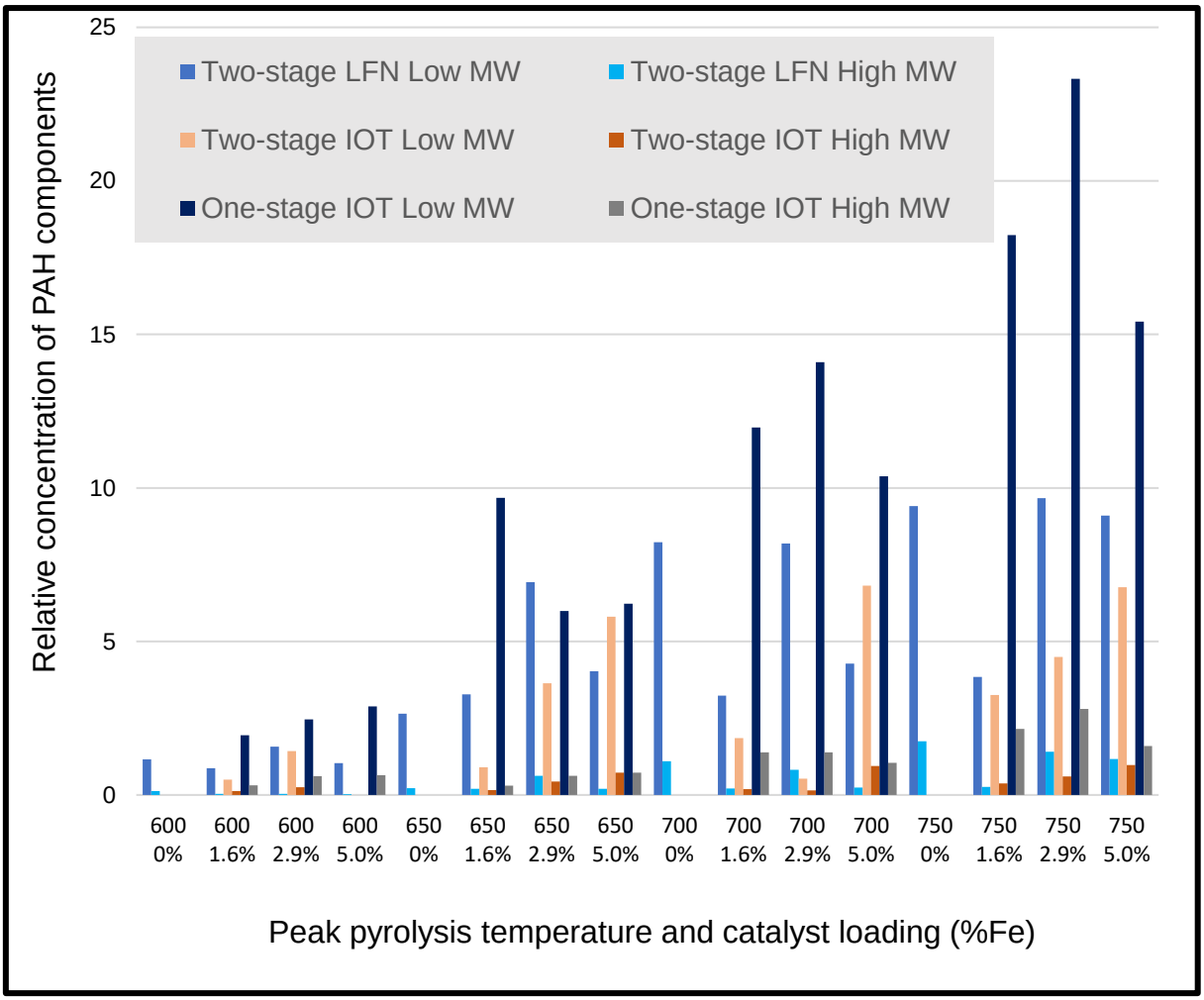

Figure 5.13: Tar reduction from one- and two-stage pyrolysis across the spectrum of pyrolysis temperatures and catalyst loadings using either LFN or IOT catalyst. **Experimental conditions:** *One-stage*: Heating rate 50°C/min to peak pyrolysis temperature 600°C-750°C in 50°C increments, held for 30 min. Sweeping gas N_2 at a space velocity of 1.6min^{-1}. Catalyst loadings of 0%, 1.6%, 2.9% and 5.0%Fe. *Two-stage*: Pre-heat second stage at 75°C/min for 10 minutes to pyrolysis temperature, then heat first stage at 50°C/min to peak pyrolysis temperature 600°C-750°C in 50°C increments, held for 30 min. Sweeping gas N_2 at a space velocity of 1.6min^{-1}. First stage catalyst loadings of 0%, 1.6%, 2.9% and 5.0%Fe; second stage catalyst loadings of 0%, ~6%, ~11%, and ~19%Fe.

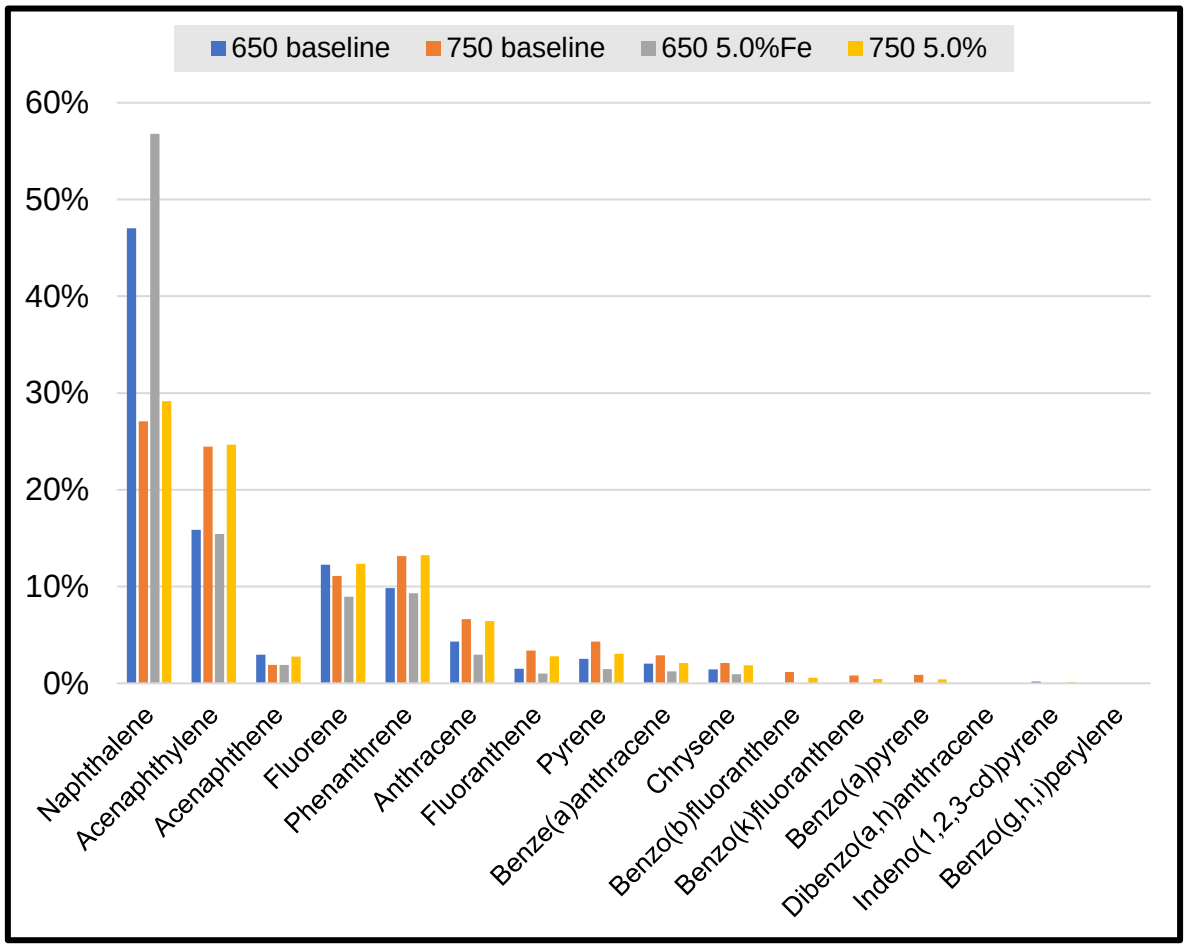

Figure 5.14: Distribution of PAHs from two-stage pyrolysis at 650°C and 750°C for baseline and 5.0%Fe catalyst loading. **Experimental conditions:** *Two-stage*: Pre-heat second stage at 75°C/min for 10 minutes to pyrolysis temperature, then heat first stage at 50°C/min to peak pyrolysis temperature 600°C-750°C in 50°C increments, held for 30 min. Sweeping gas N_2 at a space velocity of 1.6min^{-1}. First stage catalyst loadings of 0%, 1.6%, 2.9% and 5.0%Fe; second stage catalyst loadings of 0%, ~6%, ~11%, and ~19%Fe.